

# CHARACTERISATION OF SHAPE MEMORY ALLOYS BASED ON NICKEL-TITANIUM SYSTEM

## A DISSERTATION

Submitted in partial fulfillment of the  
requirements for the award of the degree

of

### MASTER OF TECHNOLOGY

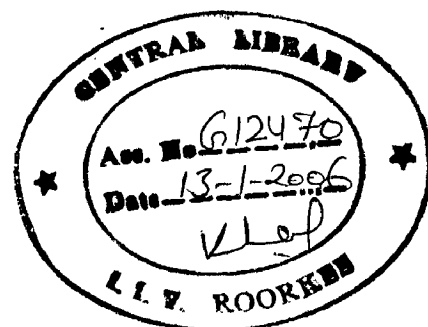
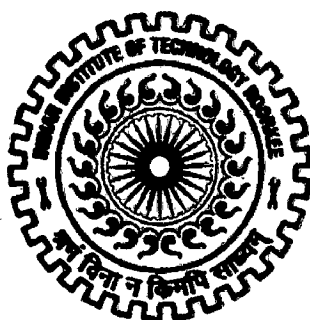
in

### METALLURGICAL & MATERIALS ENGINEERING

(With Specialization in Physical Metallurgy)

By

**K. HARI KRISHNAN**



DEPARTMENT OF METALLURGICAL & MATERIALS ENGINEERING  
INDIAN INSTITUTE OF TECHNOLOGY, ROORKEE  
ROORKEE-247 667 (INDIA)

June, 2005

A handwritten signature in black ink, appearing to be "K. Hari Krishnan", is located in the bottom left corner of the page.

## CANDIDATE'S DECLARATION

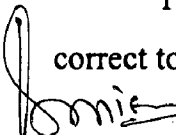
I hereby certify that the work presented in this dissertation entitled "CHARACTERISATION OF SHAPE MEMORY ALLOYS BASED ON NICKEL-TITANIUM SYSTEM" in the partial fulfillment of the requirements for the award of the degree of "MASTER OF TECHNOLOGY" in "METALLURGICAL & MATERIALS ENGINEERING" with specialization in "PHYSICAL METALLURGY", at Indian Institute of Technology, Roorkee. This is an authentic record of any own work carried out between July 2004 to June 2005. under the guidance of Dr. P.S.MISRA Professor & Dr. K.CHANDRA and Dr. D.PURI Assistant Professor, Department of Metallurgical & Materials Engineering, Indian Institute of Technology Roorkee, Roorkee.

I have not submitted the matter presented in this dissertation for the award of any other degree of this institute of any other institute.


Dated: June 30, 2005

  
(K.HARI KRISHNAN)

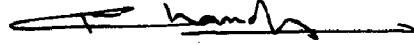
This is to certify that the above statement made by the candidate is correct to the best of my knowledge.

  
(Dr. P.S.Misra)

Professor  
Dept. of Metallurgical  
& Materials Engg.,  
IIT Roorkee,  
Roorkee - 247 667.  
(INDIA).

  
(Dr. D.Puri)

Assistant Professor,  
Dept. of Metallurgical  
& Materials Engg.,  
IIT Roorkee,  
Roorkee - 247 667.  
(INDIA).

  
(Dr.K.Chandra).

Assistant Professor,  
Dept. of Metallurgical  
& Materials. Engg.,  
IIT Roorkee,  
Roorkee - 247 667.  
(INDIA).

## ACKNOWLEDGEMENTS

---

Many individuals have assisted me during the present work. I would like to thank them all.

I express my deep sense of gratitude to **Dr.P.S.Misra**, Professor **Dr.K.Chandra** & **Dr.D.Puri**, both Assistant Professors, Department of Metallurgical and Materials Engineering, Indian Institute of Technology Roorkee, Roorkee for their inspiration and active supervision, through provoking discussing criticism and suggestion given by them during the course of this work. Without their timely and untiring help in the form of consistent guidance and encouragement, it would not have been possible to present this dissertation in its form. In addition, their experience, assiduity and deep insight of the subject helped this work always a smooth and steady course.

I am also grateful to **Dr. V.K. Tiwari**, Professor and Head, Department of Metallurgical and Materials Engineering, Indian Institute of Technology, Roorkee, Roorkee for providing me all the facilities in the department to carry out my work.

I am thankful to **Dr. G. C. Kaushal**, O.C. M. Tech. and Professor, Department of Metallurgical and Materials Engineering, Indian Institute of Technology, Roorkee, Roorkee for providing me opportunity to present this dissertation report.

I would like to express my sincere and heartfelt thanks to **The Command, Naval-Airsystem Command, MD, USA**, and **Dr. Vinod.S. Agarwala** Ph.D., P.E., FASM, FNACE, Senior Staff Scientist, **Naval-Air Systems Command, MD, USA**, who has helped and encouraged to me lot during the course of my dissertation work.

I am also thankful to **Dr.T.G.Ramesh**, Head and **Dr.S.K. Bhawmik**, Scientist, National Aero-Space Laboratory, Bangalore, who provided an opportunity to me to do wire drawing operations under the supervision of him.

Dated: June 30, 2005

  
(K. HARI KRISHNAN)

## ABSTRACT

---

This dissertation report intends to present new experimental evidence of a comprehensive investigation of the effects of low temperature ageing on the transformation behaviour of a Ni-Ti and Ni-Ti-Cu Shape memory alloys (SMA). Up to date, experimental evidence reported in the literature are exclusive of the transformation behaviour of the ageing characteristics of studied from 473 K to 993 K. The ageing temperatures investigated in this study are in the range of 423 K (new experimental evidence) and 473 K to 773 K (conventional ageing temperatures). The occurrence of the complex transformation behaviour indicates that the Ni-rich Ni-Ti and Ni-Ti-Cu alloys are unstable at even these low temperatures. This has the direct evidence and application for the property stability of Ni-Ti and Ni-Ti-Cu alloys in many applications.

This study investigates the effects on ageing (423 K to 773 K) on the transformation behaviour of a  $\text{Ni}_{54.9}\text{Ti}_{45.08}$  and Ni-49.TiCu6.6 Shape Memory Alloy (SMA). It was found that ageing in the temperature range of 423 K induced R-phase transformation in Ni-Ti and Ni-Ti-Cu SMA's. The transformation behaviours were analyzed by means of DSC, XRD, Tensile test and Resistivity measurements.

High temperature XRD was carried out to find the Transformations Temperature Region (TTR) of the aged and as-rolled samples.

The effect of cold working (% straining) on Martensite transformation was analyzed by means of XRD, DSC and resistivity methods. When the percentage straining increases means intensity of the (110)<sub>B2</sub> phase was increased progressively. This increases in intensity reveals that Ms Temperature of the SMA was increased due to the formation of the stress induced Martensite (SIM).

The effect of annealing on the Ms Temperature and As temperatures of 30% cold reduced wire samples were analyzed using DSC and tensile test. The effect of thermal cycle on the transformation hysteresis and pseudo-elasticity were analyzed by means of DSC and Tensile test.

# CONTENTS

---

	P.No
CANDIDATE'S DECLARATION	I
ACKNOWLEDEMENT	II
ABSTARCT	III
CONTENTS	IV
ABBERIVATIONS	VII
LIST OF TABLES	VIII
LIST OF FIGURES	IX
CHAPTER: 1 INTRODUCTION TO SHAPE MEMORY ALLOYS	1
CHAPTER: 2 LITERATURE REVIEW	2
2.1 History	2
2.2 Two major modes of the shape Memory Effect	4
2.2.1 Martensite transformation	4
2.3 Types of Shape memory effects	9
2.3.1 Single way shape memory effect (SWSME)	9
2.3.2 Two Way Shape Memory Effect (TWSME)	9
2.3.3 Super elasticity	10
2.3.4 Ferro elasticity	10
2.3.5 Interfacial structure and the shape memory effect	10
2.3.6 Shape Memory Martensite	11
2.3.7 Interfacial characteristics	13
2.3.8. Interfacial structure and strain accommodation	13
2.3.9 Mechanical Properties of Shape memory alloy	13
2.3.10 Pseudoelasticity	14

<b>2.3.11 Effect of strain rate</b>	<b>15</b>
<b>2.3.12 Effect of grain size</b>	<b>15</b>
<b>2.3.13 Strain memory effect</b>	<b>16</b>
<b>2.3.14 Reversible strain memory effect</b>	<b>17</b>
<b>2.3.15 Fatigue properties</b>	<b>17</b>
<b>2.3.16 Internal friction</b>	<b>17</b>
<b>2.4 Aging Characteristics of the Ni-Ti and Ni-Ti-Cu SMA</b>	<b>18</b>
<b>2.4.1 Decomposition of near-equiatomic B2 phase of Ti-Ni alloy</b>	<b>18</b>
<b>2.5 Applications of SMA</b>	<b>22</b>
<b>2.6 Formulation of the problem</b>	<b>23</b>
<b>Chapter 3 :-</b>	
<b>3.0 Experimental Details</b>	<b>24</b>
<b>3.1 Hot rolling</b>	<b>25</b>
<b>3.2 Cold rolling</b>	<b>26</b>
<b>3.3 Wire Drawing</b>	<b>26</b>
<b>3.4 Shape Memory Effect (SME) Treatment.</b>	<b>26</b>
<b>3.5 Microstructural characterization.</b>	<b>27</b>
<b>3.6 Scanning Electron Microscopy (SEM)</b>	<b>28</b>
<b>3.7 Resistivity methods</b>	<b>28</b>
<b>3.8. X-Ray Diffraction</b>	<b>29</b>
<b>3.9 Tensile test</b>	<b>29</b>
<b>Chapter 4:-</b>	
<b>4.0 Results</b>	<b>30</b>
<b>4.1.1 Ni-Ti aged in 150°C</b>	<b>30</b>
<b>4.1.2 Ni-Ti-Cu aged 150°C</b>	<b>35</b>
<b>4.1.3 Ni-Ti aged in 300°C.</b>	<b>39</b>

4.1.4	Aged 300°C in Ni-Ti-Cu	41
4.1.5	Comparison of Wire and sheet sample	45
4.1.6	DSC study of the effect of Annealing on the 30% cold reduced Ni-Ti wire	50
4.2	XRD analysis	54
4.3.	Optical microscopy study	73
4.3.1.	Effect of rolling on the microstructural changes in Ni-Ti-Cu	73
4.3.2	Effect aging treatment on Ni-Ti and Ni-Ti-Cu.	78
4.4	SEM study	83
4.5.	Tensile Test	85
4.5.1	Effect of annealing on stress-strain curve	86
4.5.2	Effect of ageing on the Tensile stress-strain Curve	88
4.5.3	Effect of temperature on the stress-strain curve of the Ni-Ti SMA	92
4.6.	Resistivity Measurements	94
Chapter 5:-		
5.0	Discussion	96
5.1.1.	Aged in 150°C in Ni-Ti system	96
5.1.2	Ageing 150°C in Ni-Ti-Cu SMA	100
5.1.3	Ageing in 300°C Ni-Ti system.	102
5.1.4	Aged 300°C in Ni-Ti-Cu SMA	104
5.2	XRD analysis.	105
6.	Future Work	108
7.	Conclusion	109
8.	Reference	110

## Abbreviations

SME- Shape memory Effect  
SMA- Shape memory alloy.  
B2 –Cubic (CsCl, Austenite structure)  
R- Rhombohedral (R-phase)  
B19'- Monoclinic martensites  
B19-Trigonal Martensite  
As-Austenite start temperature.  
Af-Austenite finish Temperature  
Ms-Martensite start temperature  
Mf- Martenite finish temperature.  
Rs- R-phase start temperature  
Rf-R-phase finish temperature.  
DSC-Differential Scanning calorimetry.  
R/ RT-Normalized resistivity  
Hrs –hours.



## List of Tables

---

TableNo	Title	P.No
Table 1	Data showing magnitude of the shear and normal components of the invariant plane strains associated with martensite reactions are difficult to measure and relatively scarce	6
Table 2	Chemical analysis of Ni-Ti and Ni-Ti-Cu	24

## List of Figures

Fig.No	Title	P.No
Fig 2.1	Detailed mechanism of the SME.	4
Fig. 2.2	Schematic diagram showing partial transformation. from the matrix phase to martensite.	15
Fig- 2.3	Stress-strain curve alloys deformed at the Ms Temperature together with a schematic curve showing the memory recovery of the alloy on heating	16
Fig 3.1	As received Ni-Ti rod	24
Fig 4.1.1	Ni-Ti as quenched from 850°C	30
Fig 4.1.2	DSC plot of the Ni-Ti aged 150°C at 4 Hrs	31
Fig 4.1.3	DSC study of the Ni-Ti aged in 150°C at 24 Hrs.	32
Fig 4.1.4	DSC study of the Ni-Ti aged in 150°C at 48 Hrs.	33
Fig 4.1.5	DSC plot of the Ni-Ti aged in 150°C in 72 hrs.	34
Fig.4.1.5.a	DSC plot of the solutionized as quenched sample from 850°C (at 1hr).	35
Fig.4.1.6	DSC curve of the Ni-Ti-Cu aged 24 hrs 150°C	36
Fig.4.1.7	DSC plot of the Ni-Ti-Cu aged 150°C at 72 hrs.	37
Fig 4.1.8	DSC study of the Ni-Ti-Cu aged 150°C at 96 hrs	38
Fig 4.1.9	DSC plot of the Ni-Ti aged in 300°C at 48 hrs	39
Fig.4.1.10	DSC plot of the Ni-Ti aged in 300°C at 72hrs	39
Fig.4.1.11	DSC curve of the Ni-Ti aged 96 hrs at 300°C	40
Fig.4.1.12	DSC curve of aged 125 hrs at 300°C sample.	41
Fig.4.1.13	DSC curve of the Ni-Ti-Cu aged in 48 hrs at 300°C	42
Fig.4.1.14	DSC plot of the Ni-Ti-Cu aged in 72 hrs at 300°C	43
Fig.4.1.15	DSC plot of the Ni-Ti-Cu aged in 96 hrs at 300°C	43
Fig.4.1.16	DSC plot of the Ni-Ti-Cu aged in 125 hrs at 300°C	44
Fig.4.1.17	DSC plot of Aged in 300°C at 48 hrs Ni-Ti wire sample.	45
Fig-4.1.18	DSC plot of aged in 48 hrs at 300°C Ni-Ti sheet sample.	46
Fig-4.1.18.a	DSC plot of the Ni-Ti wire aged in 300°C at 96hrs wire	47
Fig 4.1.19	DSC plot of the Ni-Ti-Cu of the prolong aged in 72 hrs at 300°C	48
Fig.4.1.20	DSC plot of the Ni-Ti wire aged in 300°C at 96hrs	59
Fig 4.1.21	DSC plot of the Ni-Ti annealed in 450°C at 10 minutes	50

Fig 4.1.22.a	DSC plot of the annealed in 500°C at 20 minutes Ni-Ti SMA	51
Fig.4.1.22.b	DSC curve of the Ni-Ti as drawn SMA wire	52
Fig.4.1.23	DSC plot of the Ni-Ti-Cu thermally cycled 400 cycles.	53
Fig-4.2.1	XRD spectra of the Ni-Ti aged in 300°C at 125 hrs.	54
Fig.4.2.2	XRD spectra of the Ni-Ti aged in 500°C at 24 hrs	55
Fig.4.2.3	XRD spectra of the Ni-Ti-Cu aged in 400°C at 50 hrs	55
Fig.4.2.4	XRD spectra of the Ni-Ti aged in 500°C at 150 hrs	56
Fig.4.2.5	XRD spectra of the Ni-Ti-Cu aged in 400°C at 72 hrs.	57
Fig.4.2.6	XRD spectra of the Ni-Ti-Cu as quenched from 850°C.	57
Fig.4.2.7	XRD spectra of the Ni-Ti aged in 300°C at 72 hrs.	58
Fig.4.2.8	XRD spectra of the Ni-Ti-Cu aged in 500°C at 48 hrs.	59
Fig.4.2.9	XRD spectra of the Ni-Ti as quenched from 850°C.	59
Fig.4.2.10	XRD spectra of the 30% cold worked annealed in 400°C at 20 minutes in NiTi SMA.	60
Fig.4.2.10-1	XRD spectra of the 5% reduced (strained) in Ni-Ti-Cu SMA.	60
Fig 4.2.10-2	XRD spectra of the 10% strained (Cold reduced) Ni-Ti-Cu SMA.	61
Fig 4.2.10-3	XRD spectra of the 15% strained (Cold reduced) Ni-Ti-Cu SMA	61
Fig 4.2.10-4	XRD spectra of the 20% strained (Cold reduced) Ni-Ti-Cu SMA.	62
Fig 4.2.10-5	XRD spectra of the 5%, 10%, 15% and 20% strained Ni-Ti-Cu SMA.	63
Fig.4.2.11-1	High temperature (80°C) XRD spectra of the Ni-Ti as rolled sheet.	64
Fig.4.2.11-2	High temperature (120°C) XRD spectra of the Ni-Ti as rolled sheet.	64
Fig.4.2.11-3	High temperature (150°C) XRD spectra of the Ni-Ti as rolled sheet.	65
Fig.4.2.11-4	High temperature (200°C) XRD spectra of the Ni-Ti as rolled sheet.	65
Fig.4.2.11-5	High temperature (250°C) XRD spectra of the Ni-Ti as rolled sheet.	66
Fig 4.2.11- 6	Ni-Ti as rolled high temperature XRD Spectra is super imposed.	66
Fig.4.2.12	High temperature XRD spectra of the Ni-Ti aged in 500°C at 48 hrs sample.	67
Fig.4.2.13	High temperature XRD spectra of the Ni-Ti –Cu aged 500°C at 48 hrs sample.	68
Fig.4.2.13-1	High temperature was carried out 700°C XRD spectra of the Ni-Ti –Cu aged 500°C at 48 hrs sample.	69
Fig.4.2.13-2	XRD spectra was performed in 35°C XRD spectra of the Ni-Ti –Cu aged 500°C at 48 hrs sample.	69

Fig.4.2.13-3	XRD spectra was performed in 40°C XRD spectra of the Ni-Ti -Cu aged 500°C at 48 hrs sample.	70
Fig.4.2.13-4	XRD spectra was performed in 45°C XRD spectra of the Ni-Ti -Cu aged 500°C at 48 hrs sample.	70
Fig.4.2.13-5	XRD spectra was performed in 50°C XRD spectra of the Ni-Ti -Cu aged 500°C at 48 hrs sample.	71
Fig.4.2.13-6	XRD spectra was performed in 60°C XRD spectra of the Ni-Ti -Cu aged 500°C at 48 hrs sample.	71
Fig.4.2.13-7	XRD spectra was performed in 100°C XRD spectra of the Ni-Ti -Cu aged 500°C at 48 hrs sample.	72
Fig.4.2.13-8	high temperature was carried in 150°C XRD spectra of the Ni-Ti -Cu aged 500°C at 48 hrs sample	72
Fig.4.3.1	The effect of 20% reduction rolling on Ni-Ti-Cu SMA reduced	73
Fig.4.3.2	The effect of 30% reduction rolling on Ni-Ti-Cu SMA reduced	74
Fig.4.3.3	The effect of 40% reduction rolling on Ni-Ti-Cu SMA reduced	74
Fig.4.3.4	The effect of 50% reduction rolling on Ni-Ti-Cu SMA reduced	75
Fig.4.3.5	The effect of 95% reduction (Final) rolling on Ni-Ti-Cu SMA reduced	75
Fig.4.3.6	The effect of 40% reduction rolling on Ni-Ti SMA reduced	75
Fig.4.3.7	The effect of 60% reduction rolling on Ni-Ti SMA reduced	76
Fig.4.3.8	The effect of 70% reduction rolling on Ni-Ti SMA reduced	77
Fig.4.3.8.1	Ni-Ti as quenched from 800°C (1 hour soaking time).	78
Fig.4.3.9	Ni-Ti aged in 300°C at 24 hrs.	78
Fig.4.3.11	Ni-Ti aged in 300°C at 48 hrs	79
Fig.4.3.12	Ni-Ti aged in 300°C at 72 hrs	79
Fig.4.3.13	Ni-Ti aged in 3000C at 96 hrs	79
Fig.4.3.14	Ni- Fig.4.3.14 Ni-Ti-Cu aged in 3000C at 48 hrs	80
Fig.4.3.14.1	Ni-Ti-Cu aged in 3000C at 72 hrs	80
Fig.4.3.15	Ni-Ti aged in 4000C at 24 hrs	80
Fig.4.3.16	Ni-Ti aged in 4000C at 48 hrs	81
Fig.4.3.17	Ni-Ti aged in 4000C at 72 hrs	81
Fig.4.3.18	Ni-Ti as quenched from 850°C	81
Fig.4.3.19	Ni-Ti aged in 150°C at 24 hrs	82
Fig.4.4.1	SEM picture of the aged 150°C at 48 hrs and Ni <sub>4</sub> Ti <sub>3</sub>	83

	precipitation was formed along the grain boundary and inside the grains.	
Fig.4.4.2	The martensite needles of the Ni-Ti aged in 150°C at 24 hrs	84
Fig: 4.4.3	The martensite needles of the Ni-Ti aged in 150°C at 24 hrs	84
Fig: 4.5.1	Tensile stress –strain curve of the annealed 400°C in 1 hr.	85
Fig .4.5.2	Effect on temperature on tensile stress- strain curve of the Ni-Ti SMA.	86
Fig:4.5.3	Effect of ageing characteristics of the stress-strain curve of the constant ageing time (24 hrs) in Ni-Ti-Cu SMA.	88
Fig.4.5.4	Comparison,of the ageing characteristics of the Ni-Ti in different temperatures.	89
Fig: 4.5.5	Compares the stress-strain behaviour of the aged sample with as-quenched Ni-Ti SMA	90
Fig.4.5.6	Comparison of the ageing characteristics of the Ni-Ti-Cu in different ageing temperature.	91
Fig: 4.5.7	Effect of temperature on the stress-strain curve of the Ni-Ti aged in 200°C in 24 hrs Stress-strain Curve.	92
Fig.4.5.7-a	SEM study of the Ni-Ti annealed 800°C	93
Fig.4.5.7-b	SEM study of the Ni-Ti annealed 800°C	93
Fig 5.1.1	Effect of ageing time on As temperature.	97
Fig 5.1.2	Effect of ageing time on Af temperature.	97
Fig 5.1.3	Effect of ageing time on endothermic energy (J/g)	98
Fig 5.1.4	Effect of ageing time on As temperature	101
Fig 5.1.5.	Effect of ageing time on endothermic temperature.	102
Fig 5.1.6	Effect of ageing time on As and Af temperature.	102
Fig 5.1.7.	Effect of ageing time on endothermic energy consumption.	102
Fig.5.1.8.	Effect of ageing time on As and Af temperatures.	104
Fig 5.1.9.	Effect of ageing time on endothermic energy consumption.	105

### INTRODUCTION

The shape memory effect is now generally common as the phenomenon that a specimen apparently plastically deformed at martensitic condition reverts to its undeformed original shape on heating to a somewhat higher temperature virtue of the reverse martensitic transformation. This phenomenon is very interested one compared to the ordinary plastic deformation behaviour. Thus, it has been great interest for many workers of both academic and technological fields and show found a lot of alloy systems. This effort was first found in a Au-47.5 at % cal alloy by Chang and Read, and then it was published with the discovery in Ti-Ni alloys by Buhler et al. Many other alloys such as In-Tl, Cu-Zn and Cu-Al-Ni were found between the above two and thereafter. These SM alloys have another unique property called "superelasticity" (SE) at a higher temp, which is associated with large (several-18%) non-linear recoverable strain upon loading and unloading, since these alloys have a unique properties in remembering the original shape having an actuator function and having super elasticity, they are now being used for various applications such as pipe couplings, various actuators in electrical appliances, automobile applications, antennae for cellular phones and medical implants etc. Besides, since they have the function of an actuators as well as sensors they are promising candidates for mini actuarization of actuators as such a micro actuators or micro machines or robots.

Since both SME and SE are closely related to the MT, so the detailed mechanisms of the MT's are as follows. MT is a deformation (shear process) on diffusionless transformation. The total change in shape of the crystal lattice is usually assumed to be an invariants- plane strain combining a pure shear with a change in volume. The latter is probable unimportant in most SME. If, as usual, a plate of M grows with M the parent crystal that change in shape must be accommodated by strains in the untransformed crystal.

There are a small of basic phenomenon involved directly in one or more of the mechanism responsible for the various SME stress and strain- induced nucleation and stress-directed growth.

Among shape memory metals binary alloy NiTi is probable the best known system widely investigated in past years for its particular properties related to shape memory effect and pseudoelasticity. Starting from the early 80s great attention was paid to the effect of ternary addition that can increase specific functional properties.

Copper addition increases workability of the alloy reduces the dependence of the transformation temperatures on chemical composition, reduces thermal hysteresis, increases the difference between elastic moduli of the parent and martensite phase and reduces flow stress of the alloy. It has been proved that for composition in the range 3-15 wt% Cu substituted to Ni the Thermoelastic Martensitic Transformation (TMT) is present and the functional properties of the alloys are maintained.

Although the substitution of copper maintains the TME in the  $Ni_{(50-x)}Ti_{50}Cu_x$  alloys the martensite phase is different depending on Cu content. Up to about 7wt% of Cu the transformation scheme is very similar to the binary one with a cubic body centered (B2) austenitic phase transforming to a monoclinic B19' martensite. Controversial is the presence in these alloys of the R-phase with different experimental findings. For Copper content in the range 7-15wt% a different transformation scheme is found with the B2 austenitic phase transforming to an orthorhombic B19 martensite closely followed, on the temperature scale, by the transformation to the same monoclinic structure as before (B19'). Further increase of the Cu content stabilizes the orthorhombic transformation and for Cu content higher than about 15wt% there is no evidence of the transformation to the monoclinic phase.

However, the concentration limit for the existence of the cubic-orthorhombic transformation is controversial and has never been precisely settled.

## Literature Review

### 2.1 History:

The first recorded observation of the shape memory transformation was by Chang and Read. They noted the reversibility of the transformation in Au-Cd by metallographic observation and resistivity changes, and in 1951 the shape memory effect (SME) was observed in a bent bar of Au-Cd. In 1938, the transformation was seen in brass (Cu-Zn). However, it was not until 1962 [1], when Buehler and co workers discovered the effect in equiatomic Ni-Ti, that research into the both metallurgy and potential practical uses in began in earnest. Study of shape memory alloys has continued at an increasing pace then, and more products using these materials are coming to the market each year. As the shape memory effect became better understood, a number other alloy systems that exhibited shape memory was investigated. Of all these systems, the Ni-Ti alloys, a few of the Cu base alloys and Fe based alloys have received the most development effort and Commercial exploitation.

The term shape memory alloy (SMA) is applied to that group of metallic materials that demonstrates the ability to return to some previously defined shape or size when subjected to the appropriate thermal procedure. Generally, these materials can be plastically deformed at some relatively low temperature, and upon exposure to higher temperature will return to their original shape prior to the deformation materials that exhibit shape memory only upon heating are referred to as having one-way shape memory. Some materials also undergo a change in shape upon re cooling. These materials have a two way shape memory. Although a relatively wide variety of alloys are known to be exhibit the shape memory effect, only those that can recover substantial amount of strain or that generate significant force upon changing shape are commercially interest. To date, this has been nickel titanium alloys and copper based on alloys such as Cu-Zn-Al and Cu-Al-Ni and iron based shape memory alloys such as Fe-Mn, Fe-Ni based alloys.

A shape memory alloy is further defined as one that yields a thermo elastic martensite. A detailed mechanism of the shape memory effect in crystal structure was



shown in Fig 1.1. In this case, the alloy undergoes Martensite transformation of a type that allows the alloy to be deformed by a twinning mechanism below the transformation temperature. The deformation is then reversed when twinned structure is reversed when upon heating to the parent phase.

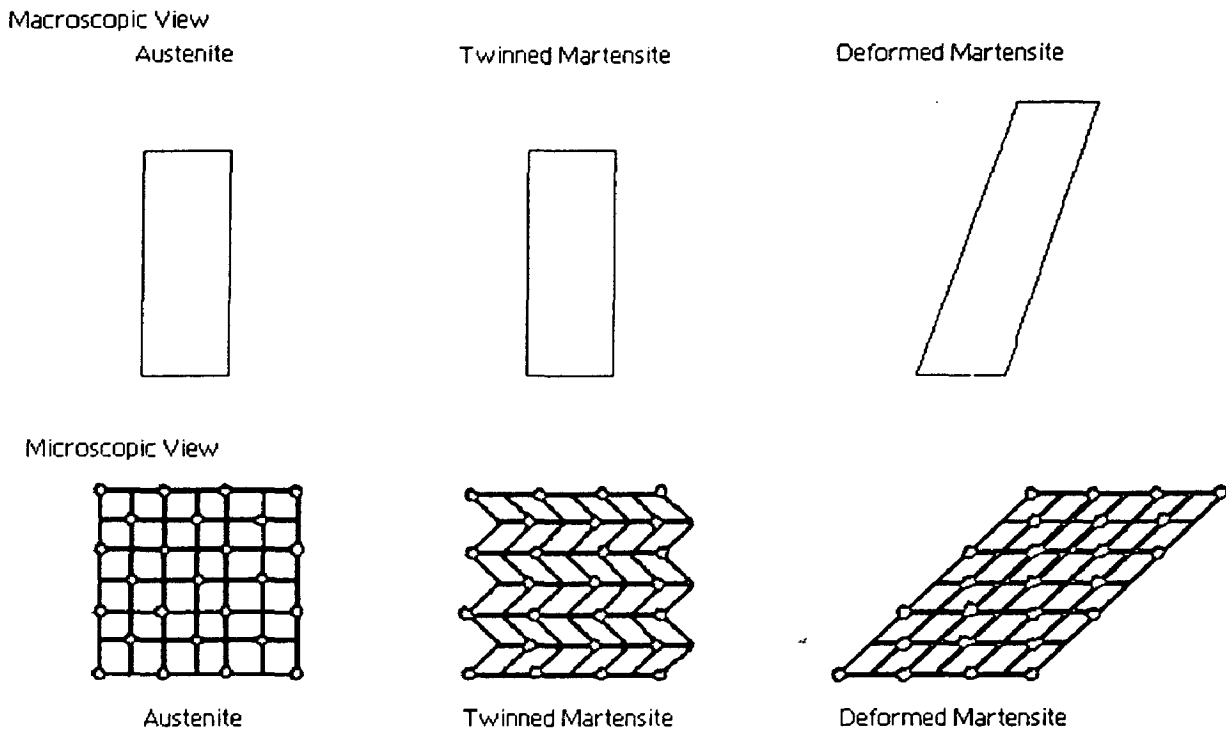


**Fig 2.1.the detailed mechanism of the SME.**

## 2.2 Two major modes of the shape Memory Effect:

There are two important shear transforms are there, these are directly associated with shape memory characteristics.

1. Martensite transformation
2. Twinning transformation

### 2.2.1 Martensite transformation:

When the temperature of a metal capable of undergoing a martensite reaction is lowered, it eventually passes through an equilibrium temperature separating the stability ranges of two different phases. Below this temperature, the free energy of the metal is lowered if the metal changes its phase from that stable high temperatures to that stable at

low temperatures. The free-energy difference is the primary driving force for a martensite reaction [2].

The phase change that occurs in a Martensite transformation is brought about by the movement of the interface separating parent phase from the product phase. As the interface moves, atoms in the lattice structure of the parent phase are realigned in to the lattice phase of the Martensite phase. The nature of the individual atomic movements in the region constituting the interface is not known, just as they are not known in deformation twinning. Nevertheless, it is undoubtedly true that displacement of atoms, Relative to their neighbors, is small in magnitude and probably more complicated than those in deformation twinning. Because of the manner in which Martensite forms, no composition change occurs as the parent lattice is converted to the product phase and diffusion in either the parent phase or product phase is not required for the reaction to continue. Martensite reactions are, accordingly, commonly referred to as diffusionless phase transformation.

The atomic realignments associated with martensite reactions produce shape change deformations just as they do in mechanical twinning. Because the new lattice which is formed has symmetry different from that of the parent phase, the deformation is, of necessity, more complicated. In mechanical twinning distortion is simple shear parallel to the twinning plane or the symmetry plane between twin and parent crystal. The twinning plane is undistorted plane; all the directions in this plane are unchanged by twinning with respect to both their magnitudes and their angular separations. The habit plane or plane on which a martensite plates form is also usually assumed to be an undistorted plane. The macroscopic shear deformation in the formation of a martensite plate is believed to be a shear parallel to the habit plane plus a simple uniaxial tensile or compressive strain perpendicular to the habit plane. A strain of this nature, known invariance of the habit plane. Neither a shear parallel to the habit plane, nor an extensions or contraction perpendicular to it will change the positions or magnitudes of vectors lying in the habit plane.

System	Phase change	Habit plane	Shear direction	Shear component of strain	Normal component of strain
Fe- 30%Ni	FCC to BCC	(9,23,33)	[156]	0.2	0.05
Fe-C (1.35%)	Bcc to fcc				
Fe-22 %Ni- 0.8%C	Fcc to bct	(3,10,15)	[132]	0.19	0.09
Pure Ti	Bcc to hcp	(8,9,12)	[111]	0.19	
Ti-11% Mo	Bcc to hcp	4 from [344] 4 from (8,9,12)	[147]	0.28-0.05	
Au-47.5% Cd)	[0.696.- 0.686,0.213]	[0.660,0.729,0.183]	0.05		
In-Tl(18- 20% Tl)	Fcc to fct	[0.013,0.993,1]	[011]	0.024	

**Table-1** Data showing magnitude of the shear and normal components of the invariant plane strains associated with martensite reactions are difficult to measure and relatively scarce.

### Stabilization:

The phenomenon of stabilization is also observed in iron-nickel alloys. The mechanism differs from that observed in the indium-thallium alloy, but the effect is the same; isothermal holding of the specimens at a temperature between  $M_s$  and  $M_f$  stabilizes the transformation so that additional supercooling is required in order to start the transformation again [3]. In the indium-thallium specimens, stabilization occurs as a result of a retardation of the movement of the interface, where as in the iron-nickel alloy, Stabilization is manifested by an increased difficulty in the nucleation of additional plates. In order for the reaction to continue, an additional increment of driving force is needed to nucleate more plates. Stabilization is also observed during the reverse transformation when martensite is reacted to form austenite.

### **The nucleation of martensite plates**

The nucleation of martensite plates is a subject of great interest and also of considerable controversy. The available experimental evidence factors the belief that martensite nuclei form heterogeneously, as is the case with nucleation in most other transformations, or changes of phases. The evidence is also strong for the assumption that the locations at which nuclei form are internal positions of high strain (dislocation configurations), commonly called strain embryos. No simple theory of martensite nucleation is yet available. This is probably due to the fact that martensite can form under two extremely different sets of conditions. First, it can form athermally, which means that it can form in a very small fraction of a second provided the temperature is lowered sufficiently to activate those nuclei which will respond in this manner. This type of nucleation apparently does not need thermal activation. The ability of martensite to form without the aid of thermal energy is also demonstrated by the fact that where the energy of thermal vibrations is vanishingly small. On the other hand, martensite is also capable of forming at constant temperature. The fact that, in this case it has a nucleation rate which is time dependent shows that thermal energy can also be a factor in the nucleation of martensite.

### **The Effect of Stress**

Because the formation of martensite plates involves a change of shape in a finite volume of matter, applied stress can influence the reaction. This is entirely analogous to the formation of deformation twins by stress. However, the formation of a martensite stress is more complicated than in the case of twinning. Nevertheless, theoretical predictions of the effect of various stress patterns on the formation of martensite have been found to agree quite well with experiment. We shall not discuss this theory in detail, but it is important to note that the  $M_s$  Temperature can be either raised or lowered as a result of applied stresses. This may be understood in terms of the following, perhaps oversimplified picture. Then if the sense of an applied shear stress is the same as the strain, the stress should aid the formation of the plate. A lower driving force for the reaction is to be expected and  $M_s$  should be raised. Similarly, if the shear-stress vector is reversed, the plate forms should be lowered. It is important to note that, in respect to this latter, a simple applied shear stress may not necessarily lower  $M_s$  because of the multiplicity of the habit planes on which

martensite can form. While; the indicated plate might not be favorably oriented to the stress, it is quite probable that there is other plate Orientations in the crystal that are [4].

**The effect of plastic deformation:**

Plastic deformation of the matrix also has an effect on the formation of martensite which is primarily to increase the sizes of internal strains and make the nucleation of martensite easier. As a result, martensite can form when the metal is plastically deformed at temperatures well above the  $M_s$  Temperature. The amount of martensite thus formed decreases, however, as the temperature is raised, and it is common practice to designate the highest temperature at which martensite may be formed by deformation as the  $M_d$  temperature. In reversible martensitic transformations, plastic deformation usually has a similar effect on the reverse transformation. The temperature at which the reverse Transformation starts is lowered by plastic deformation. The plastic deformation brings the start of the forward and reverse transformations much closer together-within approximately 100°C. The corresponding difference between  $M_s$  and  $A_s$  is 420°C.

**Twinning**

Deformation or mechanical twinning is a mode of plastic deformation while the other, Comprising martensite reactions, is a basic type of phase transformation. Twinning like slip, occurs as the result of applied stress. Sometimes may be influential in partly triggering a martensite transformation. But this is an effect of secondary importance. Martensite reactions occur in metals that undergo phase transformations, and the driving force for a martensite reaction is the chemical free energy difference between the two phases [5].

The similarity between the martensite reactions and twinning lies in the analogous way twins and martensite crystals form in both cases, the atoms inside finite crystalline volumes of the parent phase are aligned as new crystals, lattice. In twins this realignment reproduces the original crystal lattices. In twins this realignment reproduces the original crystal structure, but with new orientation. In a martensite plate, not only is a new orientation produced, but also a basically different crystalline structure. Thus, when martensite forms in steel quickly cooled to room temperature, the face centered cubic phase, which is stable at elevated temperatures, is converted into small crystalline units of a body-centered tetragonal phase. On the other hand, when twinning occurs in a metal such

as zinc, both the parent crystal and the twinned volumes still have the close-packed hexagonal structure. In both twinning and martensite transformations, each realigned volume of material suffers a change in shape which distorts the surrounding matrix. The changes in shape are quite similar. So that martensitic plates and deformation twins look alike, taking the form of small lenses or plates. The deformation accompanying mechanical twinning is simpler than that associated with martensitic reactions. This is because there is no change in crystal, merely a reorientation of the lattice. The change of shape associated with the deformation twinning is a simple shear. The sheared section still has the crystal structure and symmetry to the original crystal structure.

### **2.3 Types of Shape memory effects:**

A great many different terms have been used in conjunction with the priority anomalies referred to in the following.

#### **2.3.1 Single way shape memory effect (SWSME):**

A material apparently plastically deformed at a suitable temperature recovers, fully or partially, its origin shape on subsequent heating to a moderately higher temperature. Strains of the order of up to 8 – 10% can be thus fully recovered, the magnitude of the recoverable strain varying with the grain size texture, and the conditions under which the strain is effected. Subsequent cooling to the temperature at which deformation took place does not restore the specimen to its deformation configuration. It should be noted that a complete shape recovery has been usually implied in most of the prior work. In fact full recovery is seldom experimentally attained. In the discussion to follow we shall concentrate on the ideal, full recovery conditions, but we shall also consider the reason why these are seldom realized, and why a partial shape recovery is more generally observed.

#### **2.3.2 Two Way Shape Memory Effect (TWSME):**

Under suitable prior plastic deformation conditions in either the martensite or the parent structures a “reversible” expansion or contraction may be developed to accompany the forward transformation [7]; and a change of equal magnitude but opposite in sense will then be present in the reverse transformation. Typically the magnitude of this effect is a factor of 5- 10 lower than that attainable in the “irreversible” SME, and amounts to a dimensional change of the order of 1%.

### 2.3.3 Super elasticity:

A material deformed well past its apparent yield point fully recovers its initial shape on removing the load. A significant stress-strain hysteresis, indicative of energy absorption in the lattice, is usually observed. This behavior is due to stress-assisted martensite formation during loading, this martensite being thermally unstable except under stress. Thus unloading is accompanied by reversion to the initial structure (orientation). The temperature range within which this can be observed is  $A_f < T < M_f$  [8].

### 2.3.4 Ferro elasticity:

A stress-strain behavior undistinguished from superelasticity but occurring in material stressed while fully martensitic condition [9]. It has been frequently observed to involve a stress-assisted growth of martensite lamellae of one orientation at the expense of similar lamella of another orientation, widely interpreted as a reversible stress-assisted double transformation, within the temperature range  $A_d < T < M_r$ .

### 2.3.5 Interfacial structure and the shape memory effect:

In general martensite transformation is characterized by rapid propagation of a highly mobile interface with consecutive co-ordinate atom movements from the parent phase to product phase. In some cases uncoordinated diffusive displacements of atoms, particularly interstitials can accompany transformation or occur afterwards, but co-ordinate atom transfer is a defining feature of martensite transformation which establishes the reproducible crystallographic and geometric relationships between the parent and product phases [10]. This theory identifies the macroscopic shape change accompanying the formation of a martensite plate as an invariant plane strain  $P_1$ , with the habit plane as the invariant plane i.e. one in which macroscopic vectors are neither rotated nor changed in length by the transformation.  $P_1$  is equated to the product of the homogeneous lattice strain  $S$  which converts atoms in the parent into the product structure and orientation, and a lattice invariant shear  $P_2$  which allows the undistorted habit plane to be established. The basic matrix equation of the theory is  $P_1 = S P_2^{-1}$ . Despite the fact that

crystallographic theory only provide frame work for a mechanism, the basis of strain minimization at the macroscopic interface is of central importance to the atomic paths and extension of this principle to the fine interfacial structure yields insights into the micromechanics of transformation.

### **2.3.6 Shape Memory Martensite:**

The growth in the number of reported “shape memory alloys’ over recent decades has increased the clarity of definition of general characteristic which lead to shape memory behaviour. The single necessary and sufficient condition is Crystallographically reversible martensite phase Transformation. Martensite crystals which form from the parent crystal (by cooling and /or stress) must capable of transforming back to the original parent crystal in the original orientation on stress removal, with or without heating. The requirement of heating relates to shape memory and reversibility on stress removal applies to super elasticity. Crystallographically reversible transformation is consistent with thermoelastic transformation, but it also encompasses transformations which have a relatively large thermal hysteresis or are capable of only partial shape memory. Such transformations are clearly not thermoelastic. Prime examples, are the transformations in Ni-Ti alloys, Fe-Ni-C and partially ordered Fe<sub>3</sub>Pt. The capacity of Martensite Transformation to exhibit reversible behavior obviously depends on the maintenance of an interface capable of reversible motion and the capacity of atoms to move reversibly between sites in the two structures.

### **2.3.7 Interfacial characteristics:**

The habit (interface) plane is usually one of the three types:

- a) Planar, irrational and semi-coherent, separating a single crystal parent from a slipped and or faulted single crystal product:
- b) Planar, irrational and separating a single crystal parent from a twinned product;
- c) Curved and thus macroscopically displaced from the “true” habit plane, because of interfacial steps.

The interface plane is highly mobile, at least for the forward transformation, and it is implied that either

- i) planar sections mitigated as a unit (consisting of twin-parent volumes or a surface dislocation); or



ii) Steps consecutively sweep across the whole interface. The interface propagates of the order of the 1 km/sec. The high speed of propagation has led to the description of the interface motion as glissile, implying frictionless movement, but this is ideal condition which is approached to various degrees depending on the alloy and its conditioning. In an ideal glissile system unhindered interface motion should occur in both directions giving a completely reversible transformation.

A high degree of coherency is also implied, although in many cases the interface has been identified as semi coherent, consisting of a net of misfit dislocations which glide in both lattices. These dislocations are referred to as transformation dislocations or "anticoherency" dislocations in the terminology used by Olson and Cohen. These characteristics are general, but may not be sustained for reverse transformation as the temperature is raised. For some transformations, notably in Ni-Ti SMA and Plain carbon steels, initial glissile motion gives way to a sessile interface as an interfacial registry is disrupted by dislocations generated in either or both of the parent and martensite phases as a result of plastic accommodations of transformation strains. In addition, the interface can be immobilized by solute atoms or precipitate locking. For reversible transformation, the glissile motion and the interfacial registry are maintained, at least partially. Highly reversible transformations are exhibited by Ni-Ti, ordered Fe<sub>3</sub>Pt, and Cu-Zn-Al and Cu-Al-Ni alloys, implying good interface matching and the relative absence of plastic accommodation. Small transformation hysteresis are typical in these cases and complete transformations showing more limited reversibility, accumulation of plastic strain restricts the transformations showing more limited reversibility can occur over hundreds or thousands of cycles. For transformations showing more limited reversibility, accumulations of plastic strain restricts the number of reverse transformation cycles and /or the extent of reversibility. Interfacial friction arising from interaction with accommodation dislocations leads to a wide transformation hysteresis [11].

The term thermoelastic transformation is widely used to describe transformations with low hysteresis on stress or thermal cycling, but the essential feature is a glissile interface which can move freely both in the forward and reverse directions in response to changes in temperature or stress. In alloys which show shape memory, pseudo elasticity or rubber like behavior, this interface reversibility can be between martensite and parent, or between

twins or domains within the martensite and the martensite matrix. The characteristic feature of low friction (glissile) interface motion, at least for the forward transformations, draw attention to the nature of the interface structure which permits this behavior. Two of the striking characteristics of shape memory alloys are the existence of parent phase order and the presence of fine twinning or faulting as the lattice invariant shear, with twinning being the dominant mode.

### **2.3.8 Interfacial structure and strain accommodation:**

Many martensite plate products are fully twinned, with the twin interface boundary making a large angle with the macroscopic habit plane between the single crystal parent and the martensite plate. There are limited data on the nature of the terminating interfaces of the twin volumes, but in principle the two interface planes could be any pair of planes in the zone of the invariant line which averaged out, produce the observed macroscopic invariant plane. Different concept has been invoked to describe and/or predict these interface planes. In the simplest model, proposed by Christian, the twins can be considered to be a forced elastic coherence across the interface plane with the parent phase only interfacial discontinuity being the parallel array of intersections of the twin boundary and the habit plane (the invariant plane). For an appropriate twin ratio the hysteresis strain fields of adjacent twins cancel at distances of the order of the spacing of the twin pairs. The spacing of the twin pairs equivalent to the spacing of transformation (anti coherence) dislocations in the interface of a single crystal martensite plate.

### **2.3.9 Mechanical Properties of Shape memory alloy:**

In the last few years there have been large numbers of papers published on alloy systems which show stress martensite transformation. The main reason for the interest in these systems is their unusual mechanical especially the pseudo elasticity effect and strain memory effect (SME). All alloys which show pseudo elasticity and SME undergo reversible martensite transformation with related temperature hysteresis. These alloys are generally Beta intermetallic compounds in the Cu, Ag, Au, Ni -base alloys. Most of these systems both the matrix and martensite structures are ordered and the martensite has a twinned structure. The unusual effect of the  $\beta$ -Phase alloy was first discovered in Au-Cd by

expected since in single crystals only one martensite variant need form whilst in polycrystals, several variants (generally 5) must form in different regions of any given grain to allow for the effects of constraints due to the presence of the grain boundaries produce non-reversible deformation martensite and prevent full development of the pseudo elastic effect.

### 2.3.13 Strain memory effect:

The strain memory effect can most easily be discussed by considering a specimen having the structure of the matrix phase at a temperature close to the  $M_s$  where the martensite once formed is thermodynamically stable or metastable on stressing the matrix phase, SIM will nucleate, the particular variant or variants which form presumably being those for which the resolved shear stress in the habit plane and in the shear direction is a maximum. On release of stress, martensite won't revert back to the matrix phase since it is metastable and so there is little recovery in the dimensions of the specimen which is shown in fig.1.3 on heating, however, the martensite becomes unstable and between  $A_s$  and  $A_f$  it progressively reverts back to the matrix phase, causing the specimen to recover its original dimensions. The amount of recovery which can be obtained corresponds to the strain for complete transformation of the matrix phase to the martensite with the most favored orientation. This equals the maximum strain for pseudo elastic transformation

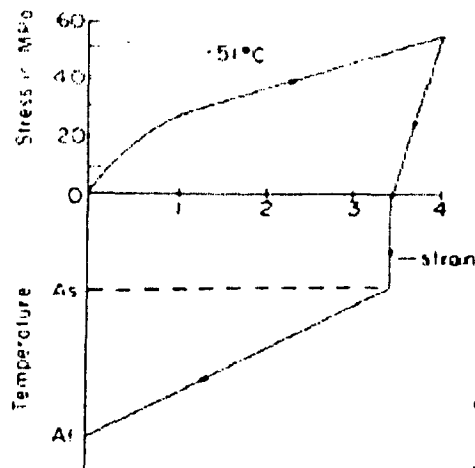


Fig- 2.3 Stress-strain curve.

Fig- 2.3 Stress-strain curve alloy deformed at the  $M_s$  Temperature together with a schematic curve showing the memory recovery of the alloy on heating [15].

twins or domains within the martensite and the martensite matrix. The characteristic feature of low friction (glissile) interface motion, at least for the forward transformations, draw attention to the nature of the interface structure which permits this behavior. Two of the striking characteristics of shape memory alloys are the existence of parent phase order and the presence of fine twinning or faulting as the lattice invariant shear, with twinning being the dominant mode.

### **2.3.8 Interfacial structure and strain accommodation:**

Many martensite plate products are fully twinned, with the twin interface boundary making a large angle with the macroscopic habit plane between the single crystal parent and the martensite plate. There are limited data on the nature of the terminating interfaces of the twin volumes, but in principle the two interface planes could be any pair of planes in the zone of the invariant line which averaged out, produce the observed macroscopic invariant plane. Different concept has been invoked to describe and/or predict these interface planes. In the simplest model, proposed by Christian, the twins can be considered to be a forced elastic coherence across the interface plane with the parent phase only interfacial discontinuity being the parallel array of intersections of the twin boundary and the habit plane (the invariant plane). For an appropriate twin ratio the hysteresis strain fields of adjacent twins cancel at distances of the order of the spacing of the twin pairs. The spacing of the twin pairs equivalent to the spacing of transformation (anti coherence) dislocations in the interface of a single crystal martensite plate.

### **2.3.9 Mechanical Properties of Shape memory alloy:**

In the last few years there have been large numbers of papers published on alloy systems which show stress martensite transformation. The main reason for the interest in these systems is their unusual mechanical especially the pseudo elasticity effect and strain memory effect (SME). All alloys which show pseudo elasticity and SME undergo reversible martensite transformation with related temperature hysteresis. These alloys are generally Beta intermetallic compounds in the Cu, Ag, Au, Ni -base alloys. Most of these systems both the matrix and martensite structures are ordered and the martensite has a twinned structure. The unusual effect of the  $\beta$ -Phase alloy was first discovered in Au-Cd by

---

chang and reading 1951 and in In-Tl by Burkhart ND Read in 1953. Interest in this field waned until the work of Buhler and associates on Ni-Ti in 1968.

### 2.3.10 Pseudoelasticity:

Pseudo elasticity occurs when SIM transformation can be produced in a range of temperature the SIM becomes unstable when unloaded. In this case the transformation strain obtained during loading is on unloading when SIM reverts back to the matrix phase [13]. A typical single crystal tensile curve illustrating pseudo elasticity is shown in Fig. 4 It can be recoverable strains of greater than 7% can be obtained, compared with less than 0.5 5 for the best co materials .The portion up to point A represents elastic deformation of the matrix. At A, SIM starts to form a to B the specimen progressively transforms to martensite specimen strained beyond point B would such deformation, depending on the alloy system. On unloading there is elastic recovery of the martensite up followed by a progressive reversion of the martensite to the matrix phase between C and D and finally recovery matrix phase. It's found that the sequence of martensite formation, with first martensite plate to form martensite plate to disappear.

Most of the recoverable strain in fig 4 is associated with the reversible martensite formation and is due to the macroscopic shear strain caused by the transformation. The magnitude of the pseudo elastic strain in tensile, compressive, shear loading can be calculated from knowledge of the habit plane of the martensite and the magnitude of the shear strain for the transformation. It has been found experimentally that the martensite variant which forms on stressing one of which the resolved shear stress of the applied stress in the habit plane and n the shear direction is a maximum. Since habit 13 plane of then martensite is irrational ,there I s the choice of the 24 possible planes and so there is always one fairly closely oriented with respect to the planar of the maximum shear.

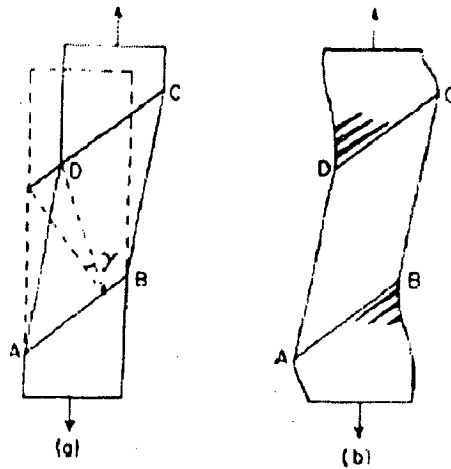


**Fig. 2.2 Partial transformation from the matrix phase to martensite.**

Fig. 2.2 Schematic diagram showing partial transformation from the matrix phase to martensite. In (a) lateral displacement of the specimen is permitted, whilst in (b) the specimen is held in position by the specimen grips.

### 2.3.11 Effect of strain rate:

The shape of the pseudo-elastic stress strain curve depends on the rate of Strain the specimen. This is due to significant temperature changes which take place in the specimen at high strain rates. These temperature changes are associated with heat of transformation ( $\Delta H$ ), there being a temperature increase during parent martensite transformation and a temperature decreasing during reverse transformation.

The maximum temperature changes in the specimen are given by  $\delta T = (\Delta H)/c$  where  $c$  is the specific heat of the martensite for the forward transformation or the specific heat of the martensite for the reverse transformation. In Cu-Al -Ni this works out to  $12^{\circ}\text{C}$ , in good agreement with the measured temperature changes at high strain rates. At lower strain rates the measured temperature increases is smaller since there's more time available for heat to be conducted away from the specimen.

### 2.3.12 Effect of grain size:

It has been established that large number of investigations that polycrystalline specimens have inferior pseudo elastic properties compared with single Crystals [14]. This is to be

expected since in single crystals only one martensite variant need form whilst in polycrystals, several variants (generally 5) must form in different regions of any given grain to allow for the effects of constraints due to the presence of the grain boundaries produce non-reversible deformation martensite and prevent full development of the pseudo elastic effect.

### 2.3.13 Strain memory effect:

The strain memory effect can most easily be discussed by considering a specimen having the structure of the matrix phase at a temperature close to the  $M_s$  where the martensite once formed is thermodynamically stable or metastable on stressing the matrix phase, SIM will nucleate, the particular variant or variants which form presumably being those for which the resolved shear stress in the habit plane and in the shear direction is a maximum. On release of stress, martensite won't revert back to the matrix phase since it is metastable and so there is little recovery in the dimensions of the specimen which is shown in fig.1.3 on heating, however, the martensite becomes unstable and between  $A_s$  and  $A_f$  it progressively reverts back to the matrix phase, causing the specimen to recover its original dimensions. The amount of recovery which can be obtained corresponds to the strain for complete transformation of the matrix phase to the martensite with the most favored orientation. This equals the maximum strain for pseudo elastic transformation

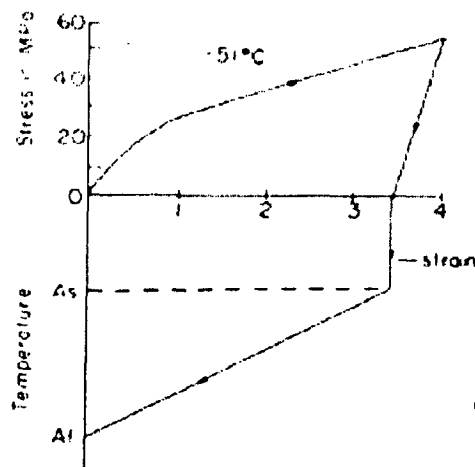


Fig- 2.3 Stress-strain curve.

Fig- 2.3 Stress-strain curve alloy deformed at the  $M_s$  Temperature together with a schematic curve showing the memory recovery of the alloy on heating [15].

### **2.3.14 Reversible strain memory effect:**

In the reversible strain memory effect, a specimen whose temperature is cycled between the martensite and parent phases shows a reversed dimensional change on both heating and cooling. Normally when a specimen is cooled through the martensite transition temperature, it shows no dimensional changes. This is because a large number of variants form in thermal martensite and any dimensional changes associated with one variant is cancelled out by opposite changes from other variants.

In the reversible strain memory effect, preferred growth favored variant occurs and this causes the preferred growth of a favored variant occurs and this causes the Dimensional change on cooling. Growth of the favored variant can occur either by cooling under the stress or by prior plastic deformation.

### **2.3.15 Fatigue properties:**

No systematic study of the fatigue properties of the Pseudo elastic behavior studied up to now. But Buehler, for example, found the fatigue life of Ni-Ti to be greater than  $10^7$  cycles at a stress level of 480 MPa. A study has just been completed of the fatigue properties of Cu-Al-Ni single studies. Specimens were cycled from zero stress to a fixed strain, and the fatigue life was found as a function of strain magnitude, temperature (relative to  $M_s$ ) and crystal orientation. The fatigue life was surprisingly short, and this means that the use of these alloys in cyclic applications is severely restricted [16].

### **2.3.16 internal friction:**

An important property of the pseudo elastic alloys is their high damping capacity at the temperatures below  $M_s$ . This makes them of potential value for sound damping and attenuation of vibrations. There is a sudden decrease in damping capacity as the temperature is raised above  $A_s$  and it is obvious that the high damping capacity is due to the martensite structure. This is easily demonstrated by comparing the resonant sound on striking a pseudo elastic metal at a temperature above  $A_s$  with dull sound obtained at lower temperatures. These alloys have good damping capacity over wide range ( $100^\circ\text{C}$ ) and as many be seen in Fig. they are much better than grey cast iron in this application [17].



The internal friction appears to have a maximum at temperatures some what below  $M_s$  and hence is associated with the structure of martensite rather than with the transformation to martensite. The main energy losses appear to be due to friction associated with reversible movement of the martensite boundaries.

## 2.4 Aging Characteristics of the Ni-Ti and Ni-Ti-Cu SMA:

In near equiatomic Ti-Ni alloy ,the shape memory effect and transformation pseudo elasticity occur in association with the thermoelastic martensitic transformation from the parent phase (beta) with a B2 structure to the phase with a monoclinic B19' structure , or more often in association with the two step transformation from the beta to a trigonal phase (so called R-phase) and then to the fine structure of the parent beta phase.

Therefore, factors such as Ni content, aging, thermal cycling treatment which affect the structure are important for controlling the memory behavior.

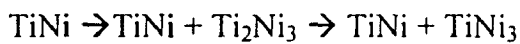
### 2.4.1 Decomposition of near-equiatomic B2 phase of Ti-Ni alloy:

Ti-Ni alloys with nickel contents exceeding 50.5 at % decompose on cooling slowly from a high temperature or on aging at a temperature below 973 K (700°C) after quenching from a high temperature [18].

a) Ageing at temperature below 953 K(680°C)



b) Ageing at temperature between 953 K and 1023 K (750°C)



c) Ageing at temperature between 1023 K and 1073 K (800°C)



In any of the three temperature ranges the final products of decomposition is a mixture of  $\text{TiNi}_3$  and  $\text{TiNi}$ . The  $\text{Ti}_3\text{Ni}_4$  and  $\text{Ti}_2\text{Ni}_3$  phase are metastable. In the range (a), the three phase  $\text{Ti}_3\text{Ni}_4$ ,  $\text{Ti}_2\text{Ni}_3$  and  $\text{TiNi}_3$  appear in this sequence, which is the order of increasing nickel content of the product phases. In the range (b), only the  $\text{Ti}_2\text{Ni}_3$  phase appears before the  $\text{TiNi}_3$  appears, and in the range (c) the  $\text{TiNi}_3$  forms directly from the initial  $\text{TiNi}$ .

The  $\text{Ti}_3\text{Ni}_4$  phase forms in the early stages of aging at low temperatures as fine platelets with coherency to the matrix and affects the properties of the Ti-Ni alloys. The  $\text{Ti}_3\text{Ni}_4$  phase has a rhombohedral structure.

The  $\text{Ti}_2\text{Ni}_3$  phase which has been interpreted to be a product of a peritectoid reaction ( $\text{TiNi} + \text{TiNi}_3 \rightarrow \text{Ti}_2\text{Ni}_3$ ) is now understood to form as an intermediate phase prior to the formation of the final product,  $\text{TiNi}_3$ . The eutectoid reaction ( $\text{TiNi} + \text{TiNi}_3 \rightarrow \text{Ti}_2\text{Ni}_3$ ) which was once proposed 36.8 at % does not exist. It appears that  $\text{Ti}_4\text{Ni}_2$  was misinterpreted as  $\text{Ti}_2\text{Ni}$  since these two phases are similar in structure. The  $\text{Ti}_4\text{Ni}_2$  oxide forms easily and is commonly observed in Ti-Ni alloys.

It is known that near equiatomic Ni-Ti shape memory alloys exhibit three different phases, the  $B_2$  phase, which has a CsCl structure, the  $B19'$  phase, which is monoclinic, and the R-phase (R), which is rhombohedral. The  $B_2$  phase is often referred to as the austenite (A) whereas the  $B19'$  phase is referred to as the martensite (M). Among these phases three transformations are possible, the  $B_2 \leftrightarrow$  monoclinic transformation ( $B_2 \leftrightarrow M$ ), the  $B_2 \leftrightarrow$  rhombohedral transformation ( $B_2 \leftrightarrow R$ ) and the rhombohedral  $\leftrightarrow$  monoclinic transformation ( $R \leftrightarrow M$ ). All three transformations involve lattice distortions and are martensitic in nature. Consequently, the transformations are sensitive to variations in metallurgical and mechanical conditions as well as chemical composition. Therefore, under different pretreatment and testing conditions, with the interplay of transformation hysteresis, various combinations of these transformations have been observed.

Among the three transformations, the  $B_2 \leftrightarrow M$  and  $R \leftrightarrow M$  transformations are characterized by large lattice distortions and large transformation hysteresis. Due to the

large lattice distortions, these transformations introduce structural defects to the microstructure during the processes and, at the same time, are sensitive to influences of structural defects. Therefore, these transformations have relatively low thermal and mechanical stability for their functional properties. In contrast, the  $B2 \leftrightarrow R$  transformation is characterized by a small lattice distortion and a small temperature hysteresis. The small lattice distortion implies less damage to the microstructure during transformation and lower sensitivity to structural modifications, hence higher reversibility and higher property stability. The small thermal hysteresis implies high response rate and high reversibility. Owing to these unique advantages, the R-phase transformation is of particular importance for many applications, such as actuators and sensors [ 19].

The study of the R-phase transformation began with the identification of the phase by Honma et al. in 1972 [20]. since then many studies have been carried out to characterize its behaviour [21–28]. In fully annealed binary near-equiatomic Ti–Ni alloys, usually only the  $B2 \leftrightarrow M$  transformation is observed. The  $B2 \leftrightarrow R$  transformation can be introduced by many different ways. Addition of third elements, such as Fe and Al [29, 30], is effective in suppressing the  $B2 \leftrightarrow M$  transformation to lower temperatures to reveal the  $B2 \leftrightarrow R$  transformation. For binary near-equiatomic Ti–Ni alloys (Ni<50.4 at.% practically), cold working [22], partial annealing after cold work [19] and thermal cycling [18-20] have been found to cause the appearance of the  $B2 \leftrightarrow R$  transformation prior to the  $B_2 \leftrightarrow M$  transformation. For Ni-rich Ti–Ni alloys (Ni>50.5at.% practically), ageing after solution treatment causes the R-phase transformation [19]. A good account on factors affecting the R-phase transformation for earlier studies is given in reference [29]. Among these various means, ageing treatment for Ni-rich Ti–Ni alloys is found to be the most versatile method, since it can be applied to pre-shaped components and the characteristics of the R-phase transformation can be adjusted within certain range by controlling ageing conditions. Commercial Ni-rich Ti–Ni alloys are usually aged at above 700°K for relatively short times for optimum pseudoelasticity. Under this condition they usually exhibit transformation behaviour involving  $B2 \leftrightarrow R \leftrightarrow M$  on cooling and  $M \leftrightarrow B2$  or  $M \leftrightarrow R \leftrightarrow B2$  on heating. In some recent years, however, some complex transformation behaviours have been reported in the literature.

Zhu and Gotthardt first reported an internal frictional measurement of a two-stage martensitic transformation following a single-stage R-phase transformation on cooling in a Ti-51at.%Ni alloy after ageing at 773°K[30].

Favier et al. reported the first DSC measurement of a similar transformation behaviour in a Ti-50.2at.%Ni and proposed that the peculiar transformation behaviour was related to the formation of precipitates [31].

In parallel, Stroz et al. reported similar two-stage martensitic transformation behaviour induced by partial annealing after cold working, and proposed a mechanism based on consideration of stress fields associated with dislocations [32].

Since then a number of investigations have been reported on the phenomena, with three particularly devoted to the discussion of possible mechanisms responsible for ageing-induced multiple-stage transformation behaviour.

Bataillard et al. [33] reported on a TEM in situ investigation of the transformation behaviour of a Ti-51at. %Ni. They observed at TEM scale two discrete steps of martensite formation from the R-phase in regions near  $Ti_3Ni_4$  precipitates, corresponding to “stressed” and “unstressed” regions. Based on this observation they proposed a mechanism for the multiple stage martensitic transformation behaviour based on stress relaxation considerations. They proposed a mechanism based on a scenario that martensite forms in a “burst” manner once nucleated whereas the R-phase forms in a normal thermoelastic manner, in conjunction with a consideration of composition distribution caused by precipitation, but without any experimental evidence to support the claim. This hypothesis explicitly requires the martensite to nucleate with an under cooling at  $M_s$ , a finite temperature below the thermodynamic equilibrium temperature  $T_0$  between the  $B_2$  and the martensite, and to propagate with zero under cooling at  $T_0$ . Such scenario depicts a condition of system instability and violates the basic thermodynamic requirement for a thermoelastic martensitic transformation, which specifies a continuous equilibrium with a continuously increasing driving force for the transformation. Shortly after, the same group proposed another explanation based on TEM evidence of inhomogeneous distribution of  $Ti_3Ni_4$  precipitates], dividing the matrix into two spatially distinctive regions: grain boundary regions where  $Ti_3Ni_4$  precipitates concentrate and grain interior regions which relatively precipitate free. Whereas proving logical reasoning of the discrete steps of

transformations, this hypothesis is unable to explain the observations of similar ageing-induced multiple-stage transformation in specimens where the distribution of  $Ti_3Ni_4$  precipitates is uniform [34] or where there is no obvious  $Ti_3Ni_4$  precipitates. In Conclusion, whereas there is a common acceptance that ageing-induced multiple-stage transformation behaviour is related to the formation of Ni-rich precipitates, no convincing explanations to the mechanisms have been established. The lack of experimental evidences largely contributes to the absence of such an understanding.

This dissertation work intends to present new experimental evidence of a comprehensive investigation of the effects of low temperature ageing on the transformation behaviour of a Ti-50.9Ni alloy. Up to date, experimental evidences reported in the literature are exclusive of the transformation behaviour involving multiple-stage martensitic transformation and single-stage R-phase transformation. This paper presents the first comprehensive study of ageing-induced multiple-stage R-phase transformation. Such an investigation is also of practical importance. The ageing temperatures investigated in this study is in the range of 473–573°K, some 100–200°K Below the conventional ageing temperature range of Ti-Ni. The occurrence of the complex transformation behaviours indicates that Ni-rich Ti-Ni alloys are unstable at even these low temperatures.

## **2.5 Applications of SMA:**

- 1) Orthodontic Ti-Ni wire
- 2) Antenna for the portable phone
- 3) Eye glass Frame
- 4) Air-craft smart structures

## 2.6. FORMULATION OF PROBLEM:

Shape memory Ni-Ti and Ni-Ti-Cu alloys have received considerable research and wide use for its special mechanical properties like pseudo-elasticity, Super elasticity and shape memory effect, which have been shown to be a consequence of its martensite transformation. Shape memory alloys used as micro sensor and micro actuator is a promising candidate either in common industry or in aviation industry.

In order to complete the actuation, the shape memory alloys actuators possess a narrow thermal hysteresis loop. Creation of narrow thermal hysteresis loop in actuators were achieved formation R-phase ( $\text{Ni}_4\text{Ti}_3$ ) in SMA.

R-phase transformations were induced with the help of ageing treatment, annealing treatment and thermo-mechanical cycles. In R-phase transformation regions having low thermal hysteresis along with energy consumption in phase transformation and distortion in parent lattice are very low.

The main aim of our investigation is to find out the possible treatment to stabilize the R-phase transformations and low thermal hysteresis loop. Once R-phase stabilized means, the performance of the Air-Craft actuator increased considerably. So, the main focus of my dissertation was to control and stabilize the R-phase transformation for improving the performance of Air craft Actuators and Sensors.

EXPERIMENTAL DETAILS

The alloy compositions and transformations temperatures of the polycrystals that have been studied are listed in Table 2. The polycrystals denoted by NiTiNOL (Nickel-Titanium Naval Ordnance Laboratory) and NiTiNOL-Cu had been obtained as 12mm rod in Ni-Ti and 12.5 mm rod in Ni-Ti-Cu from THE COMMAND, NAVAL-AIR SYSTEMS COMMAND, MD, USA through Dr. Vinod S. Agarwal, NAVAL-AIR SYSTEMS COMMAND, Senior Staff Scientist, MD, USA. The as received materials were shown in the following Fig. 3.1.

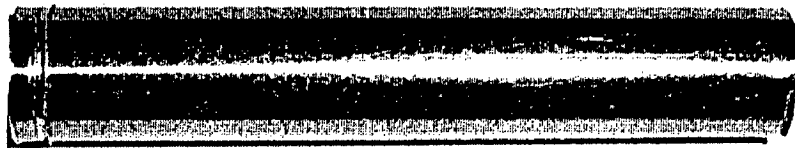


Fig.3.1. as received Ni-Ti rod.

The transformation temperatures of the polycrystals are studied with DSC and listed in Table-2.

SMA alloy	Element	%Wt
NiTiNOL	Ni	54.9
	Ti	45.08
	C	288ppm
	H	211 ppm
NiTiNOL-Cu	Ni	49.14
	Ti	45
	Cu	6.6
	O	193 ppm
	C	410 ppm

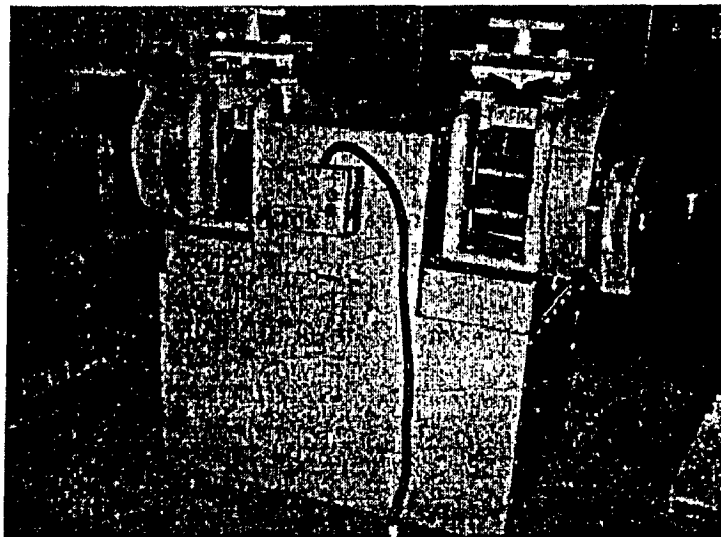
As received samples were subjected to the normalizing for 36 ks (1hour) in tube furnace. The specimens of DSC were cut from the ingots. After normalizing treatment other sample are subjected to rolling operation to convert rod to 0.5mm thickness sheet.

There are two steps in rolling process depending upon the thickness of the materials.

1. Up to 4mm thickness – Hot rolling.
2. 4 mm to 0.5mm thickness – Cold rolling.

### 3.1 Hot rolling:

The ingots were hot rolled (at 850°C) into sheets (3mm in thickness) with a 10% reduction of per pass. Controlling deformation in hot rolling is very critical issue because whenever the samples ingots subjected to high % Reduction, the rolling will start to struck. To verify this problem, careful control of the % reduction plays very important role. Formation of oxide layer  $TiO_2$  over the surface of the ingots, sometimes may lead to formation of surface roughness. To remove this problem, ingots are subjected to pickling process. (70%  $HNO_3$ , 25% $HF$ , 5%  $H_2O$  mixture). The pickling operation was carried out each and every 1mm reduction.





### **3.2 Cold rolling:**

Cold rolling is used to produce sheet with superior surface finish and dimensioned tolerances compared with hot rolled strip. Cold rolling was carried out 500°C intercritical annealing with 30% reduction. So the reduction achieved by cold rolling was 95%.

In establishing the reduction in each pass, it is desirable to distribute the work as uniformly as possible over the various passes without falling very much below the maximum reduction for each pass. Generally 0.10mm thickness in each pass is desirable. The lowest percentage reduction around 0.05mm is taken on the last pass to permit better control of flatness and surface finish.

The surface tolerance for cold rolling is very much important than hot rolling. The oxide layer must be removed with pickling process. High surface finish is required in each and every pass; otherwise it may lead to the formation of crack or affect the surface finish of the sheet.

### **3.3 Wire Drawing:**

Wire drawing was performed in NAL (National Aero-Space Laboratory) under the supervision of Dr.S.K Bhawmik, Scientist, NAL, Bangalore, India.

Hot wire drawing was performed the diameter of the wire up to 3 mm and after 3 mm to 0.5 mm thickness reduced in cold drawing operation.

### **3.4. Shape Memory Effect (SME) Treatment:**

After rolling and wire drawing, products are subjected to the normalizing treatment at 500°C (723 K) for 3.6 ks in tube furnace followed by water quenching.

### 3.5 MICROSTRUCTURAL CHARACTERIZATION

Samples prepared as described in previous section were then undergone microscopic examination. Preparation of specimens for microscopic examination is mentioned below.

#### **Rough grinding:**

The surface of the specimen had made plane by means of a specially designed motor driven grinder and emery belt. In order not to alter superficially the structure of the metal undergoing grinding, the specimen was kept cool by frequently dipping it into water during the grinding operation.

#### **Fine Grinding:**

Emery papers used in the preparation of metallographic specimen has fineness no. 1/0, 2/0, 3/0 and 4/0. Fineness of these every papers increases from 1/0 to 4/0 gradually, i.e. 4/0 is the finest paper.

#### **Polishing Technique:**

Fine polishing of a metallographic specimen is for the purpose of removing from the surface of the specimen the fine scratches introduced during the last grinding operation, and of ultimately producing a highly polished scratch-free surface.

The success in final polishing, as well as the time consumed in this operation, depends largely upon the care that has exercised during the preceding grinding operations. It must be emphasized that both time and effort will be wasted if an attempt is made to final-polish a specimen containing deep and coarse scratches that were not removed completely in last grinding operation. In such cases the specimen should be reground, with more attention paid to the uniformity of scratch fineness before final polishing. Fine polishing was done on a wheel polishing machine with abrasive aluminum slurry spread on a velvet cloth attached wheel.

### **Microscopic Examination:**

After preparing samples they were examined under optical microscope for different magnification & their photographs were taken. All the samples were examined in un-etched condition. Fig.4.3 shows the optical microscope used for microscopic examination.

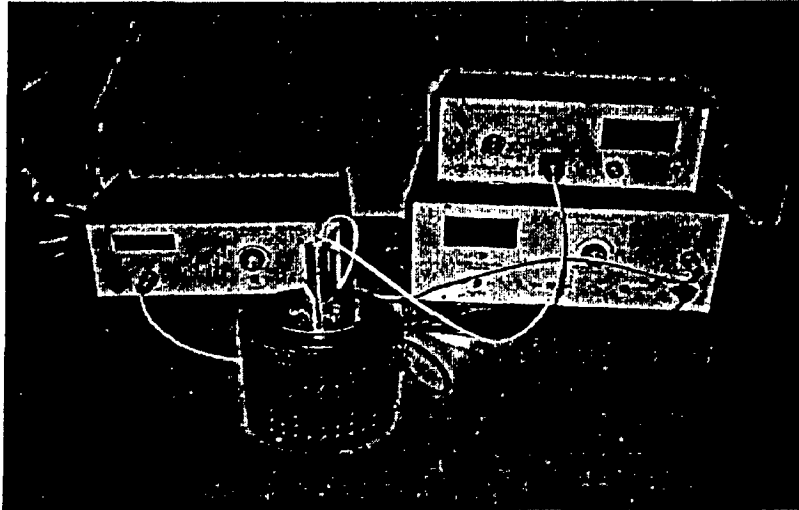


### **3.6 Scanning Electron Microscopy (SEM):**

After wear testing the worn surfaces of all specimens had been analyzed through scanning electron microscopy. Here 9-10 mm length of worn pin samples from worn surfaces had been cut in such a way that the worn surface could not be damaged. Now these samples had been used in scanning electron microscope for study of mode of wear in these samples. For this purpose use was made of LEO, 435 VP scanning electron microscope (SEM).

### **3.7 Resistivity methods:**

Four probe resistivity methods was used to analyze the transformation temperatures of the sample. The components of the resistivity methods were follows.



1. Constant power source: 100 mA.
2. Variable volt-meter. - 20  $\mu$ V to 20 mV.
3. Induction Furnace.

### **3.8. X-Ray Diffraction:**

Bruker D06 series of the XRD instruments used for analyzes the sample. High temperature XRD was performed with hot stage XRD, temperature control within  $\pm 1^\circ\text{C}$ . Target:  $\text{CuK}\alpha$ .

### **3.9 Tensile test:**

Tensile test was of a wire sample were performed in S-series, H25K-S Materials testing machine.

## RESULTS

### 4.1.1. Ni-Ti aged in 150°C

DSC curve of the Ni-Ti solutionized (As-quenched) from 850°C was shown in Fig 4.1.1. As temperature of the sample as compared to the as-quenched Ni-Ti sample. Ms Temperature of the as-quenched sample 60°C and As temperature of the Ni-Ti SMA as quenched sample 77°C reduced from 96°C in as received condition. Transformation hysteresis in this austenite phase transformation 37°C and transformation thermal hysteresis in this B19' phase 29°C.

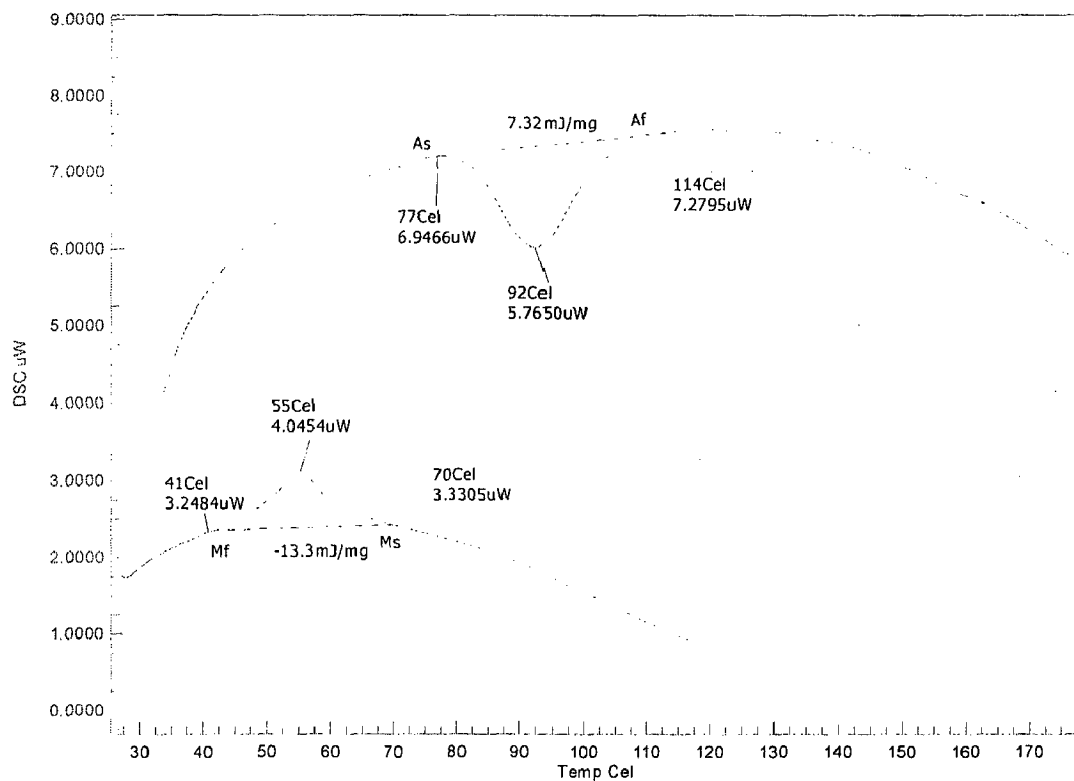
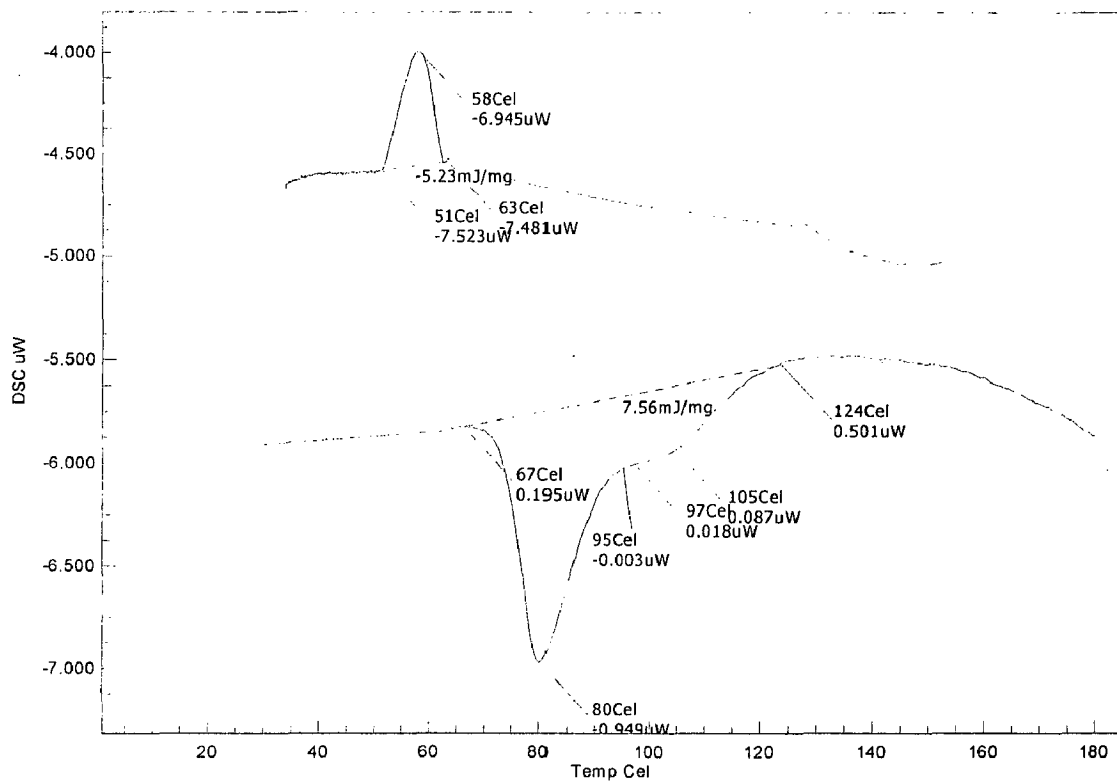
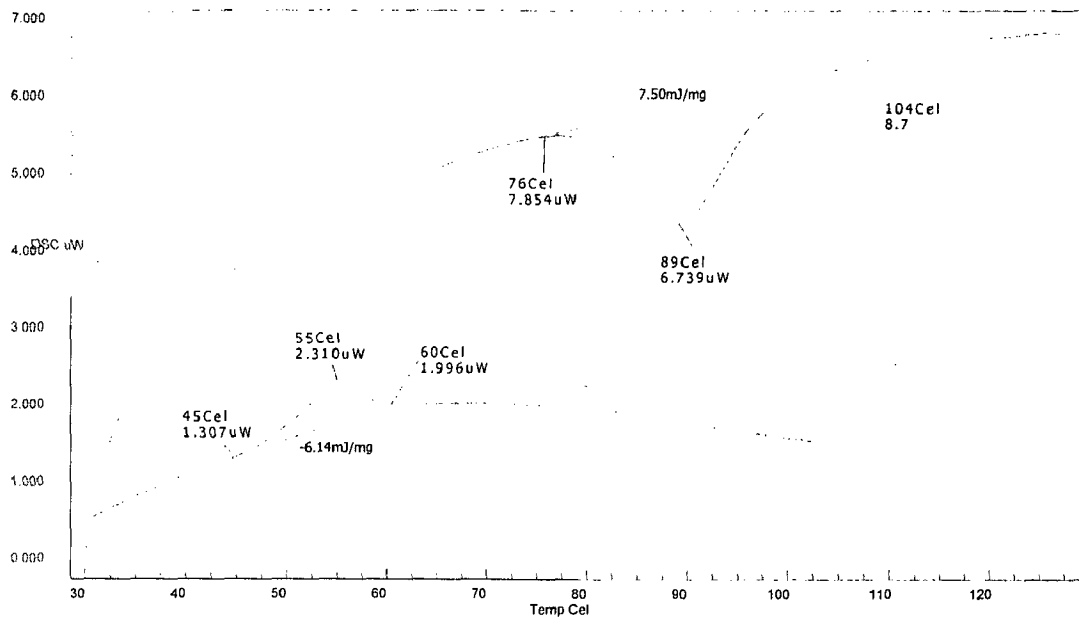


Fig-4.1.1 DSC plot of Ni-Ti as quenched from 850°C

DSC plot of the Ni-Ti aged 150<sup>0</sup>C at 4 Hrs was shown in Fig. There's no difference in As temperature of the sample as compared to the as-quenched Ni-Ti sample. But there was a large difference in the Ms temperature of the sample, which was reduced to 60<sup>0</sup>C as compared to 70<sup>0</sup>C in the as-quenched sample. This difference in Ms (B19'-Monoclinic structure) temperature of the sample indicates that the change in composition of the sample in aged four hours in 150<sup>0</sup>C at 4 Hrs. So the thermal hysteresis in B2 cubic structure of this phase change is 28<sup>0</sup>C. Here the transformation sequences was B2 (Austenite)↔ B19' (monoclinic).



**Fig: 4.1.2 The DSC plot of the Ni-Ti aged 150<sup>0</sup>C at 4 Hrs**



**Fig. 4.1.3. DSC plot of the Ni-Ti SMA aged in 150<sup>0</sup>C at 24 hrs**

DSC curve of the Ni-Ti aged 150<sup>0</sup>C at 24 Hrs as shown in the Fig 4.1.3. Here, As temperature of the sample was reduced to 67<sup>0</sup>C (as compared to as quenched sample 77C). The following parameters were studied in this DSC curve. As = 72<sup>0</sup>C Af = 97<sup>0</sup>C Ms = 63<sup>0</sup>C Mf = 51<sup>0</sup>C. The transformation thermal hysteresis in the B2 Cubic phase I equal to 25<sup>0</sup>C and the B19' phase equal to 12<sup>0</sup>C. In B19' phase transformation hysteresis was very low but energy released in this phase transformation very high as compared to B2 phase (4.10 J/g). The reason for high energy released in this B19' transformations were high amount of lattice distortions occurred in this shear transformations than B<sub>2</sub> Cubic phase transformation.

Ms Temperature of this aged sample was reduced to 63<sup>0</sup>C and thermal hysteresis in this total transformation is equal to As-Ms = 9<sup>0</sup>C. Thermal hysteresis in martensite transformation is equal to 12<sup>0</sup>C.

DSC study of the Ni-Ti aged in 150<sup>0</sup>C at 48 Hrs was shown in Fig-4-1.4. There is some surprising results were obtained in this aged sample. One exothermic peak was





obtained while heating the sample; it was started at 65°C and ended to 85°C with little exothermic energy -4.23 J/g and thermal hysteresis 20°C. There are three endothermic peaks were obtained. Two peaks belong to R-Phase (it was the combinations of the two R-Phases –R1 and R2 Phase). R-phase indicates in this aged sample belong to Ni<sub>4</sub>Ti<sub>3</sub> orthorhombic structure. Third phase may belong to NiTi Cubic B<sub>2</sub> structure.

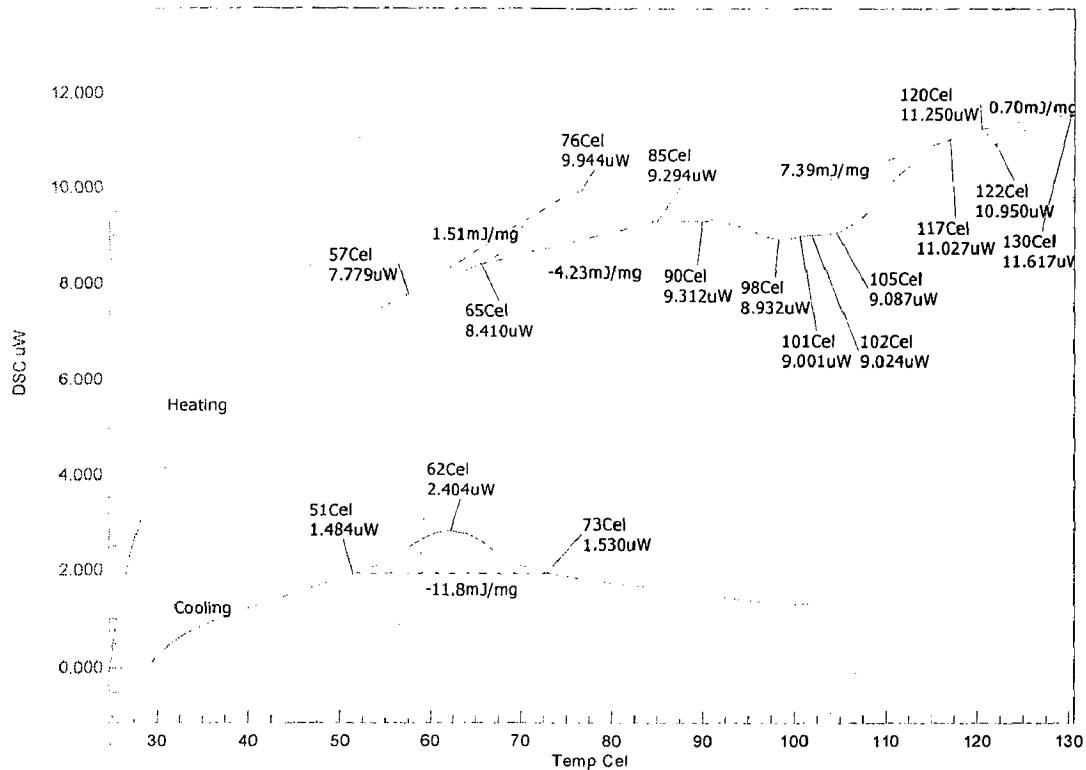


**Fig-4.1.4 DSC Plot of the Ni-Ti aged in 150°C at 48 Hrs.**

Currently, there is no experimental evidence available formation of this exothermic peak on heating; it may due to formation of the Burst transformation because most of the austenite transformations were endothermic, only martensite transformations were exothermic. Martensite transformations were appeared only on cooling and it will proceed due to chemical driving force and shear strain accumulated while deforming the lattice structure (SIM-Stress Induced Martensite).

Presently, we can not give any conclusion about this transformation, because the transformation is opposing to the nature of the B19' ↔ R ↔ B2 transformation.



While cooling R-phase was started from 75<sup>0</sup>C and ended to the Rf =51<sup>0</sup>C with the thermal hysteresis equals to 22<sup>0</sup>C. Unfortunately, our DSC could not work below room temperature; not possible to measure the Ms and Mf temperatures of this aged sample.

DSC study of the Ni-Ti aged 150<sup>0</sup>C at 72 Hrs were shown in the following Fig-4.1.5 Compared with the 48 Hrs aged at 150<sup>0</sup>C Ni-Ti sample, here two R-peaks were merged and formed in one single R-peak transformation. So, we may conclude that R1 and R2 phases are formed between 48 hrs and 72 hrs aged at 150<sup>0</sup>C. Thermal hysteresis in R phase transformation was reduced to 16<sup>0</sup>C as compared to 27<sup>0</sup>C in aged 48 hrs R- Phase transformation. So, we may guess saturation of R- phase transformation occur around 55 to 65 hrs. Future work may focus to find the exact ageing time to merge of this R-phase transformation. B2-phase was started at 84<sup>0</sup>C and ended 107<sup>0</sup>C with thermal hysteresis of this B2-phase transformation 23<sup>0</sup>C.

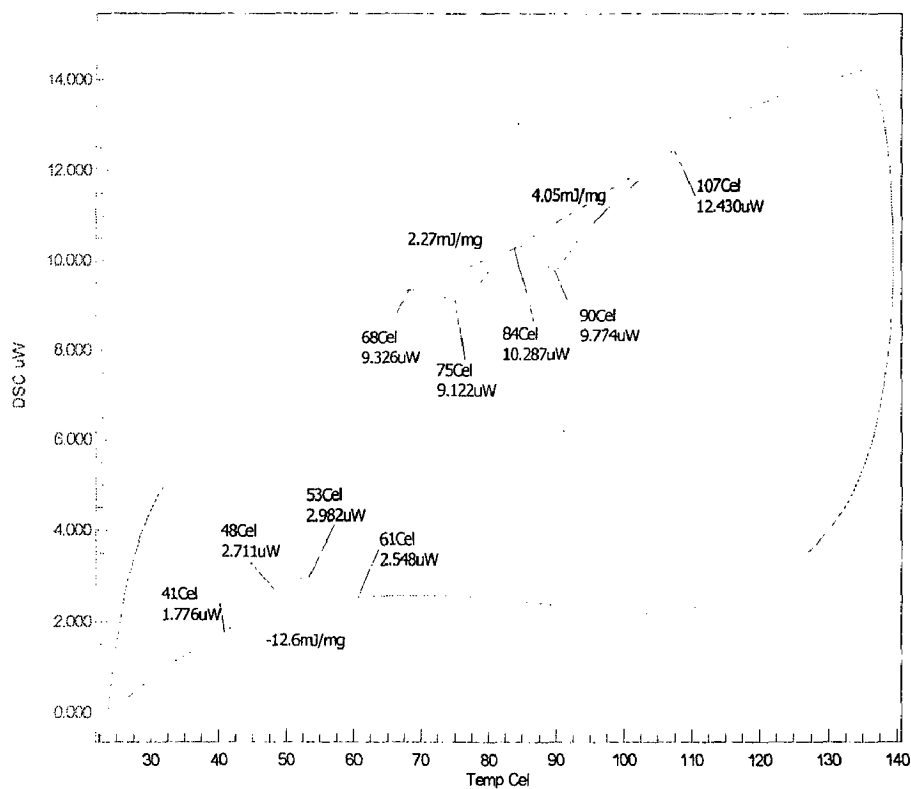


**Fig: 4.1.5. DSC plot of the Ni-Ti aged in 150<sup>0</sup>C in 72 hrs.**

#### 4.1.2. Ni-Ti-Cu aged 150°C

Fig.4.1.5 a. shows the DSC plot of the solutionized as quenched sample from 850°C (at 1hr). From this plot the following parameters were studied.

$M_s=55^\circ\text{C}$   $A_s=60^\circ\text{C}$ ,  $A_f=81^\circ\text{C}$   $A_s=42^\circ\text{C}$ .

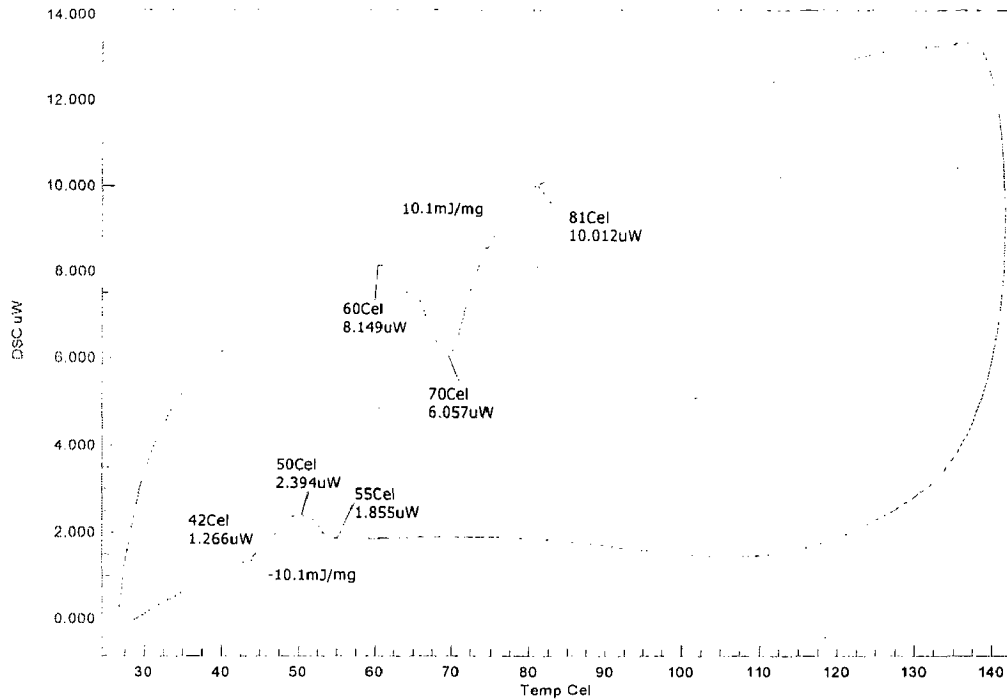


**Fig.4.1.5 a. DSC plot of the solutionized as quenched sample from 850°C (at 1hr).**

The thermal hysteresis in  $B_2$  phase transformation was  $21^\circ\text{C}$  with endothermic energy  $10.1 \text{ J/g}$ . The thermal hysteresis in  $M$  phase transformation was  $13^\circ\text{C}$  with exothermic energy around  $-10.1 \text{ J/g}$ . The phase transformation mechanism was  $B_2 \rightarrow B_{19}'$  on heating,  $B_{19}' \rightarrow 2$  on cooling. So there is no formation of  $R$ - phase transformation in heating or cooling. Thermal hysteresis of the  $B_2 \rightarrow B_{19}'$  phase transformation was  $A_s - M_s = 60 - 55 = 5^\circ\text{C}$ .

Fig.4.1.6 shows the DSC curve of the Ni-Ti-Cu aged 24 hrs  $150^\circ\text{C}$ .  $A_s$  temperature of the sample was raised to  $96^\circ\text{C}$  from  $60^\circ\text{C}$  (in as quenched sample).  $R$ - Phase transformation was appeared in Ni-Ti-Cu aged in  $150^\circ\text{C}$  at 24hrs. The following parameters were studied from this figure.

$R_s=72^\circ\text{C}$   $R_f=93^\circ\text{C}$   $A_s=96^\circ\text{C}$   $A_f=121^\circ\text{C}$



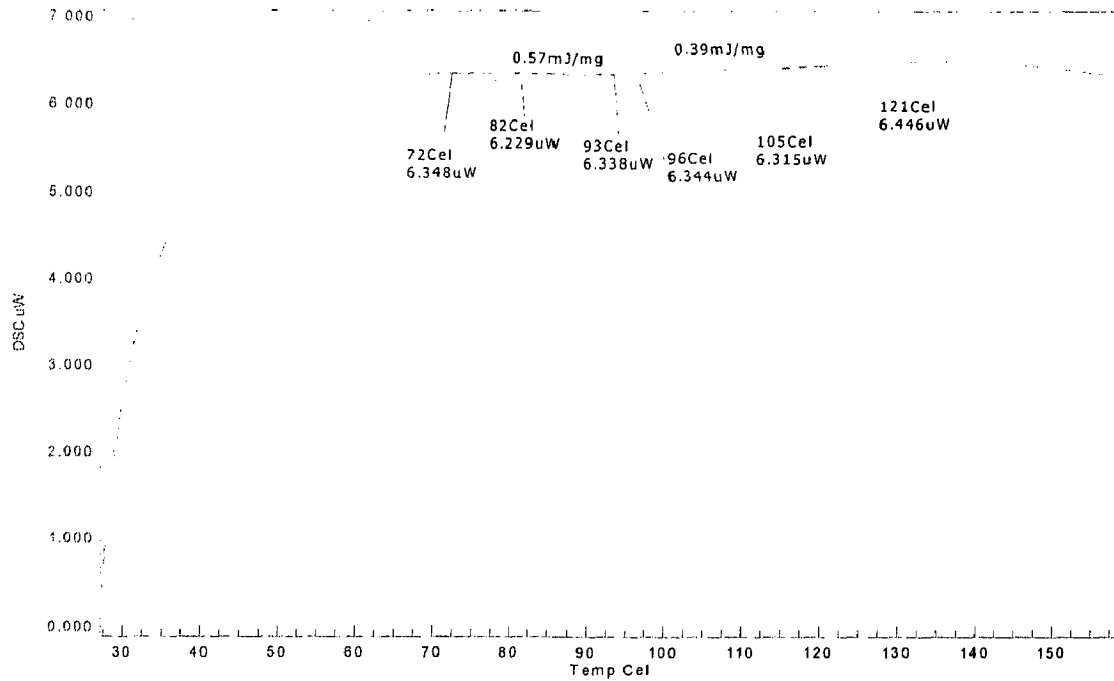


**Fig.4.1.6. the DSC plot of the Ni-Ti-Cu aged in 150°C at 24 hrs**

The change in the austenite transformation temperature indicates change in composition during the formation of the austenite (It may due to formation of  $Ni_4Ti_3$  precipitates in grain boundary; it will create heterogeneity in the distribution of the Ni content in the microstructure). So the Change in the transformation temperature is to prove for change in composition.

Here, the transformation sequence as follows.

$B2 \rightarrow R \rightarrow 19'$ . But the energy consumed in the above transformations were less 0.39 J/g compared with an quenched sample 10.1J /g. the Ni-Ti-Cu aged 48 hrs 150°C. The following parameters are studied from their DSC curve.

$A_s=80^\circ C$ ,  $A_s=97^\circ C$ ,  $R_s=80^\circ C$ ,  $R_f=70^\circ C$  compared with ageing 24 hrs sample, no separate R-phase and B2-phase peaks appeared because R-phase and B2 phase transformation peaks were merged in this transformation. This is the special characteristics future of this aged 48 hrs at 150°C sample. There is no significant change in  $M_s$  Temperature as compared to solutionized sample, only 7°C was raised in this transformation.

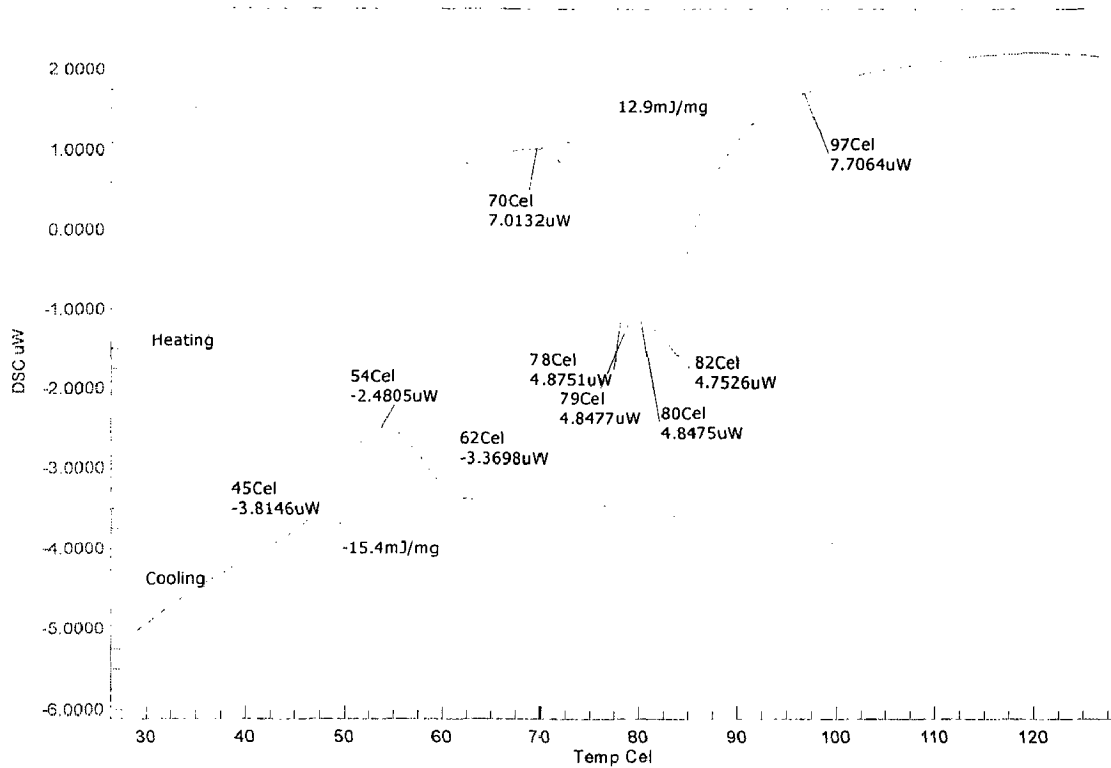


**Fig.4.1.7. DSC plot of the Ni-Ti-Cu aged in 48 hrs at 150°C**

**Fig.4.1.7** shows the DSC plot of the Ni-Ti-Cu aged 150°C at 72 hrs. The following parameters are studied from this graph.

$M_s=57^{\circ}\text{C}$ ,  $A_s=84^{\circ}\text{C}$ ,  $A_f=99^{\circ}\text{C}$ ,

$M_f=43^{\circ}\text{C}$ ,  $R_s=72^{\circ}\text{C}$ ,  $R_f=81^{\circ}\text{C}$ .

Thermal hysteresis in Martensitic phase transformation was  $14^{\circ}\text{C}$  with exothermic energy  $-7.25\text{mJ/mg}$ . The total thermal hysteresis in  $M\leftrightarrow A$  transformation is  $A_s-M_s=84-57=27^{\circ}\text{C}$ .

**Fig 4.1.8** shows the DSC study of the Ni-Ti-Cu aged 150°C at 96 hrs. R-phase transformation was not appeared in this graph. From this graph, We may conclude that R-phase transformation was vanished in long time aged at 96hrs. So the transformation sequence on heating is  $B19'\leftrightarrow B2$  (phase) on cooling  $B2\leftrightarrow B19'$  (phase),  $M_s=61^{\circ}\text{C}$ ,  $M_f=45^{\circ}\text{C}$ .

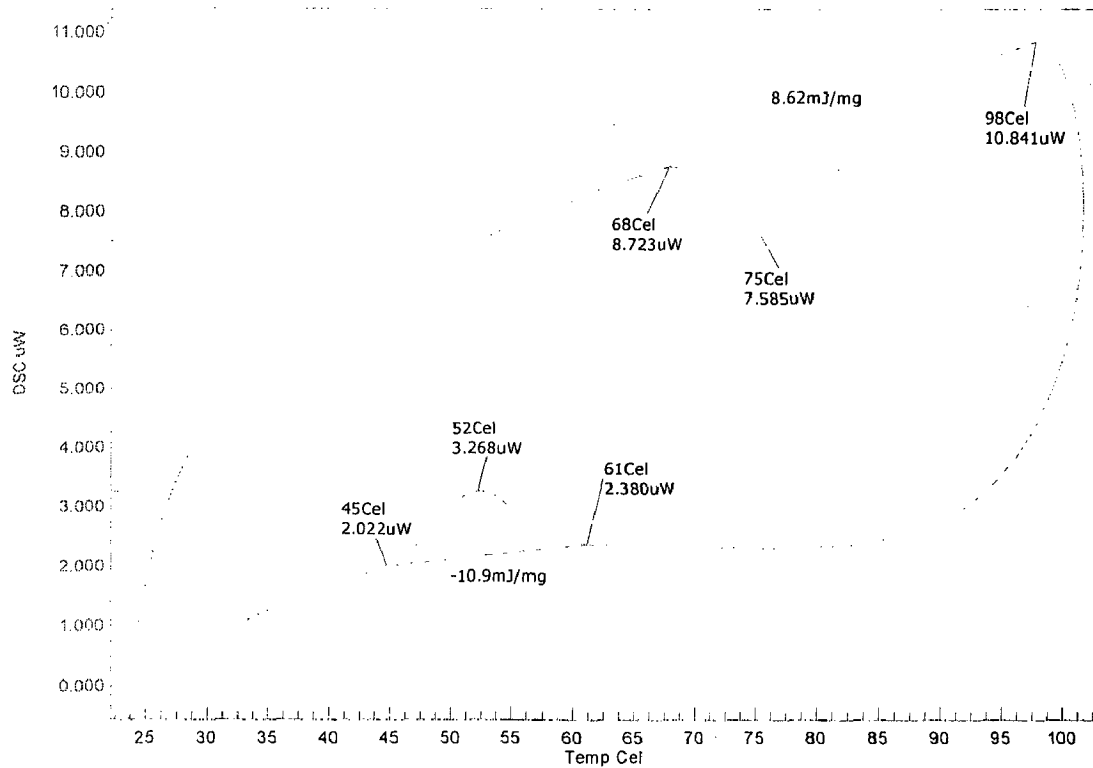


**Fig.4.1.8. DSC plot Ni-Ti-Cu aged in 150°C at 96 hrs**

There is no significant effect in  $M_s$  temperature of this aged samples. There's the slight change in  $M_s$  temperature, it was increased to 4°C as compared to Ni-Ti-Cu aged 72 hrs at 150°C.

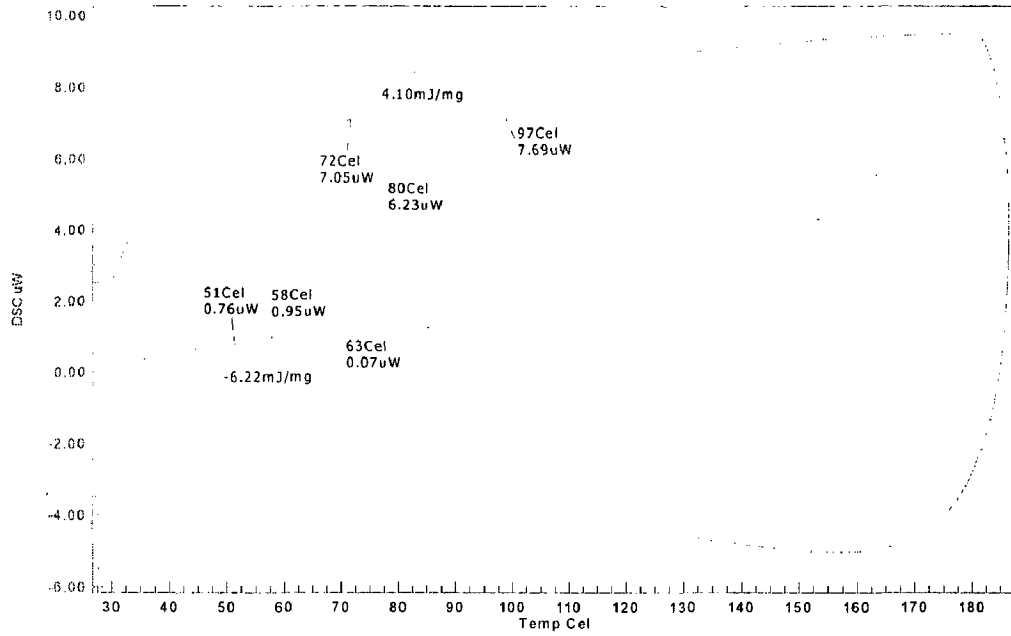
#### 4.1.3 Ni-Ti aged in 300°C.

Ni-Ti and Ni-Ti-Cu samples are subjected to ageing treatment at 300°C at deform intervals 24h, 48h, 72h and 96h. The main objective of this ageing treatment to study the control and stabilize the transformation temperatures, hysteresis loops of the transformation and R-phase thermal hysteresis transformation characteristics.

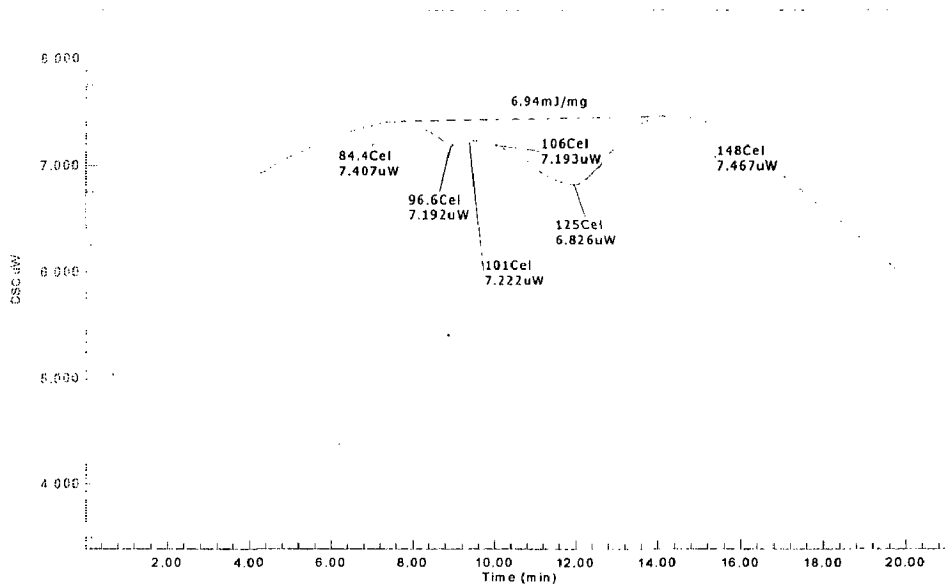
#### Ni-Ti aged in 300°C at 48 hrs

Fig 4.1.9 shows the DSC plot of the Ni-Ti aged in 300°C at 48 hrs. From this graph  $A_s=80^\circ\text{C}$  and  $A_f=121^\circ\text{C}$  temperature were understood. Thermal hysteresis of this B2 phases transformations equal to 31°C. There is the large thermal hysteresis observed in this curve.





**Fig.4.1.9. DSC plot of the Ni-Ti aged in 300°C at 48 hrs**



**Fig.4.1.10. DSC plot of the aged in 300°C at 72 hrs.**

**Ni-Ti Aged in 300°C at 72 hrs**

Fig.4.1.10 shows DSC plot of the Ni-Ti aged in 300°C at 72hrs, from this graph the following parameters are studied.  $A_s=106^{\circ}\text{C}$ ,  $A_f=148^{\circ}\text{C}$ ,  $R_s =84.4^{\circ}\text{C}$ ,  $R_f =101.6^{\circ}\text{C}$ . R phase formation occurs in this sample only after 48 hrs aged at 150°C. The formation R phase involves reduction of thermal hysteresis in high temperature region (B2 phase). Thermal hysteresis is R phase region was  $(R_f-R_s) =27^{\circ}\text{C}$ .

**Ni-Ti aged in 300°C at 96 hrs.**

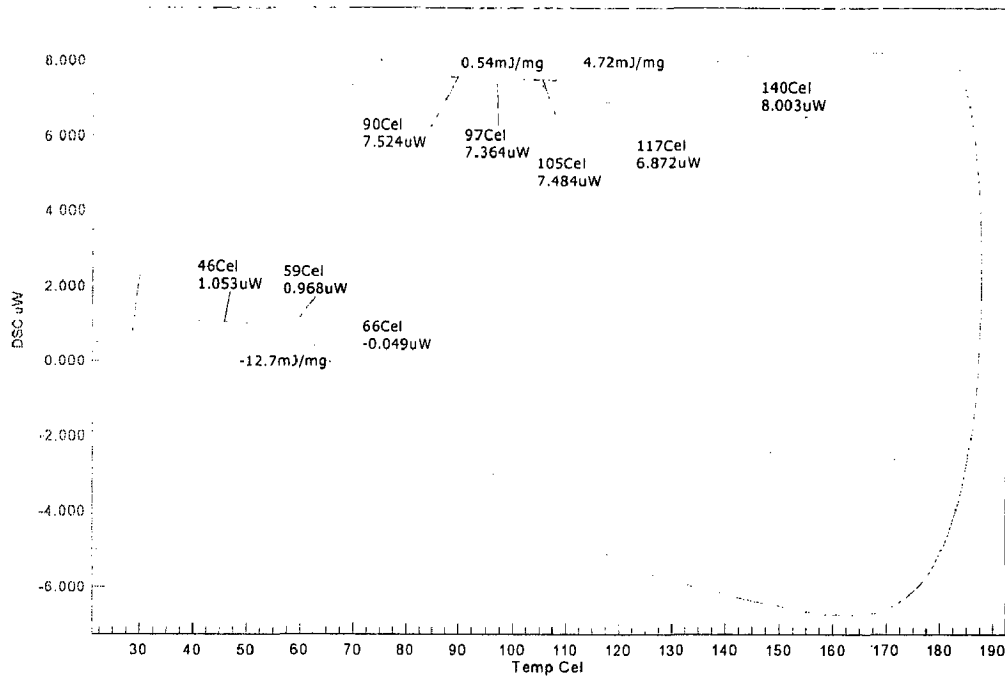


**Fig.4.1.11 DSC plot of the Ni-Ti aged in 96 hrs at 300°C**

**Fig.4.1.11** shows the DSC curve of the Ni-Ti aged 96 hrs at 300°C. Clearly separation of R-phase peaks and B2 phase peaks are appeared in the aged sample.  $R_s=90^\circ\text{C}$ ,  $R_f=103^\circ\text{C}$ ,  $A_s=105^\circ\text{C}$ ,  $A_f=140^\circ\text{C}$ . Thermal hysteresis in  $M \rightarrow A$  phase transformation is equal to  $A_s - R_s = 105 - 90 = 15^\circ\text{C}$ , we may conclude from the above discussion that R-phase transformation was stabilized at 96 hrs aged at 300°C. While cooling from  $B_2 \rightarrow B_{19}'$  transformation  $M_s=66^\circ\text{C}$  and  $M_f=46^\circ\text{C}$  with the exothermic energy 12.7 J/g were studied from this graph.

So the transformation sequence on heating  $B_{19}' \rightarrow R \rightarrow B_2$

On cooling  $B_2 \rightarrow M$ .

**Ni-Ti aged in 300°C at 125 hrs.**

**Fig.4.1.12** shows the DSC curve of aged 125 hrs at 300°C sample. R phase has pronounced effect in this aged sample as compared to aged 96 hrs at 300°C. But the high temp  $B_2$  phase has appeared in the scattered manner.



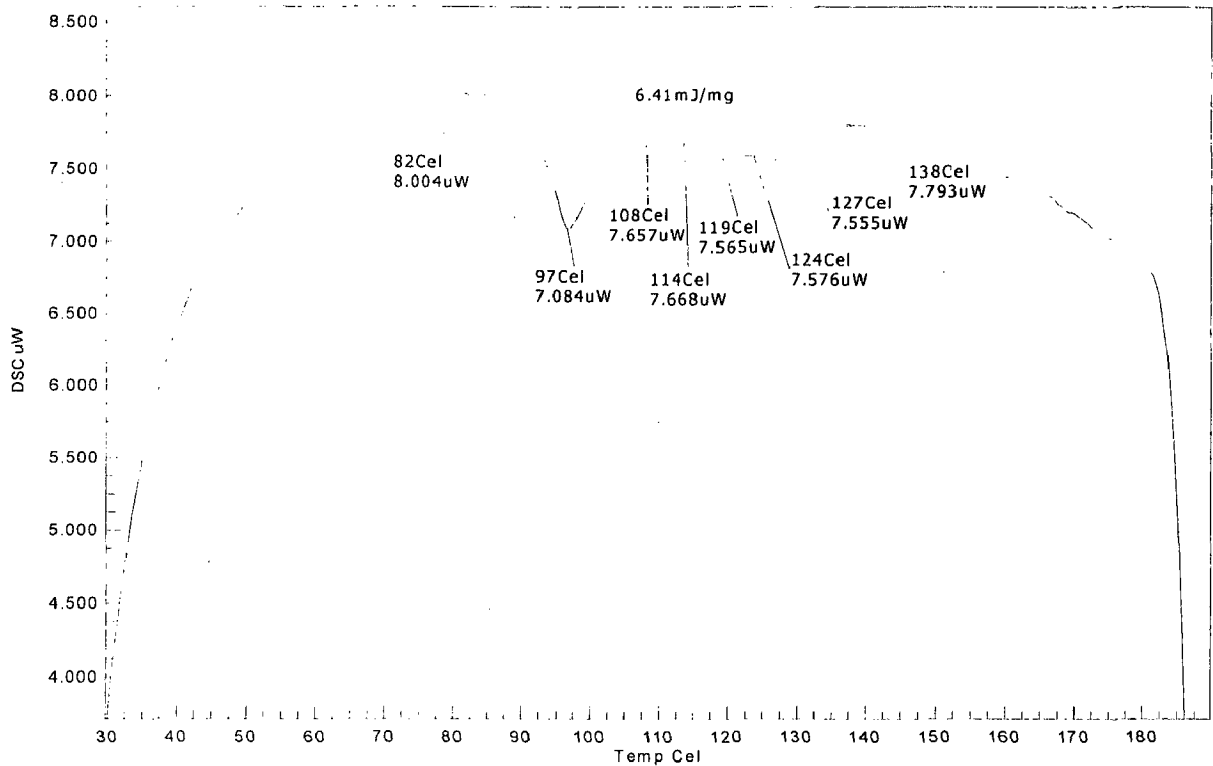


**Fig.4.1.12 DSC plot of the aged 125 hrs at 300°C sample**

There is the large variation in ups and downs appeared in this B2 phase region. It may be due to formation of second R-phase ( $R_2$  phase) or second high temperature rather than B2 phase. Future work should be focused in this transformation region.

$R_s=82^\circ\text{C}$ ,  $R_f=108^\circ\text{C}$ ,  $R_{2,s}=114^\circ\text{C}$ ,  $R_{2,f}=123^\circ\text{C}$ ,  $A_s=124^\circ\text{C}$ ,  $A_f=138^\circ\text{C}$ .

Total energy consumed in this high temperature phase transformations were 6.41mj/mg. There are three endothermic peaks identified in this aged samples.

R1,R2,B2 phase.

So, the transformation sequences were

$B19' \rightarrow R \rightarrow R_2(\text{or})B2, 1 \rightarrow B2$ .

#### 4.1.4 Aged 300°C in Ni-Ti-Cu

Ni-Ti-Cu SMA aged in 300°C Ni-Ti-Cu at 48 hrs



**Fig.4.1.13** shows the DSC curve of the Ni-Ti-Cu aged in 48 hrs at 300°C. R phase transformations were observed in the curve at  $R_s = 86^\circ\text{C}$  and  $R_f = 113^\circ\text{C}$ ,  $A_s = 114^\circ\text{C}$  and  $A_f = 134^\circ\text{C}$ . Thermal hysteresis in these R-phase regions equals to  $28^\circ\text{C}$  and energy observed in this R-phase transformation equal to  $3.19 \text{ J/g}$ . Thermal hysteresis in the  $B_2$ -phase region were  $20^\circ\text{C}$  and energy observed in the transformation equal to  $10.3 \text{ J/g}$ .

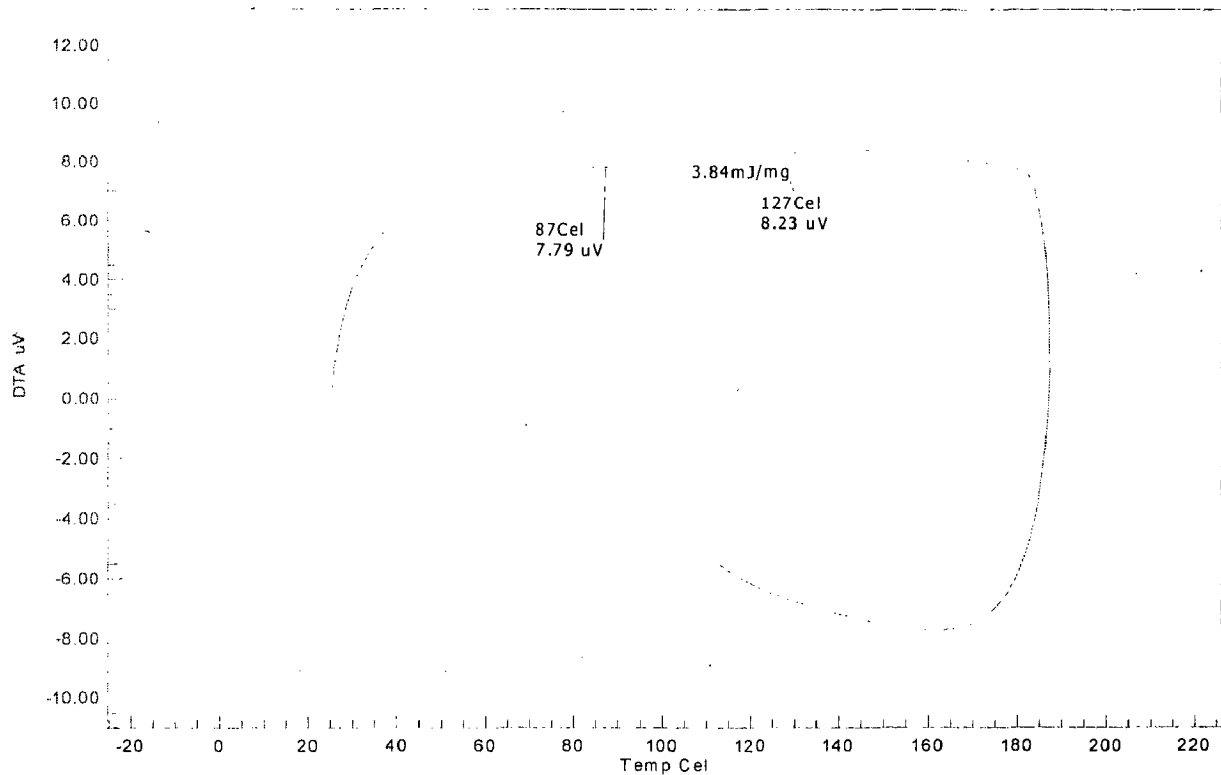


**Fig.4.1.13.** DSC plot of the Ni-Ti-Cu in aged 48 hrs at 300°C

**Fig.4.1.14** shows the DSC plot of the Ni-Ti-Cu aged in 72 hrs at 300°C. R phase transformations were observed in the curve at  $R_s = 72^\circ\text{C}$  and  $R_f = 89^\circ\text{C}$ ,  $A_s = 90^\circ\text{C}$  and  $A_f = 118^\circ\text{C}$ . Thermal hysteresis in this R-phase regions were observed  $17^\circ\text{C}$  and energy absorbed in this R-phase transformation equal to  $1.56 \text{ J/g}$ . Thermal hysteresis in the  $B_2$ -phase region were  $29^\circ\text{C}$  and energy observed in the transformation equal to  $3.33 \text{ J/g}$



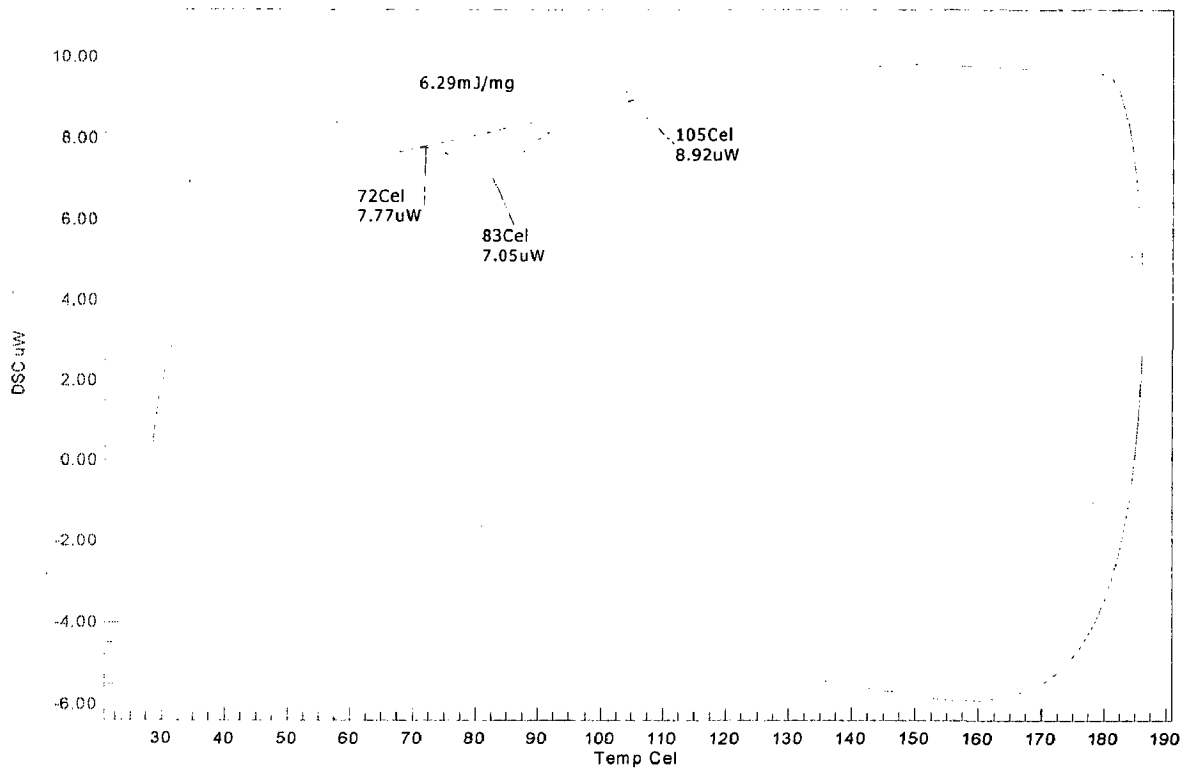


**Fig.4.1.14 DSC plot of the Ni-Ti-Cu aged in 72 hrs at 300°C**

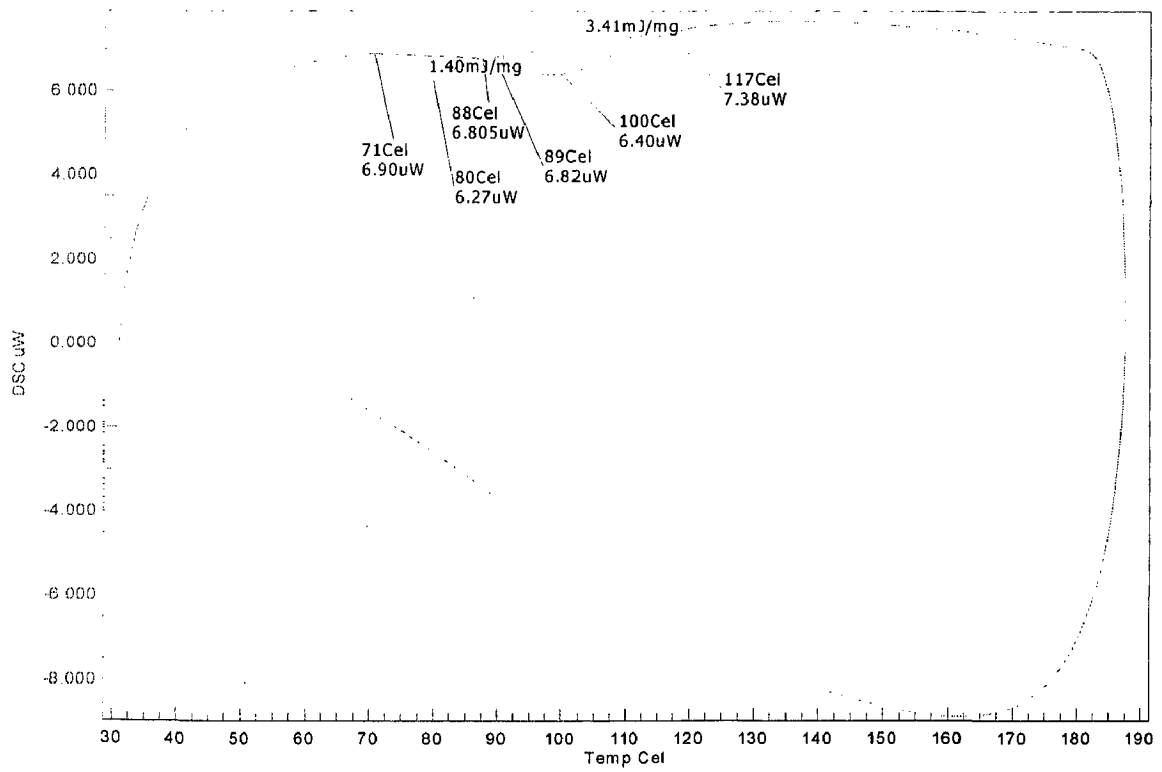


**Fig.4.1.15 DSC plot of the Ni-Ti-Cu aged in 96 hrs at 300°C**





**Fig.4.1.15** shows the DSC plot of the Ni-Ti-Cu aged in 96 hrs at 300°C.No R-phase transformations were observed in this DSC plot. The following parameters were observed in this plot:  $A_s = 69^\circ\text{C}$  and  $A_f = 104^\circ\text{C}$ . Thermal hysteresis in this B2-phase regions was  $35^\circ\text{C}$  and energy absorbed in this R-phase transformation equal to 6.2 J/ g.

**Fig.4.1.16** shows the DSC plot of the Ni-Ti-Cu aged in 125 hrs at 300°C.No R-phase transformations were observed in this DSC plot. The following parameters were observed in this plot:  $A_s = 73^\circ\text{C}$  and  $A_f = 107^\circ\text{C}$ . Thermal hysteresis in this B2-phase regions was  $35^\circ\text{C}$  and energy absorbed in this R-phase transformation equal to 13.2 J/ g.

**Fig.4.1.16.a** shows the DSC plot of the Ni-Ti aged in 500C at 96 hrs. the following parameters were studied from this plot.

$M_f = 33^\circ\text{C}$ ,  $M_s = 115^\circ\text{C}$ ,  $A_s = 116^\circ\text{C}$  and  $A_f = 152^\circ\text{C}$

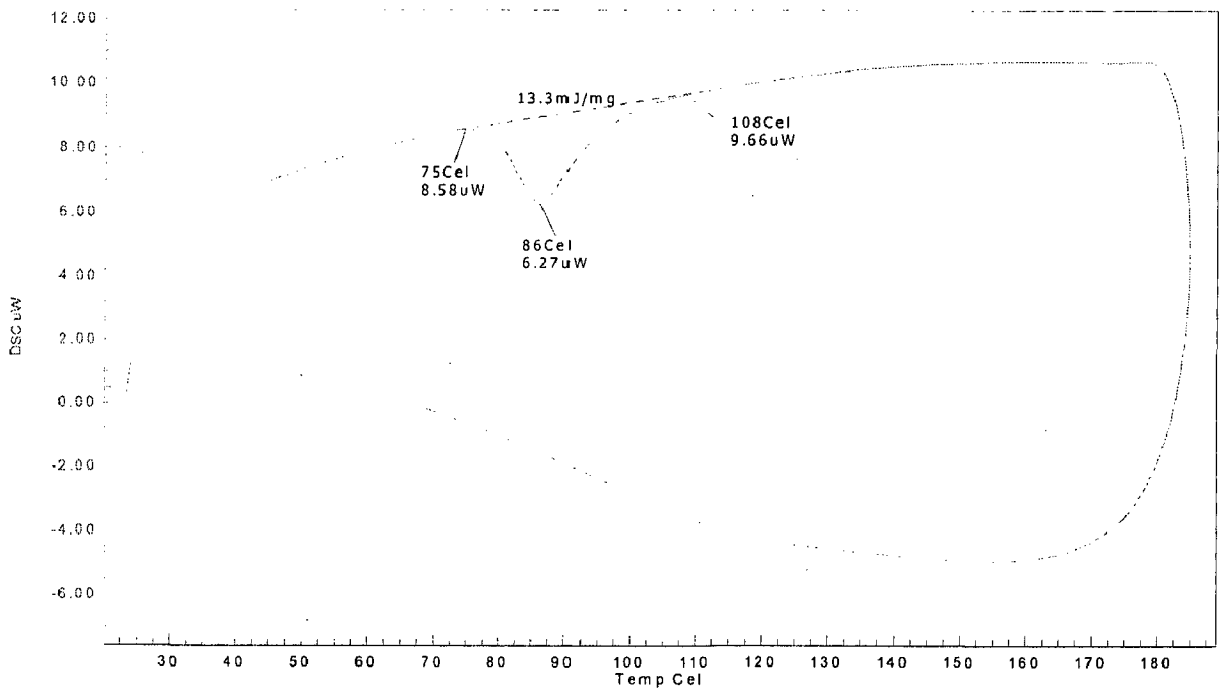


**Fig.4.1.16 DSC plot of the Ni-Ti-Cu aged in 125 hrs at 300°C**



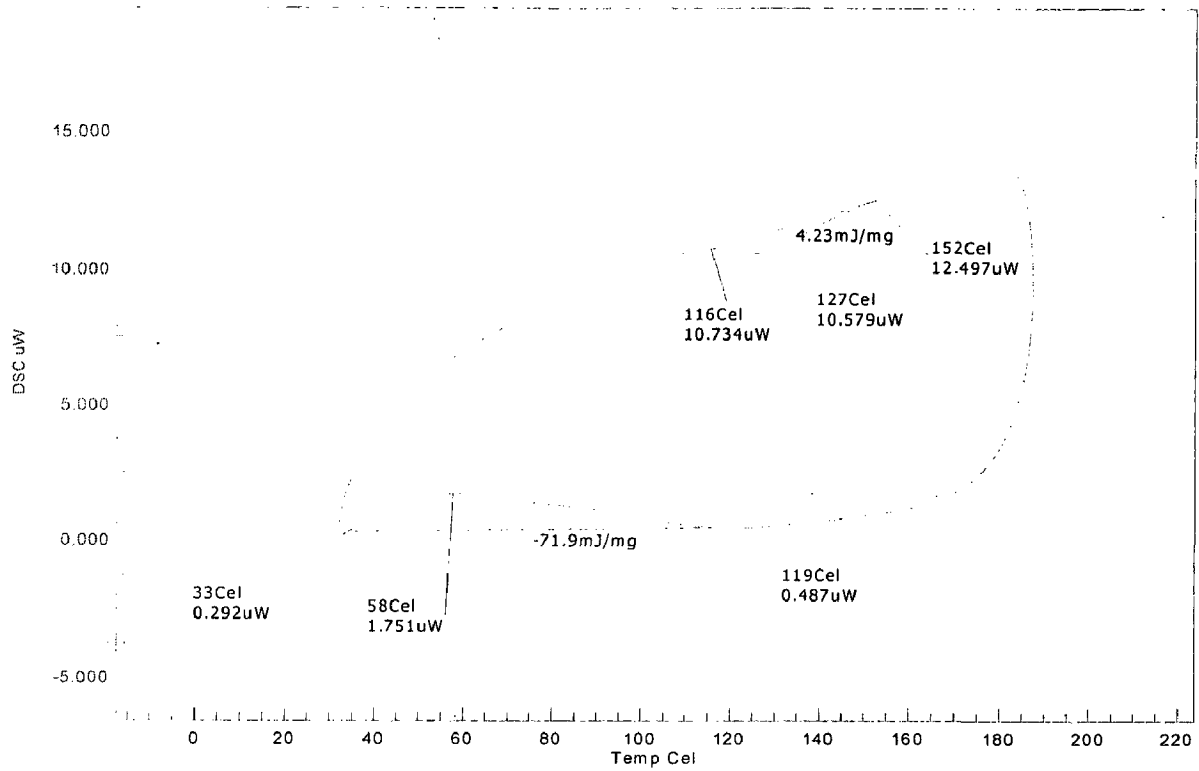


**Fig.4.1.16-a DSC plot of the Ni-Ti aged in 500°C at 96 hrs**

#### **4.1.5 Comparison of Wire and sheet sample:**

##### **Differences in ageing behaviour of the wire and sheet of Ni-Ti and Ni-Ti-Cu:**

**Fig.4.1.17** the aged in 300°C at 48 hrs Ni-Ti wire sample with thermal hysteresis 41°C in B2 (Austenite) phase formation and thermal energy of this transformation (endothermic energy) was 10.2 J/g.

While heating:

B19' → B2

While cooling:

B2 → B19'

**Fig-4.1.9** shows the aged in 48 hrs at 300°C Ni-Ti sheet with R-phase thermal hysteresis 30°C. Total energy consumed in this phase transformation was 11.2 J/g.



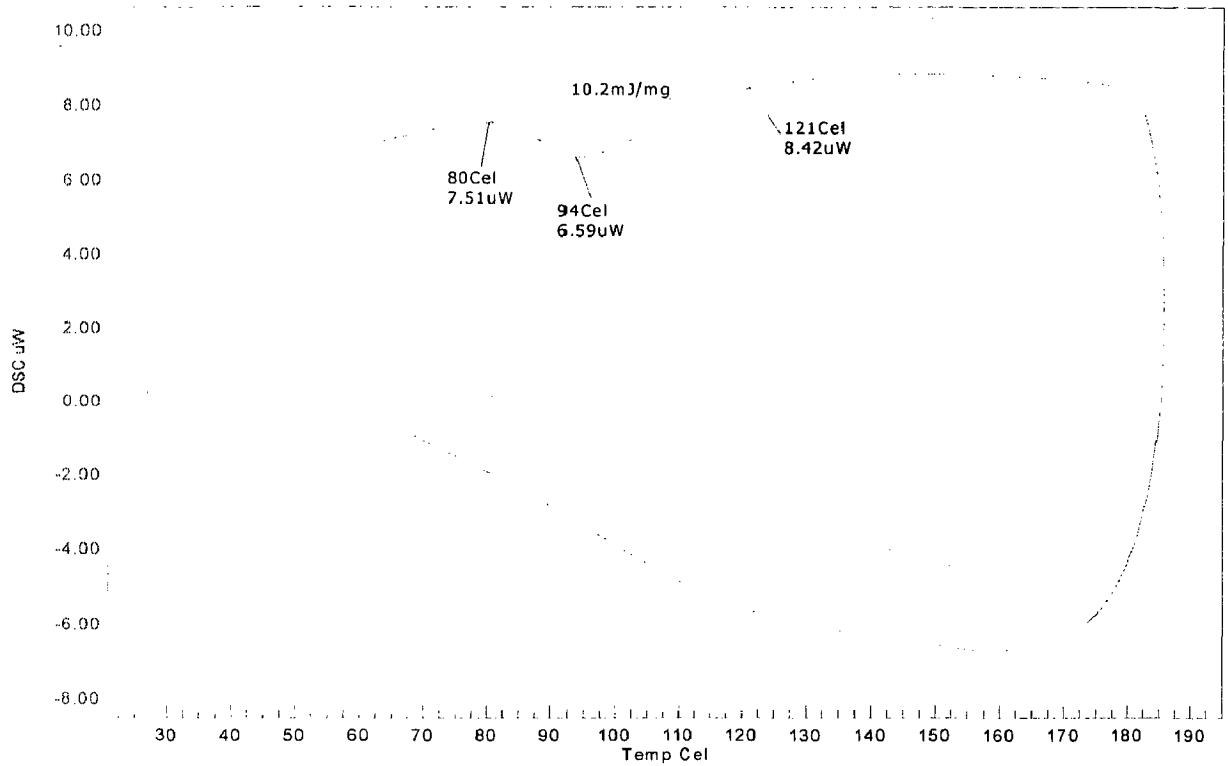


**Fig.4.1.17 DSC plot of the aged 48 in 300<sup>0</sup>C at 48 hrs Ni-Ti wire sample**

While heating:

B19'(monoclinic) → R( Ni<sub>4</sub>Ti<sub>3</sub>) → B2(Cubic)

While cooling:

B<sub>2</sub>(Cubic) → R → B19'.

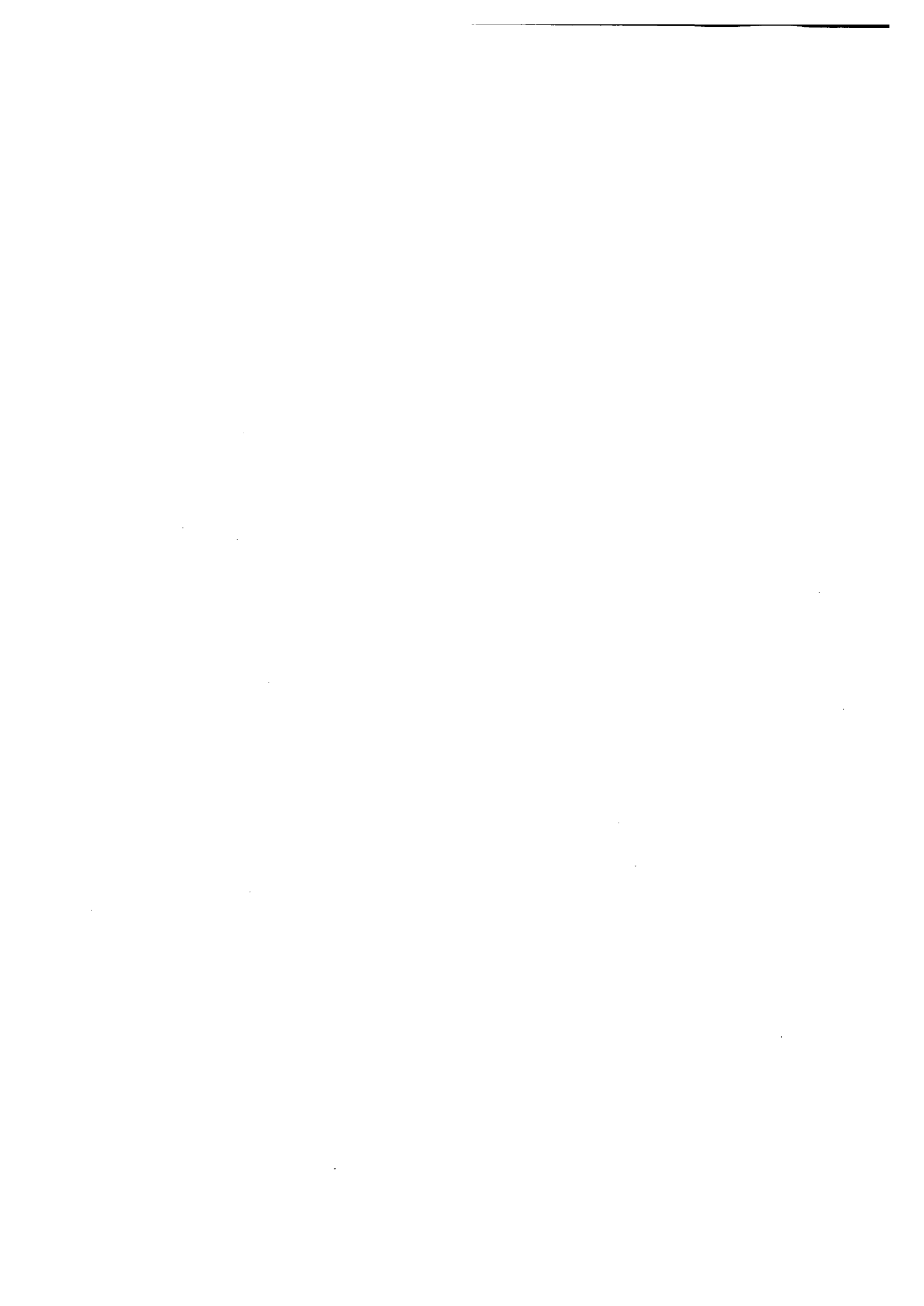
Fig-24 shows Ni-Ti aged in 72 hrs at 300<sup>0</sup>C wire with R-phase thermal hysteresis 17<sup>0</sup>C and B2 phase thermal hysteresis 29<sup>0</sup>C.

While heating:

B19'(monoclinic) → R( Ni<sub>4</sub>Ti<sub>3</sub>) → B2(Cubic)

While cooling:

B<sub>2</sub>(Cubic) → R → B19'.



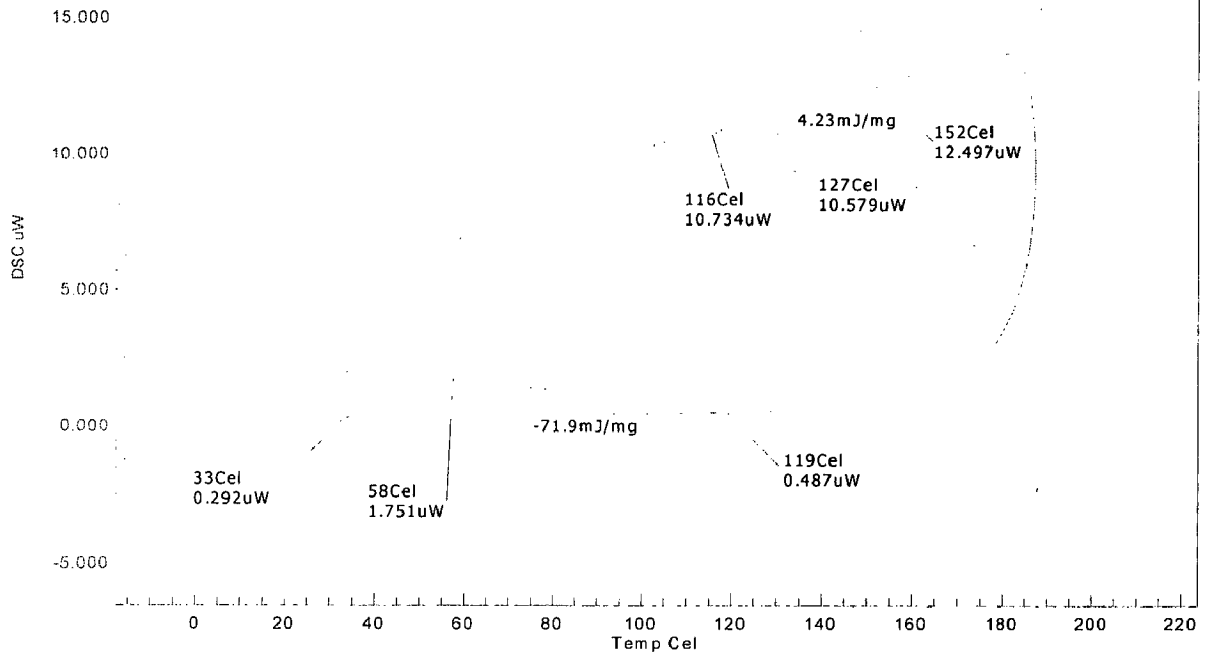


**Fig-4.1.18 DSC plot of the Ni-Ti wire aged in 300°C at 96hrs**

**Fig-4.1.18** shows the DSC plot of the Ni-Ti wire aged in 300°C at 96hrs wire, only B2 phase with thermal hysteresis 35°C.

As=69°C and Af= 104°C.

**Fig.4.1.11** shows Ni-Ti aged 96 hrs at 300°C solid sample (with no R-phase peak), only B2 phase with large thermal hysteresis 41°C.

As=86°C and Af=127°C.

While heating:

B19' → B2

While cooling:

B2 → B19'.





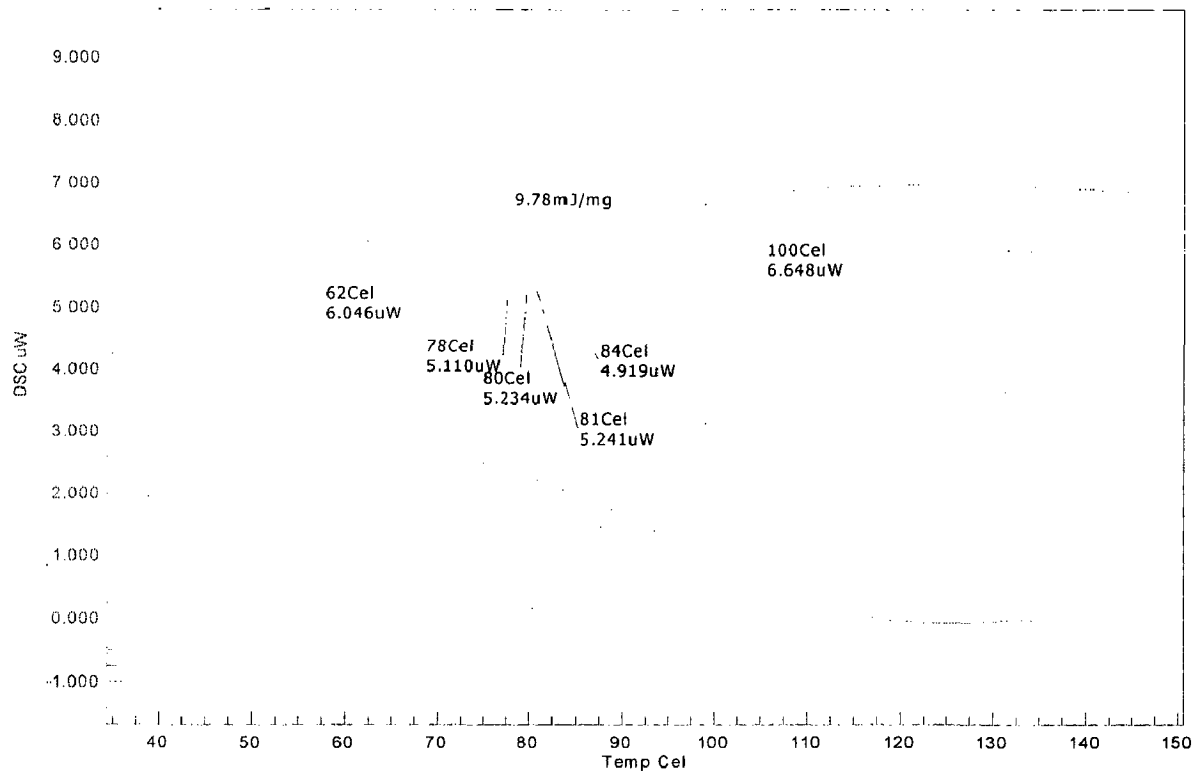


**Fig 4.1.19 DSC plot of the Ni-Ti-Cu (wire) prolonged aged in 72 hrs at 300<sup>0</sup>C**

**Fig 4.1.19** shows the DSC plot of the Ni-Ti-Cu of the prolonged aged in 72 hrs at 300<sup>0</sup>C. Up to 48 hrs aging, there is no effect (No R-phase) on the heating curve, only As and Af appeared. But aging about 72 hrs in 300<sup>0</sup>C shows the peak As temperature was separated in to two parts M→ R→A, while heating curve, R-phase was appeared at 70<sup>0</sup>C and Rf was appeared at . From this DSC plot, it was observed that prolonged ageing time promotes formation of the R-phase transformation. The reason for this effect due to formation of Ni<sub>4</sub>Ti<sub>3</sub> precipitates in grain boundaries. But aged at 48 hrs, no formation of the Ni<sub>4</sub>Ti<sub>3</sub> precipitates, no R-phase peak was formed in this transformation.

**Fig.4.1.14** shows Ni-Ti-Cu aged in 300<sup>0</sup>C at 72 hrs. DSC plot shows that R-phase was stabilized in this aged time.

**Fig:4.1.15** shows the DSC plot of the Ni-Ti sheet aged in 300<sup>0</sup>C at 96hrs. As temperature of the sample was 68<sup>0</sup>C and Af temperature of the sample was raised from 104<sup>0</sup>C, and the energy consumed in this transformation was 6.2 J/g. **Fig.4.1.20** shows the DSC plot of the Ni-Ti wire aged in 300<sup>0</sup>C at 96hrs. As temperature of the sample was 86<sup>0</sup>C



and Af temperature of the sample was raised from 127<sup>0</sup>C, and the energy consumed in this transformation was 6.2 J/g

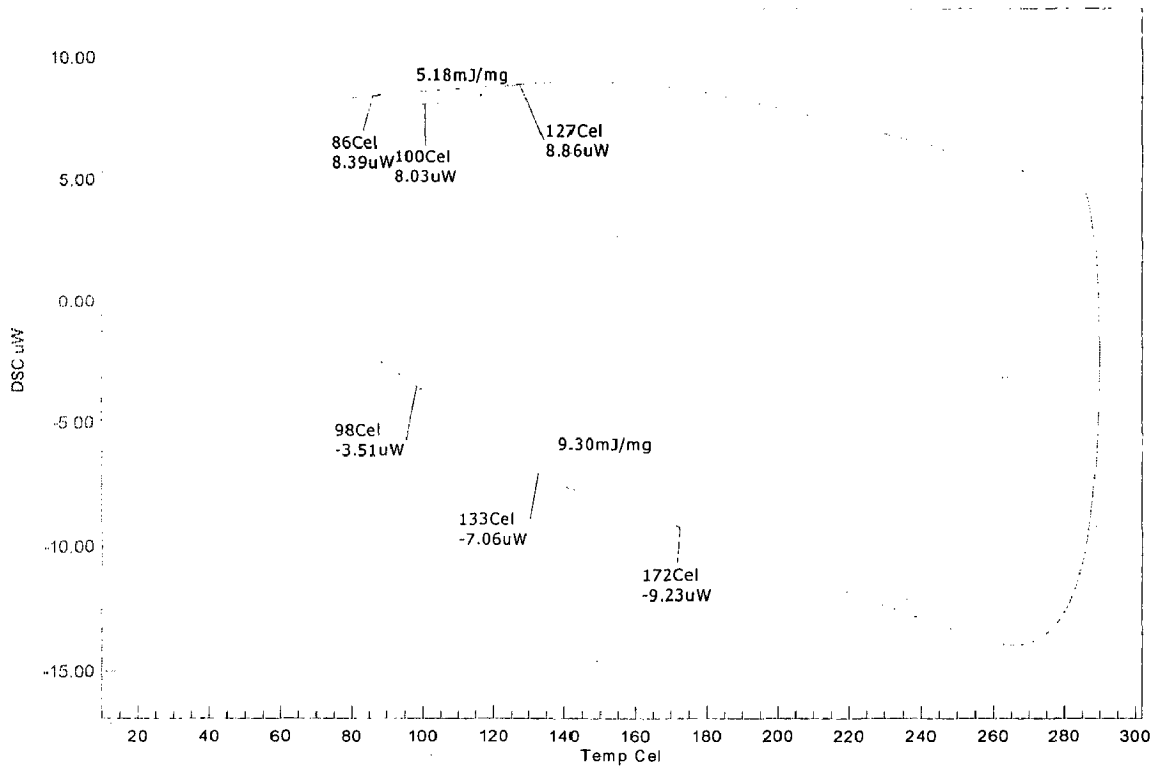
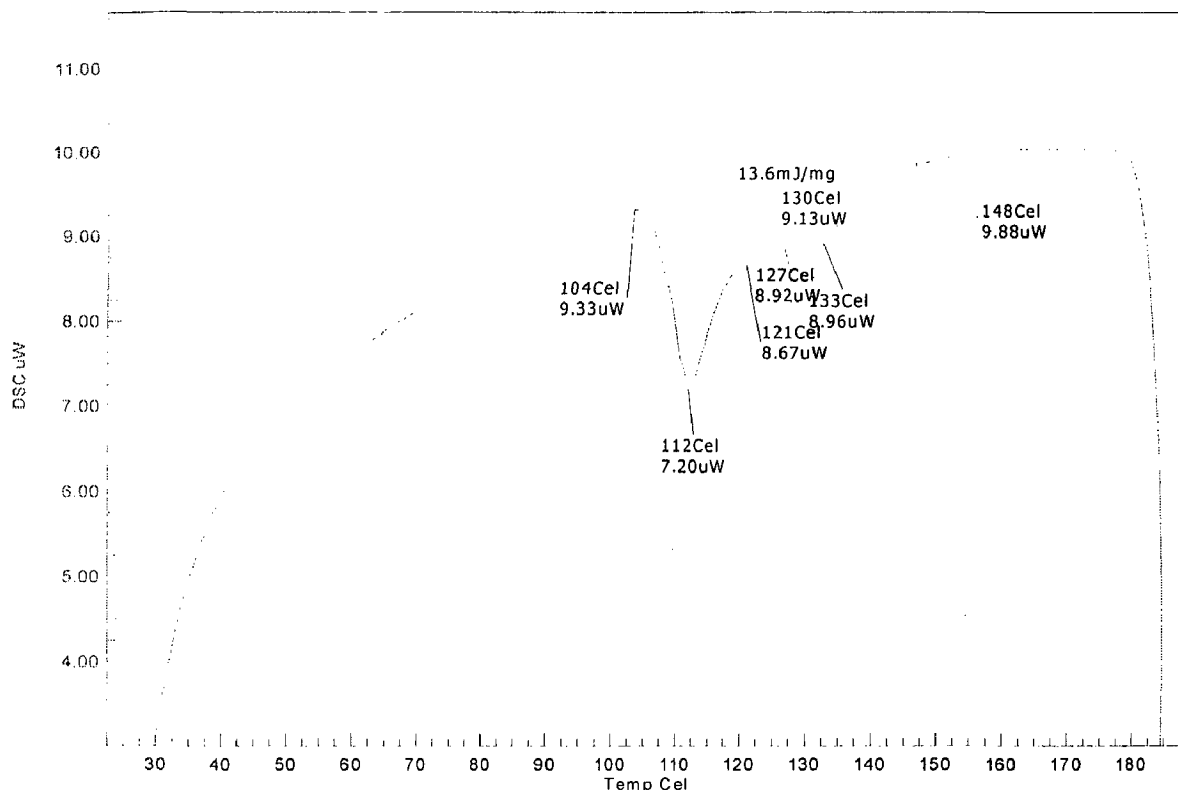


**Fig.4.1.20 DSC plot of the Ni-Ti wire aged in 300<sup>0</sup>C at 96hrs**

Fig-25 shows the DSC plot of the Ni-Ti-Cu aged in 300<sup>0</sup>C at 125 Hrs. Here, there is no second peak which corresponds to the formation of the R-phase. From this DSC plot, we may conclude that R-phase vanished due to over ageing. While, in over ageing R-phase Ni<sub>4</sub>Ti<sub>3</sub> precipitates were dissolved. So that R-phase peaks were not observed in this aged sample. We can not say anything about this, why R-phase peaks were disappeared in this prolonged aged sample. Peoples may think like that, due to over aged sample, grain size increases and for this reason R-phase was disappeared. Of course, grain size play very important role in SMA's to improve mechanical properties like pseudoelasticity etc., but I think, it will not play any role in R-phase transformation. Because R-phase transformations were entirely dependent upon the Ni<sub>4</sub>Ti<sub>3</sub> precipitates.

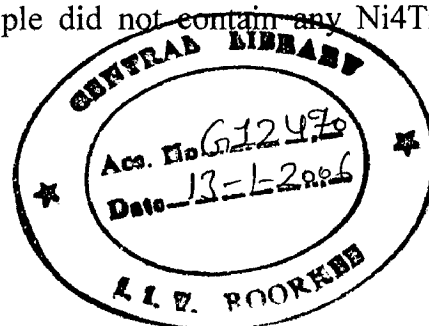
#### 4.1.6 DSC study of the effect of Annealing on the 30% cold reduced Ni-Ti wire.

DSC results of 30% deformed Ni-Ti SMA alloy annealed at different temperatures and different time intervals as shown in the figures-.



**Fig 4.1.21 DSC plot of the Ni-Ti annealed in 450°C at 10 minutes**

Fig 4.1.21 indicates DSC plot of the Ni-Ti annealed in 450°C at 10 minutes. There were two distinct peaks are appeared in this DSC plot. This two peaks are confirmed the formation of Ni<sub>4</sub>Ti<sub>3</sub> (Rhombohedral), R-Phase and B2 cubic (austenite) phase formation. The first peak corresponds to formation of R- peak and second peak B2-cubic phase on heating. Between first and second peak some intermediate peaks with low thermal hysteresis. Comparing with 30% cold reduced as drawn fresh wire. As temperature of the as drawn fresh wire was 128°C and Af = 153°C. There is no R-peak formed in as drawn fresh wire. This indicates that as drawn fresh wire sample did not contain any Ni<sub>4</sub>Ti<sub>3</sub> precipitates. [35-38]



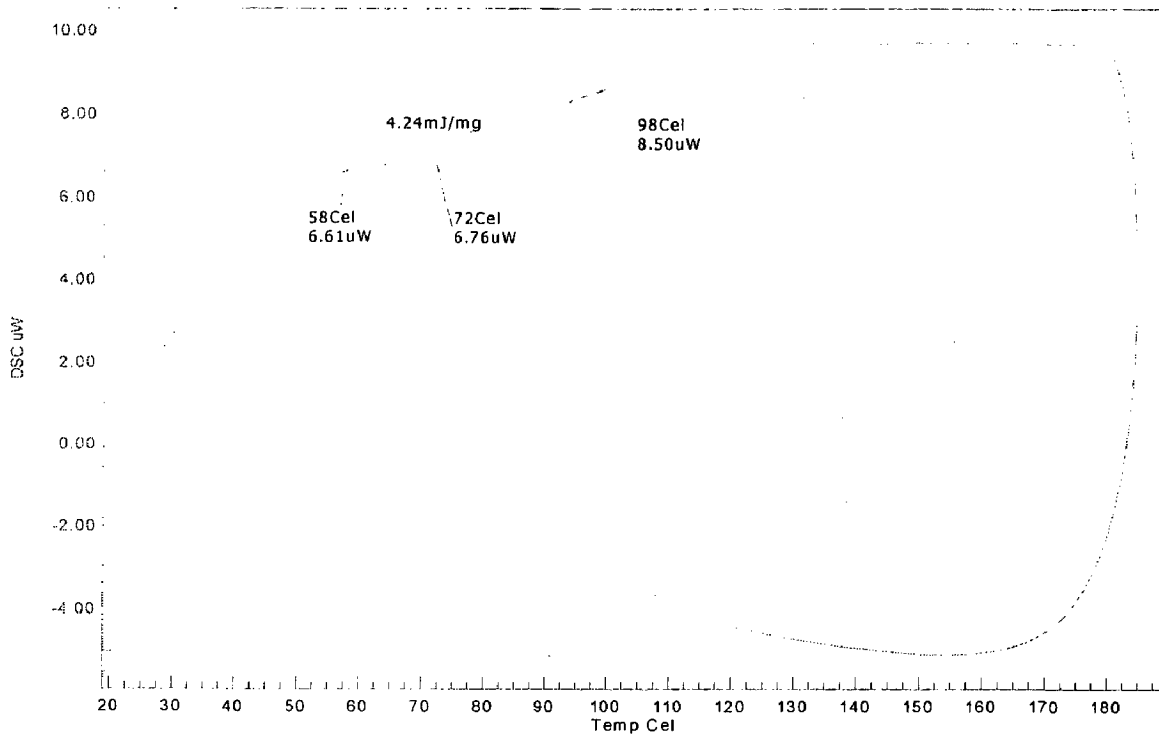


**Fig 4.1.22. DSC plot of the annealed in 500<sup>0</sup>C at 20 minutes Ni-Ti SMA**

The following sequences were followed in annealed 450<sup>0</sup>C at 10 minutes.

While heating: B19' (monoclinic) → R (Ni<sub>4</sub>Ti<sub>3</sub>) → B2 (Cubic)

While cooling: B2 (Cubic) → R → B19'. But as in the case of the 30% cold reduced wire sample: While heating: B19' → B2; While cooling: B2 → B19'. There is no formation of R-phase in the 30% cold reduced sample.

**Annealed 20 minutes at 500<sup>0</sup>C:**

Fig 4.1.22 shows DSC plot of the annealed in 500<sup>0</sup>C at 20 minutes Ni-Ti SMA with no R-phase peak only Austenite phase with the thermal hysteresis of this B2-phase transformation equal to 40<sup>0</sup>C.

The following results were interpreted in this DSC plot.

As=58<sup>0</sup>C and Af=90<sup>0</sup>C.

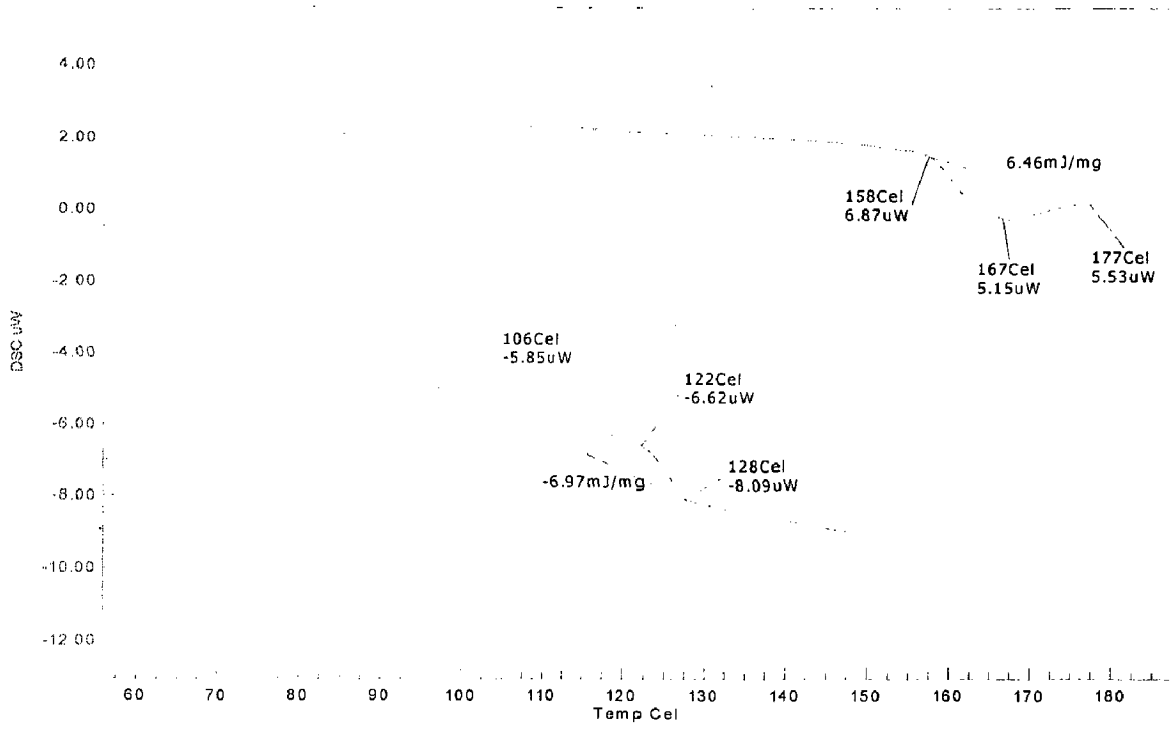


**Fig 4.1.22 DSC plot of the annealed in 500<sup>0</sup>C at 20 minutes Ni-Ti SMA**

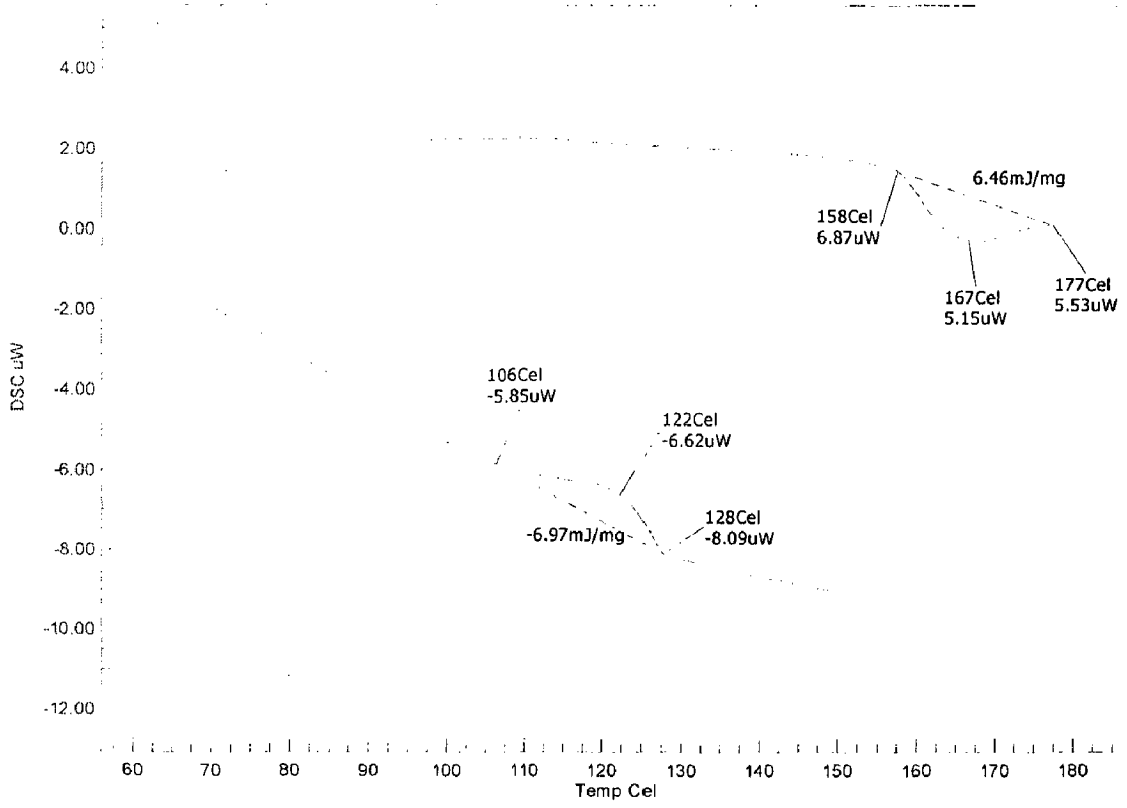


**Fig.4.1.23 DSC plot of the Ni-Ti as drawn SMA wire**

**Fig.4.1.23** show the DSC curve of the Ni-Ti as drawn SMA wire. As temperature of the sample was raised from 96<sup>0</sup>C (as received) to 158<sup>0</sup>C Ni-Ti (30 % cold reduced as drawn) sample. Ms Temperature of the as-quenched sample was raised very high values 128<sup>0</sup>C. Transformation hysteresis in the austenite phase transformation was 19<sup>0</sup>C and Martensite phase transformation was 22<sup>0</sup>C.

### Thermal cycling Methods:

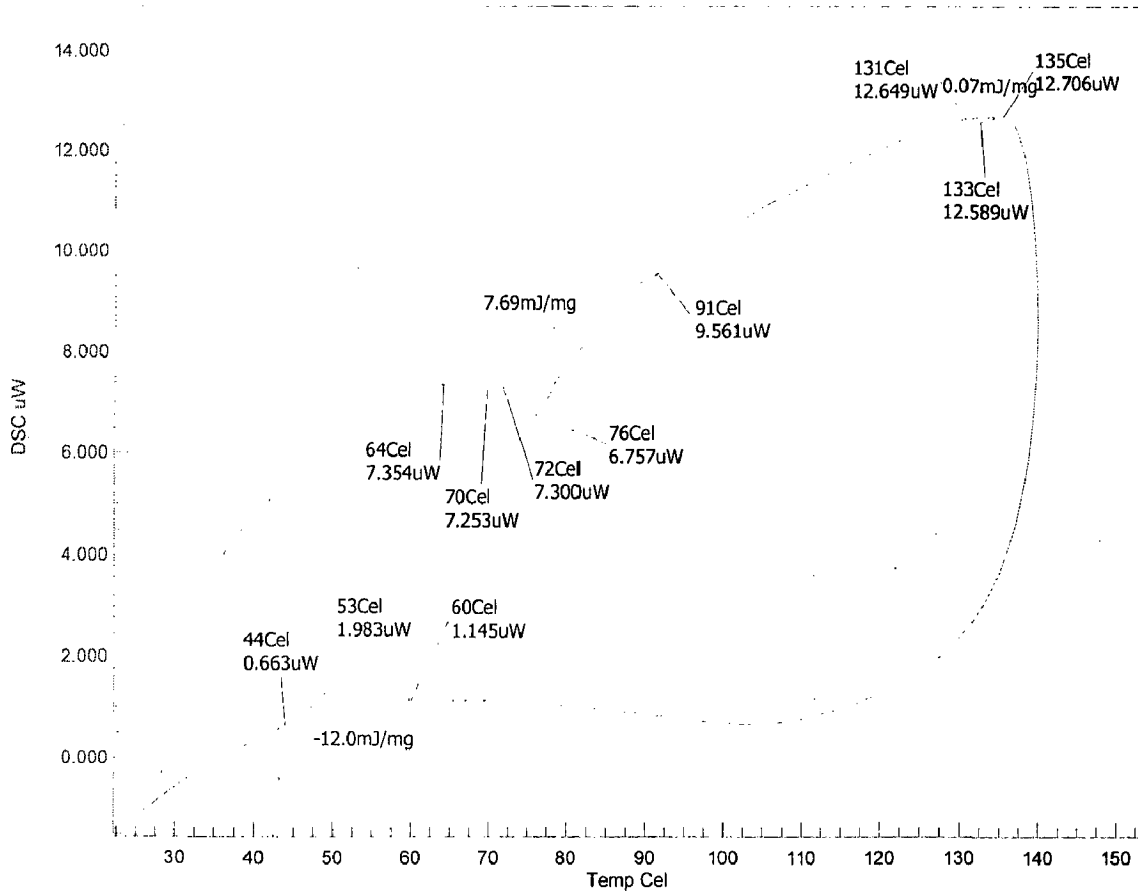


**Fig.4.1.24 DSC plot of the Ni-Ti-Cu Shape memory trained specimen.**

Fig.4.1.24 shows the Ni-Ti-Cu specimen as quenched from 850<sup>0</sup>C and given thermal cycles with the help of the constant current source (1 A current in 1.5 minutes), after 1.5 minutes cooling will occur. While thermal cycled wire showing the R-phase transformations, it will be very useful for designing the actuators in Fighter craft.

R1,s = 64<sup>0</sup>C R1,f=72<sup>0</sup>C R2,s=72<sup>0</sup>C R2,f=91<sup>0</sup>C, As=131<sup>0</sup>C and Af=135<sup>0</sup>C.



## 4.2 XRD analysis

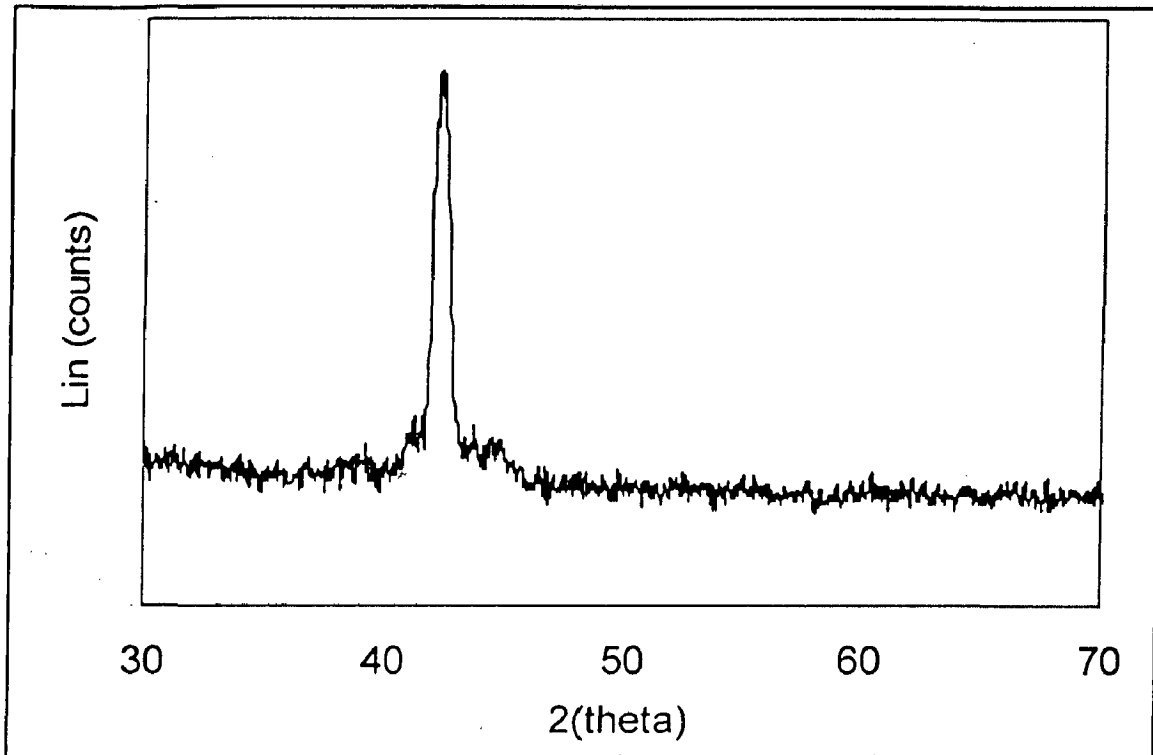
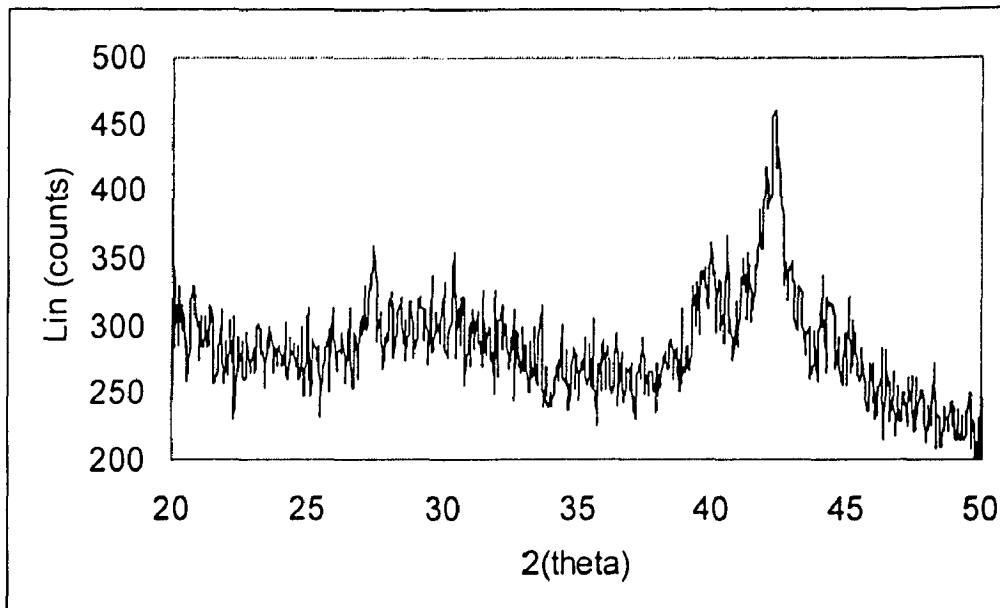


Fig-4.2.1 XRD spectra of the Ni-Ti aged in 300<sup>0</sup>C at 125 hrs.

Fig 4.2.1 shows XRD spectra of the Ni-Ti aged in 300<sup>0</sup>C at 125Hrs. Only one major peak was appeared in this spectra corresponds to the formation of Ni<sub>4</sub>Ti<sub>3</sub> precipitates (R-phase, Rhombohedral crystal structure) in (122) plane.

a=11.235 Å c=5.0789 Å C=.4521 S.G= R3(148).



**Fig.4.2.2 XRD spectra of the Ni-Ti aged in 500<sup>0</sup>C at 24 hrs.**

Fig.4.2.2 shows the XRD spectra of the Ni-Ti aged in 500<sup>0</sup>C at 24 hrs.

$d=2.13287\text{\AA}$  corresponds to the formation of the R-phase with (011) plane, Ni<sub>4</sub>Ti<sub>3</sub> precipitation.

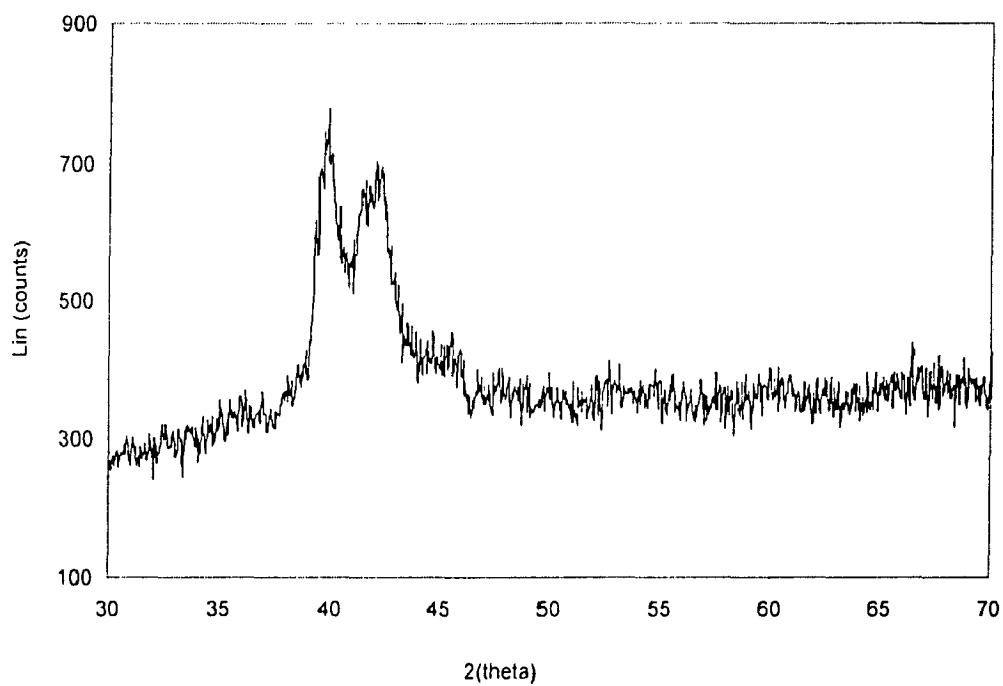


**Fig.4.2.3 XRD spectra of the Ni-Ti-Cu aged in 400<sup>0</sup>C at 50 hrs**

Fig.4.2.3 shows XRD spectra of the Ni-Ti-Cu aged in 400<sup>0</sup>C at 50 hrs. (011)R,(202) B19' (monoclinic) phases were appeared

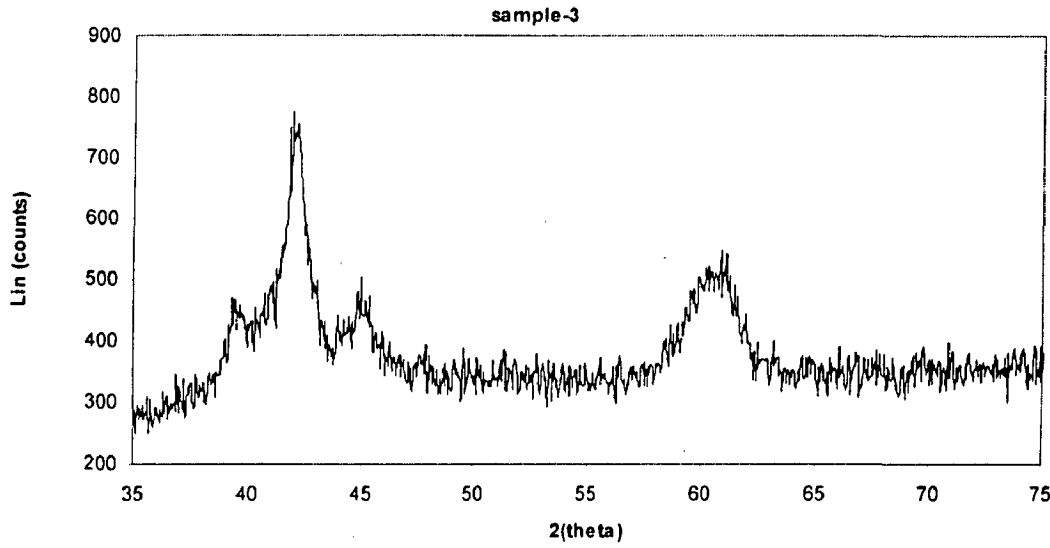


Fig.4.2.4 XRD spectra of the Ni-Ti aged in 500<sup>0</sup>C at 150 hrs.

$d=2.13287\text{\AA}$  corresponds to the formation of the R-phase with (011) plane, Ni<sub>4</sub>Ti<sub>3</sub> precipitation

$d=2.01 \rightarrow$  NiTi monoclinic B19' martensites in (012).

$d=2.29$  NiTi monoclinic B19' martensitic structure in (002)

$d=1.53 \rightarrow$  NiTi monoclinic B19' martensitic structure in (003).

In this XRD spectrum 3 monoclinic phases were observed.

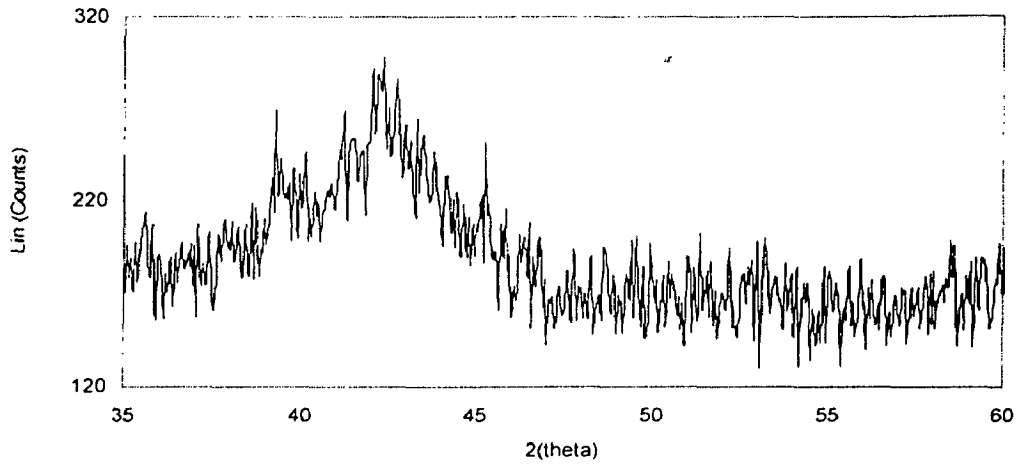


**Fig.4.2.5 XRD spectra of the Ni-Ti-Cu aged in 400<sup>0</sup>C at 72 hrs.**

Fig.4.2.5 shows the XRD spectra of the Ni-Ti-Cu aged in 400C at 72 hrs.  $d=2.13287\text{\AA}$  corresponds to the formation of the R-phase with (011) plane,  $\text{Ni}_4\text{Ti}_3$  precipitation.

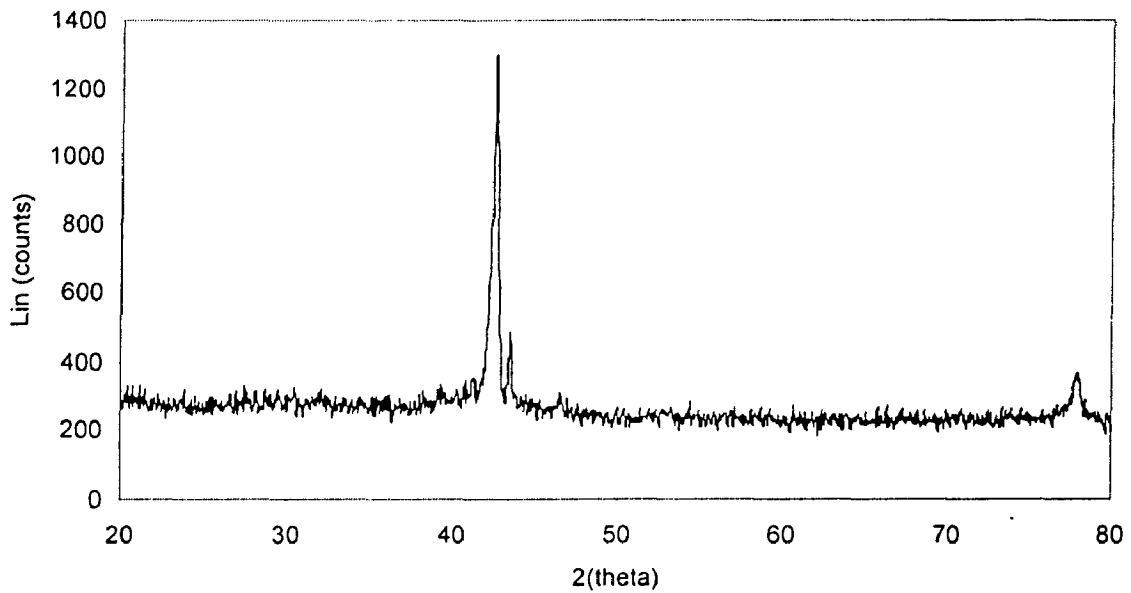


**Fig.2.4.6 XRD spectra of the Ni-Ti-Cu as quenched from 850<sup>0</sup>C.**

Fig 2.4.6 shows XRD spectra of the Ni-Ti-Cu as quenched form B2 structure. There is the only one peak available, represented the formation of the B2 cubic crystal structure. B2 structure was retained at room temperature. S.G-Pm3m (110)<sub>B2</sub>

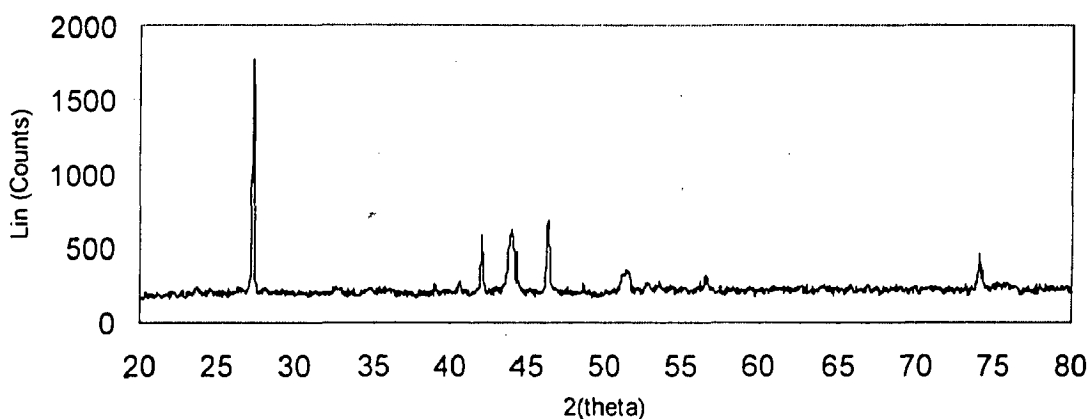


Fig.2.4.7. XRD spectra of the Ni-Ti aged in 300<sup>0</sup>C at 72 hrs.

Fig 4.2.7 shows the XRD spectra of the Ni-Ti aged 300<sup>0</sup>C at 72 hrs.

$d=2.14293\text{Å}^0$  correspond to the formation of the R-phase R(011) with Rhombohedral crystal structure (Ni<sub>4</sub>Ti<sub>3</sub>).

$d=1.9587\text{Å}^0$  indicates hexagonal R-phase transformation in (202) plane.

$d=2.054\text{Å}^0$  represents to the formation of the Ni<sub>4</sub>Ti<sub>3</sub> precipitates R-phase in (111) plane.

There is no peak available for monoclinic B19' [crystal structure]. So we may conclude that the B19' phase peak occurred below the room temperature.  $d=2.217\text{Å}^0$  corresponds to the formation of hexagonal Ni<sub>3</sub>Ti phase.

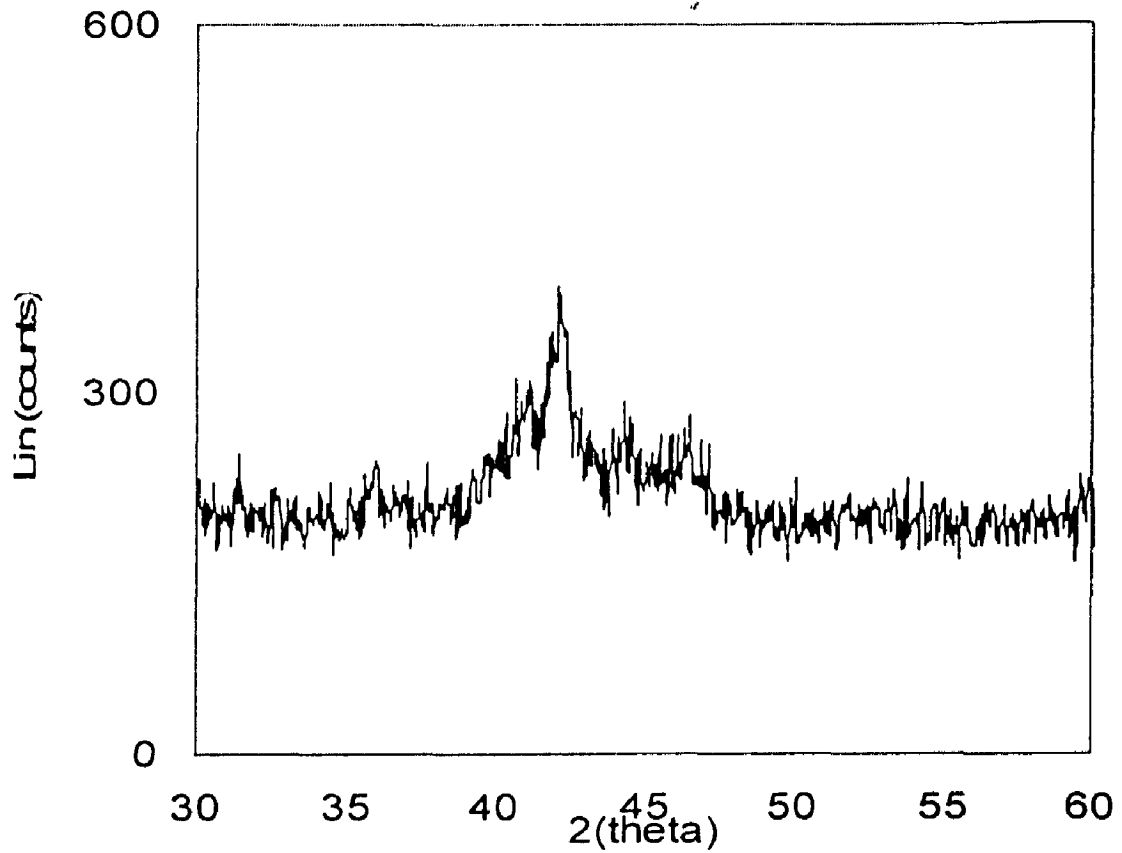


**Fig.2.4.8. XRD spectra of the Ni-Ti-Cu aged in 500<sup>0</sup>C at 48 hrs.**

Fig.2.4.8 shows XRD spectra of the Ni-Ti-Cu aged in 500<sup>0</sup>C at 48 hrs. (011)R, (202) H phases were appeared in the diffraction peak profile.

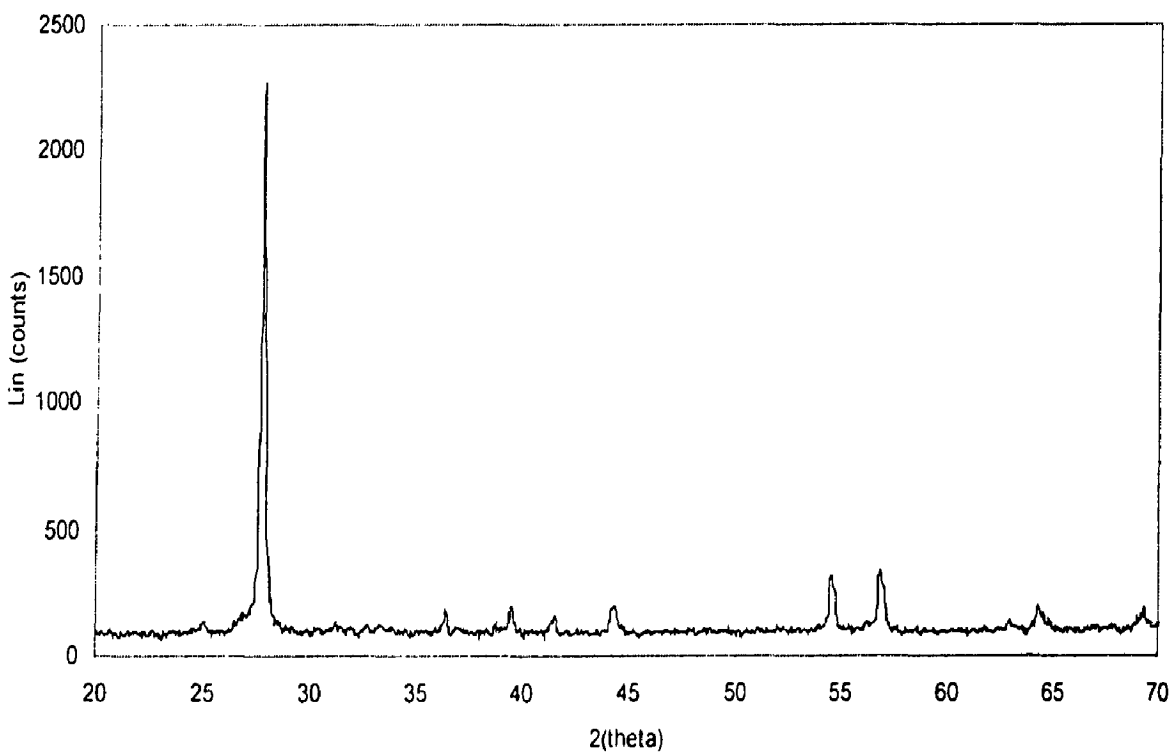


Fig.2.4.9 shows XRD spectra of the Ni-Ti as quenched from 850°C. (011)R, (020)-B19' phases were presents in this diffraction profile.

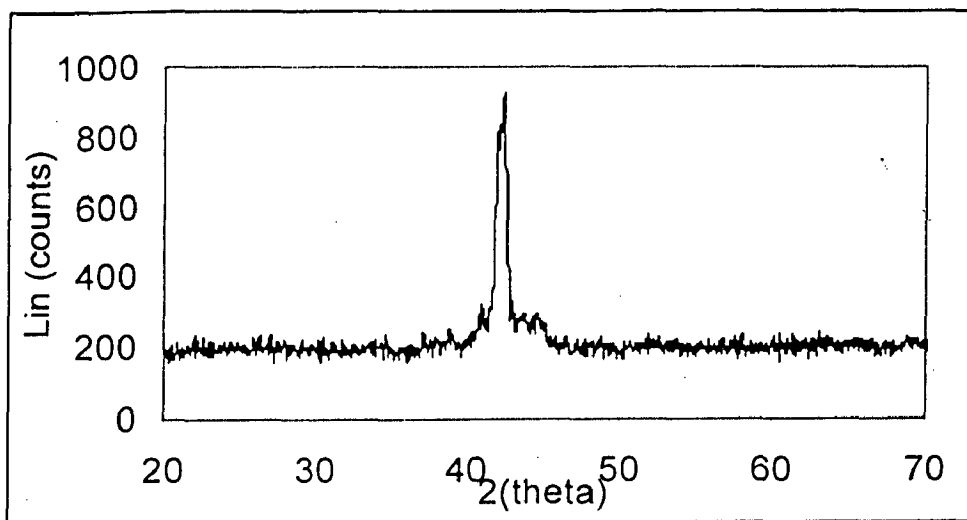


Fig.4.2.10 XRD spectra of the 30% cold worked annealed in 400°C at 20 minutes in NiTi SMA.

$d=2.13287\text{\AA}$  corresponds to the formation of the R-phase with (011) plane,  $\text{Ni}_4\text{Ti}_3$  precipitation.  $d=2.03012\text{\AA}$  represents to the formation of the NiTi Monoclinic B19' martensite phase.  $d= 2.20317 \rightarrow$  NiTi M (012), Monoclinic, B19' structure. So, the annealed 20 minutes in 400°C XRD spectra having R-phase and B19' phase.

2-51

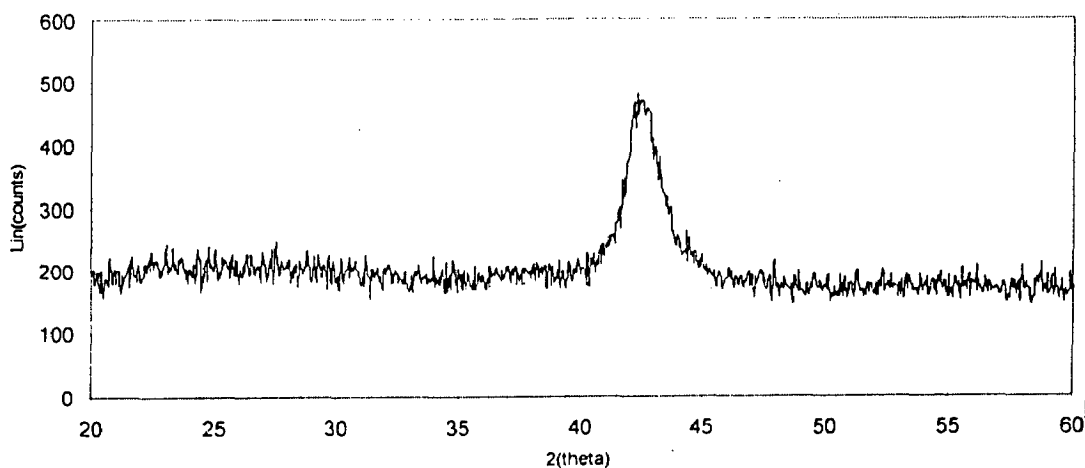
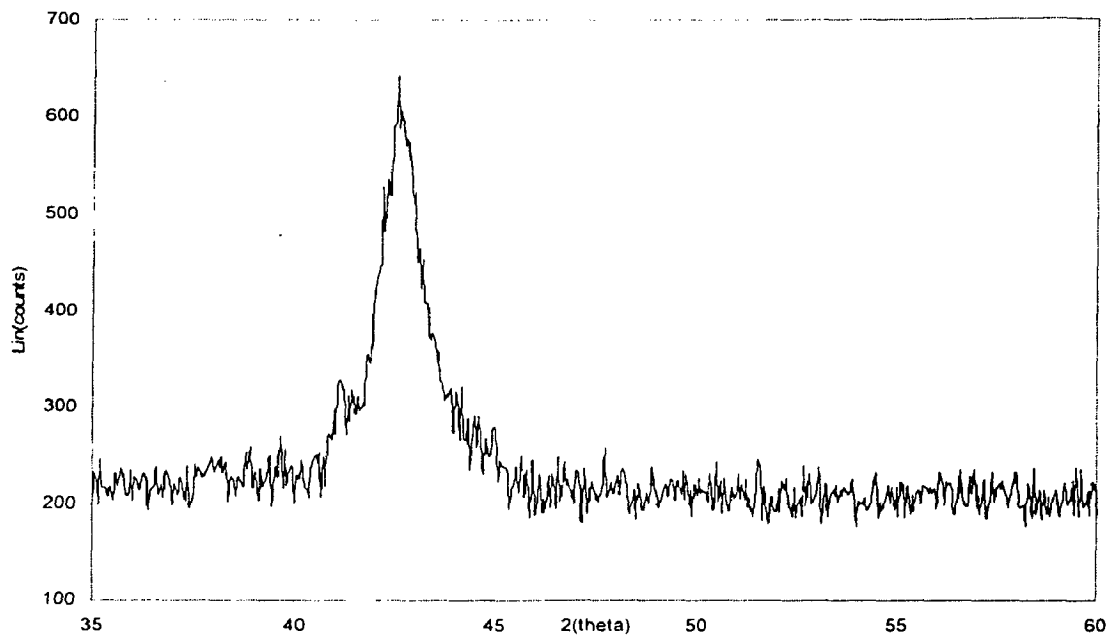
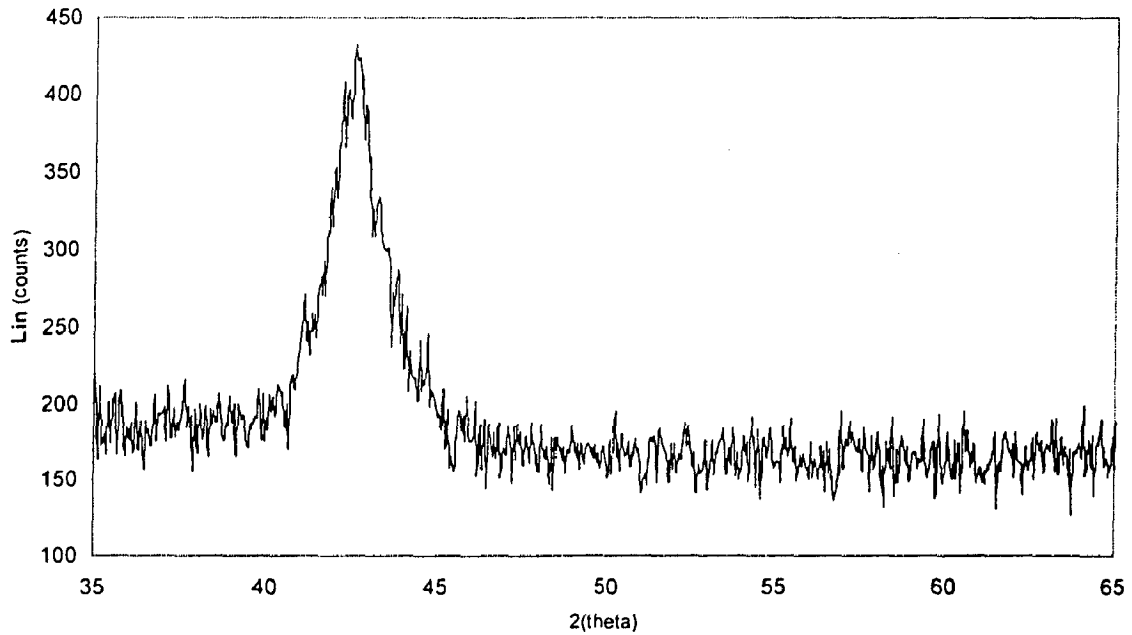


Fig.4.2.10-1 XRD spectra of the 5% reduced (strained) in Ni-Ti-Cu SMA.



**Fig 4.2.10-2 XRD spectra of the 10% strained (Cold reduced) Ni-Ti-Cu SMA.**



**Fig 4.2.10-3 XRD spectra of the 15% strained (Cold reduced) Ni-Ti-Cu SMA.**



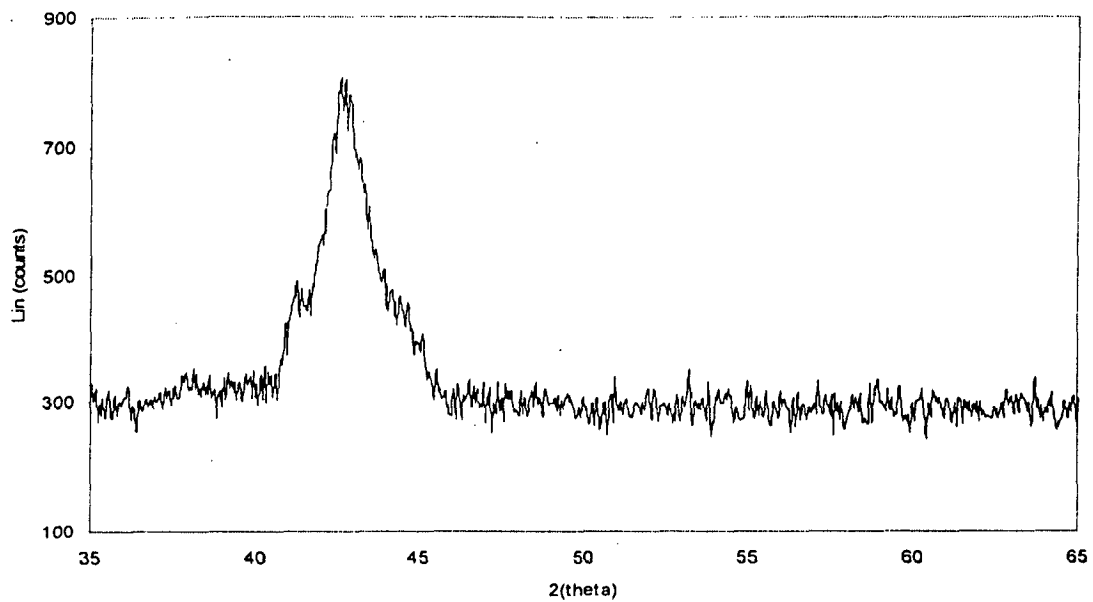


**Fig 4.2.10-4 XRD spectra of the 20% strained (Cold reduced) Ni-Ti-Cu SMA.**

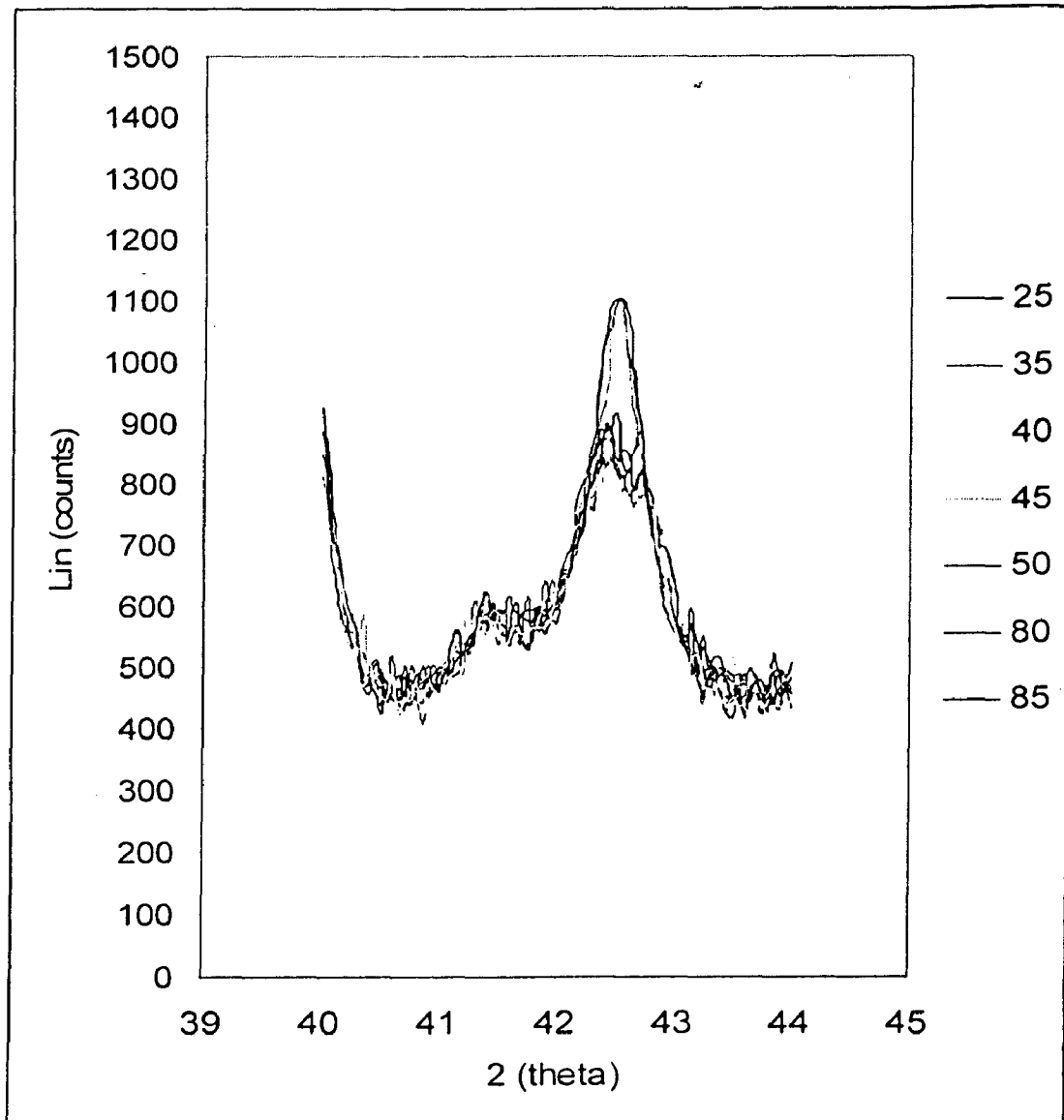


**Fig 4.2.10-5 XRD spectra of the 5%, 10%, 15% and 20% strained Ni-Ti-Cu SMA.**

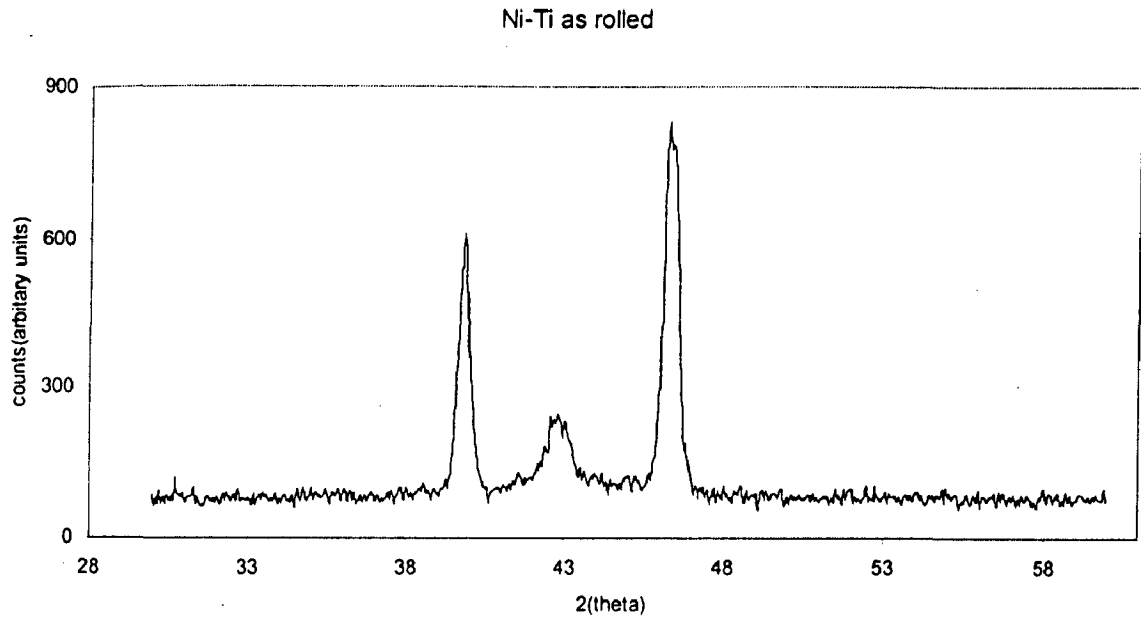


**Fig.4.2.11-1 High temperature (80<sup>0</sup>C) XRD spectra of the Ni-Ti as rolled sheet.**

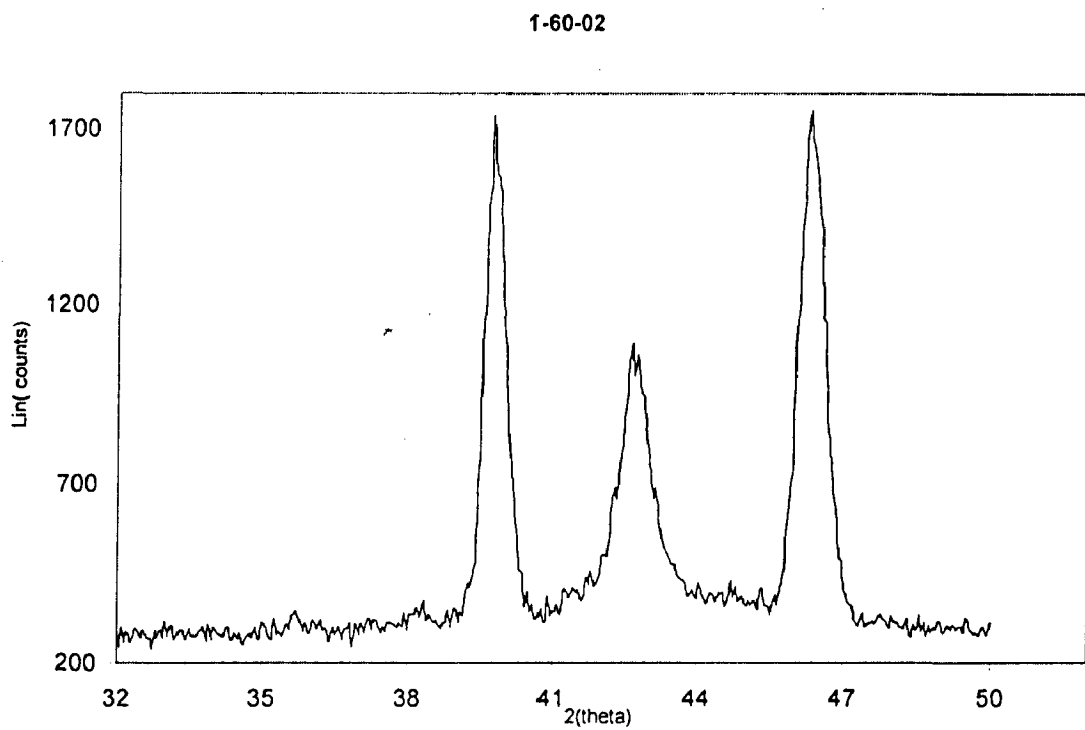


**Fig.4.2.11-2 High temperature (120<sup>0</sup>C) XRD spectra of the Ni-Ti as rolled sheet.**

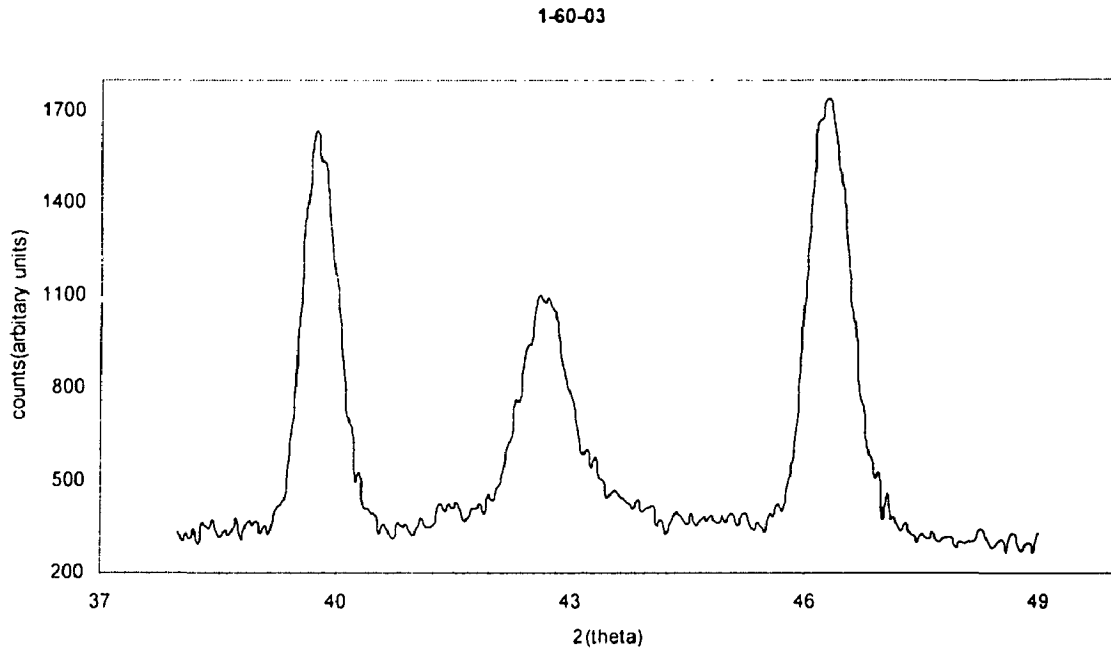


Fig.4.2.11-3 shows high temperature (150<sup>0</sup>C) XRD spectra of the Ni-Ti as rolled sheet.

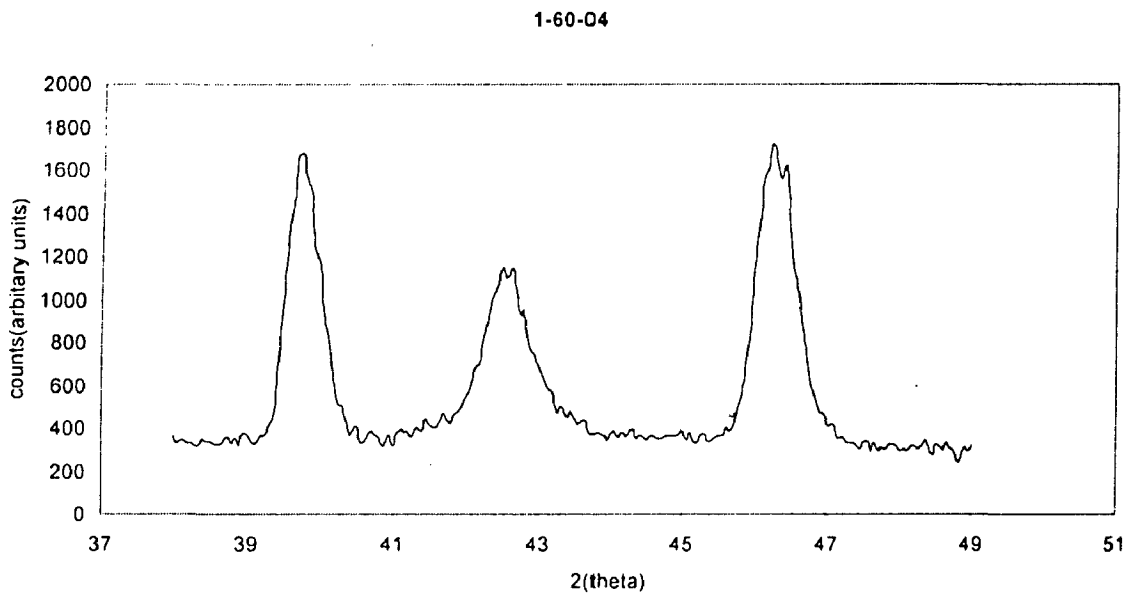


Fig.4.2.11-4 shows high temperature (200<sup>0</sup>C) XRD spectra of the Ni-Ti as rolled sheet.

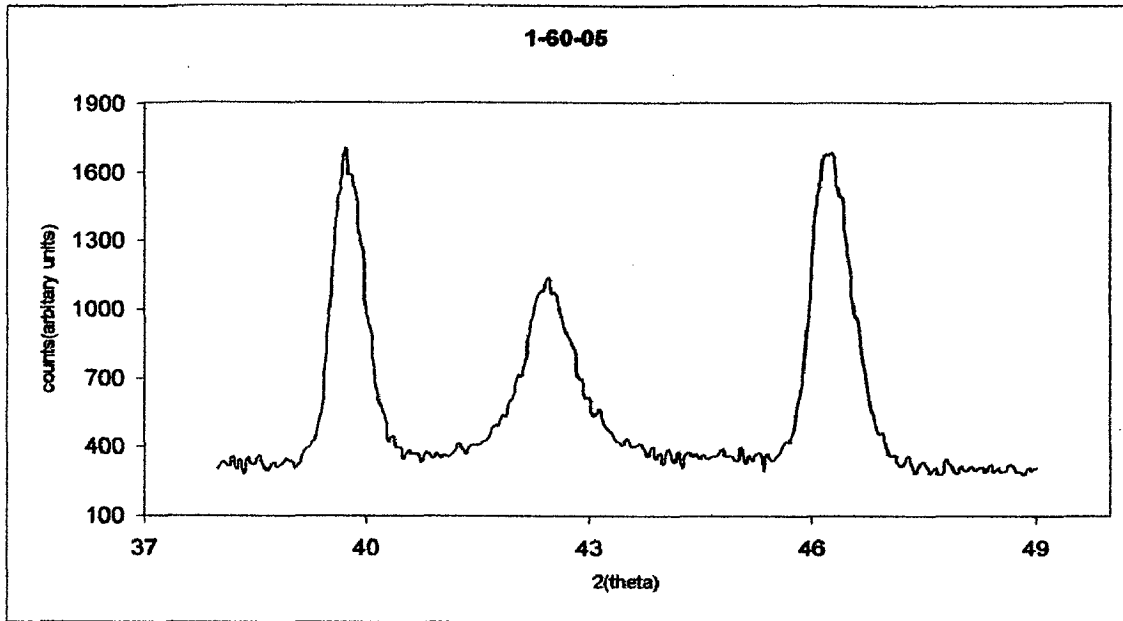


Fig.4.2.11-5 shows high temperature (250°C) XRD spectra of the Ni-Ti as rolled sheet.

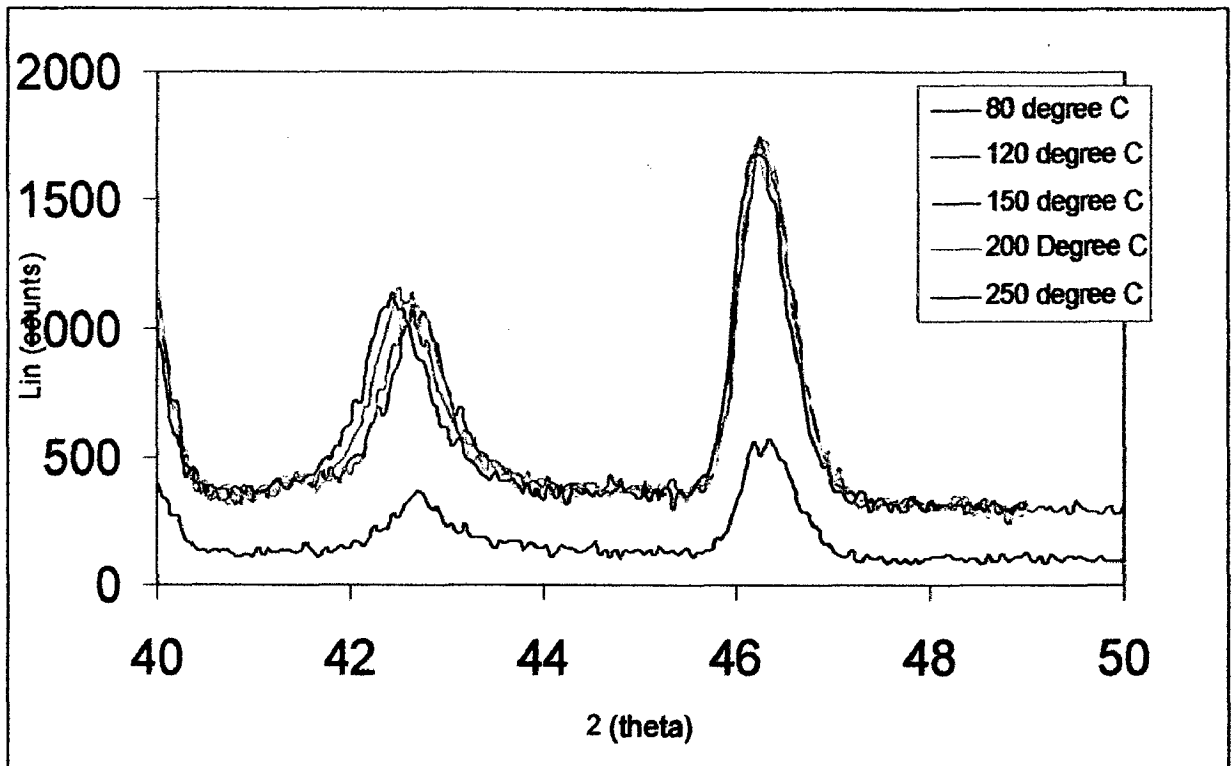


Fig 4.2.11- 6 shows all of the above Ni-Ti as rolled high temperature XRD Spectra is super imposed.

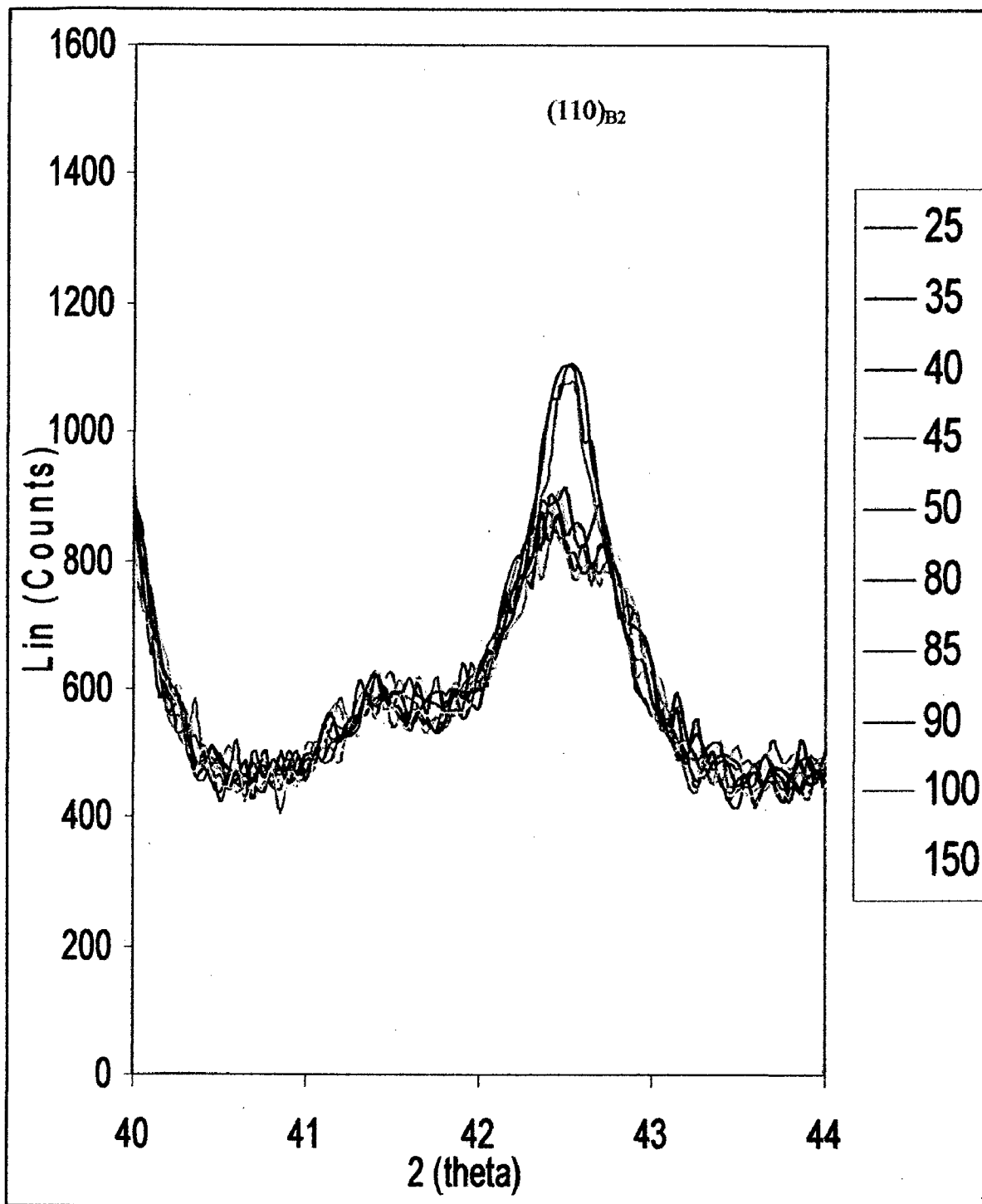


Fig.4.2.12 high temperature XRD spectra of the Ni-Ti aged in 500°C at 48 hrs sample.

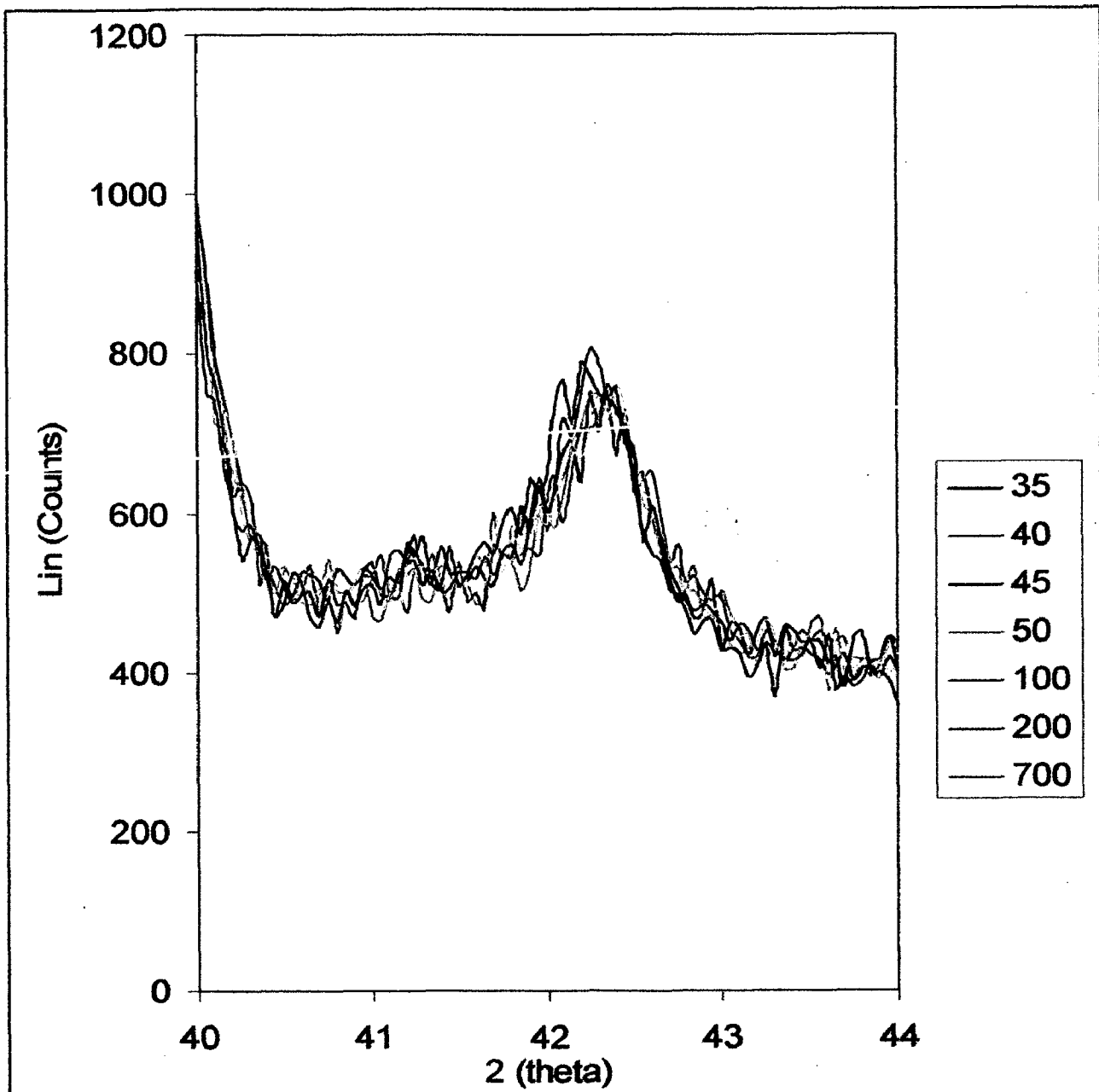


Fig.4.2.13 High temperature XRD spectra of the Ni-Ti-Cu aged 500°C at 48 hrs sample.

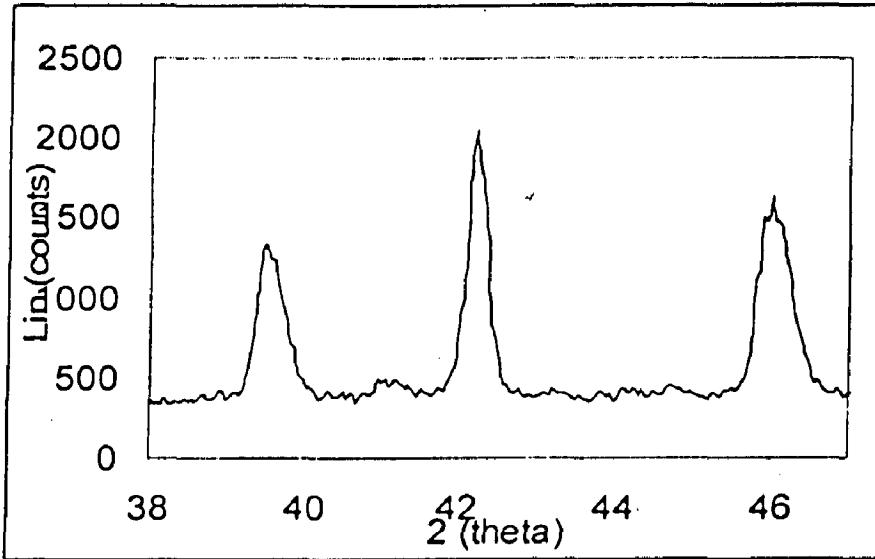


Fig.4.2.13-1 high temperature was carried out 700<sup>0</sup>C XRD spectra of the Ni-Ti -Cu aged 500<sup>0</sup>C at 48 hrs sample.

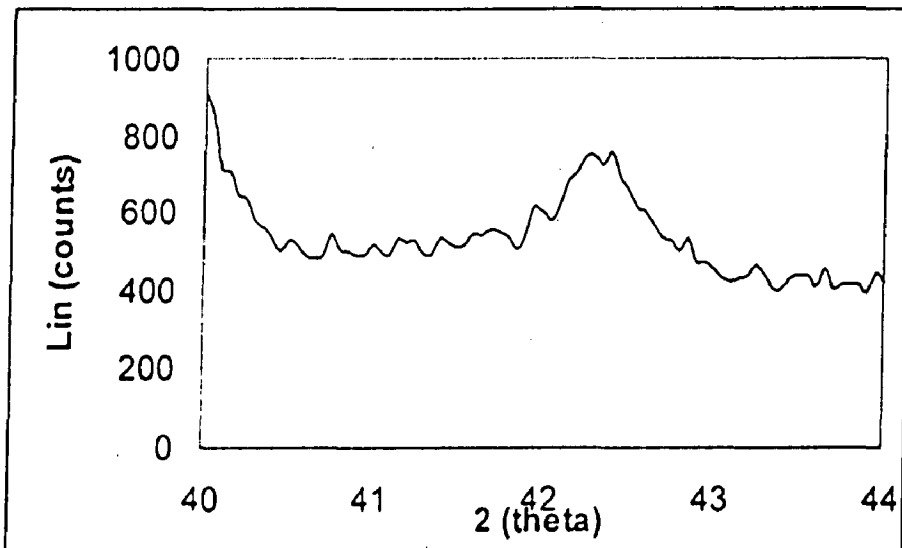


Fig.4.2.13-2 XRD spectra was performed in 35<sup>0</sup>C XRD spectra of the Ni-Ti -Cu aged 500<sup>0</sup>C at 48 hrs sample.



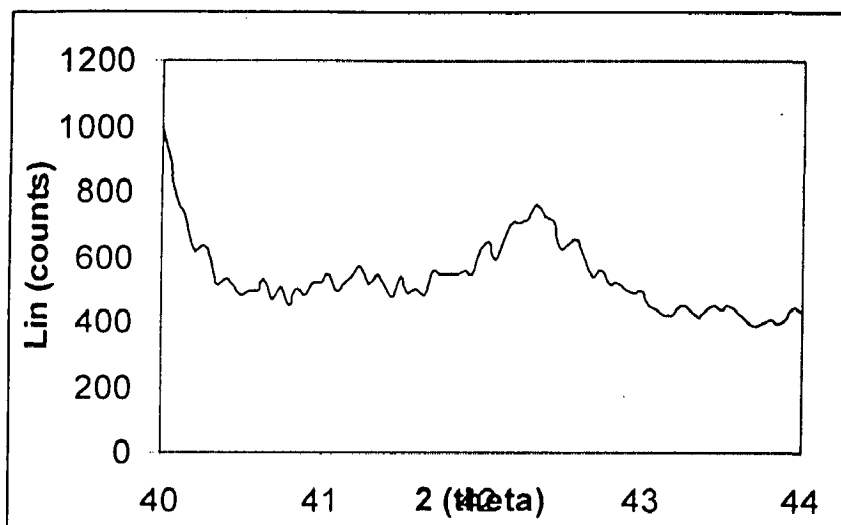


Fig.4.2.13-3 XRD spectra was performed in 40<sup>0</sup>C XRD spectra of the Ni-Ti -Cu aged 500<sup>0</sup>C at 48 hrs sample.

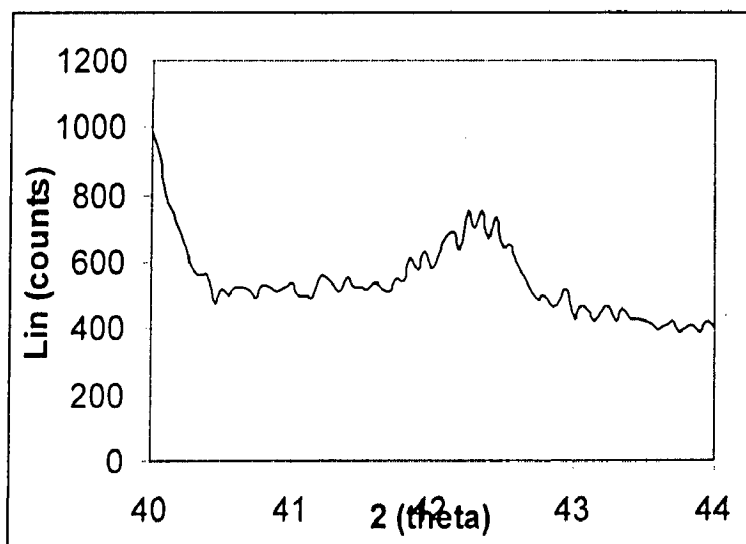


Fig.4.2.13-4 XRD spectra was performed in 45<sup>0</sup>C XRD spectra of the Ni-Ti -Cu aged 500<sup>0</sup>C at 48 hrs sample.

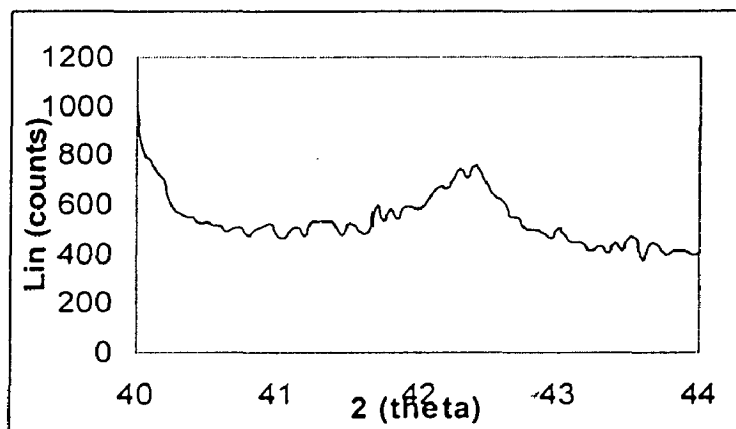


Fig.4.2.13-5 XRD spectra was performed in 50<sup>0</sup>C XRD spectra of the Ni-Ti –Cu aged 500<sup>0</sup>C at 48 hrs sample.

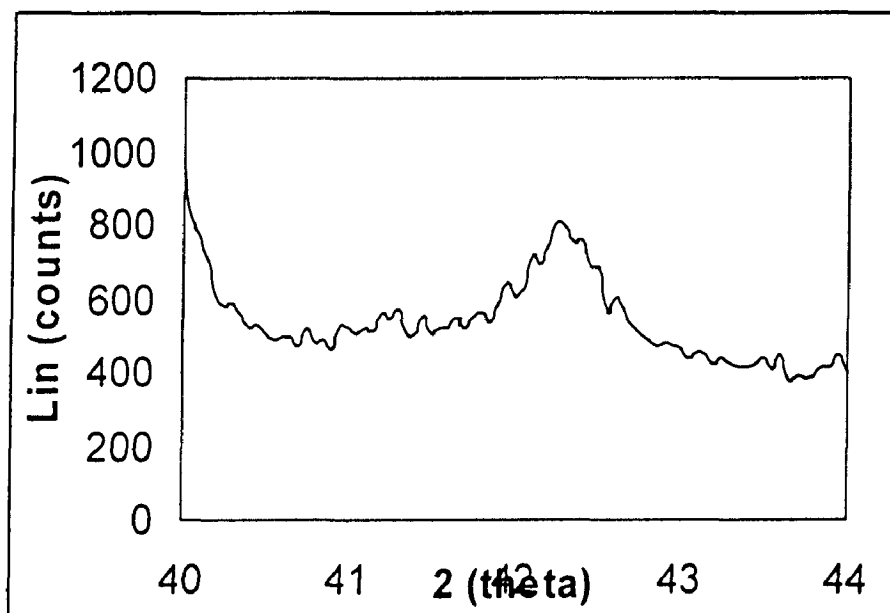


Fig.4.2.13-6 XRD spectra was performed in 60<sup>0</sup>C XRD spectra of the Ni-Ti –Cu aged 500<sup>0</sup>C at 48 hrs sample.

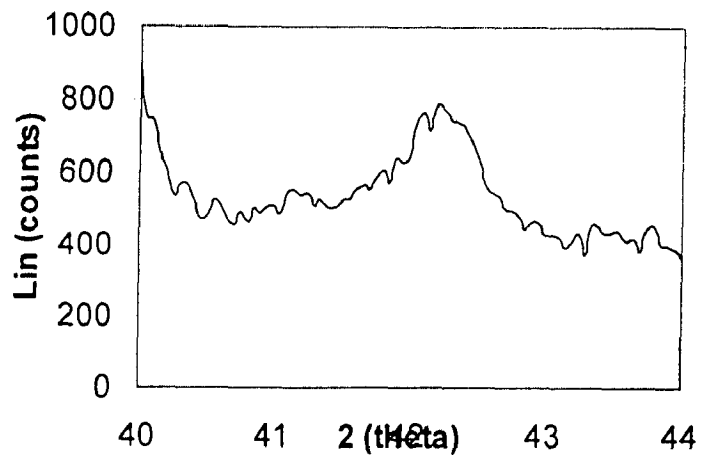


Fig.4.2.13-7 XRD spectra was performed in 100<sup>o</sup>C XRD spectra of the Ni-Ti -Cu aged 500<sup>o</sup>C at 48 hrs sample.

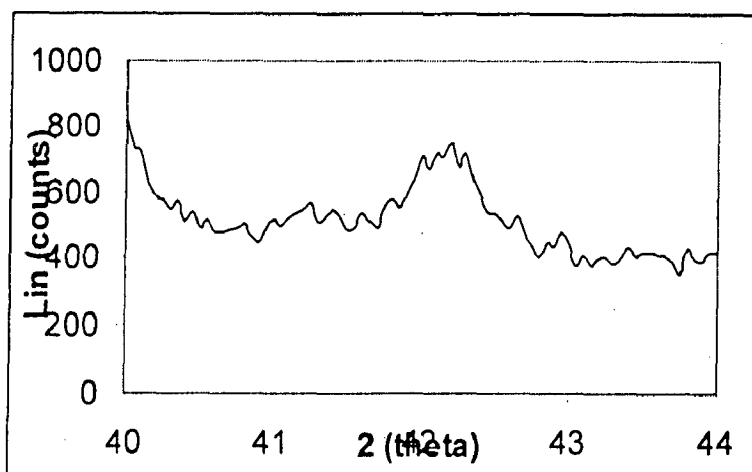


Fig.4.2.13-8 high temperature was carried out 150<sup>o</sup>C XRD spectra of the Ni-Ti -Cu aged 500<sup>o</sup>C at 48 hrs sample.

### 4.3. Optical microscopy study:

Optical microscopy is one of tool to characterize the SMA. But the limitations in this tool are, not used to identify the phase transformation mechanism through microstructural changes with out hot stage. Any how, we used for this study to study the martensite needles, response of rolling and Stress induced twin re-arrangement.

#### 4.3.1. Effect of rolling on the microstructural changes in Ni-Ti-Cu:

Series of optical microstructures shows the effect of rolling on the Ni-Ti-Cu SMA. In Fig.4.3.1 to 4.3.5 shows some rolling textures on the surface of the specimen. Hot rolling was carried with in the single pass rolling mill. The rolling temperature was 800<sup>0</sup>C. Fig.4.3.6 shows the last reduction was performed with intermediate annealing in 500<sup>0</sup>C at 5 minutes. Martensite needles were appeared in this microstructure.

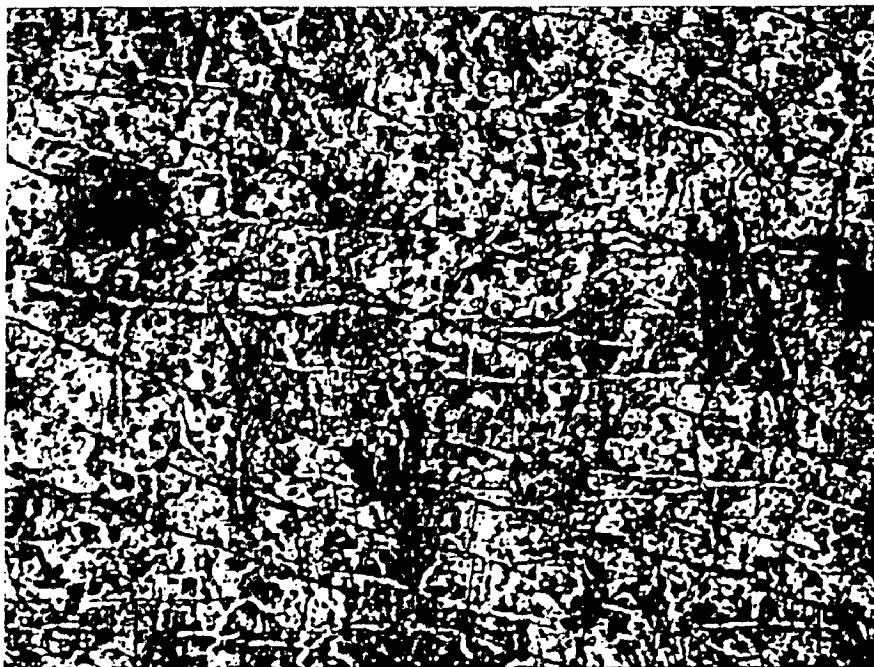


Fig.4.3.1 shows the effect of 10% reduction rolling on Ni-Ti-Cu SMA reduced (Magnification: 100X).

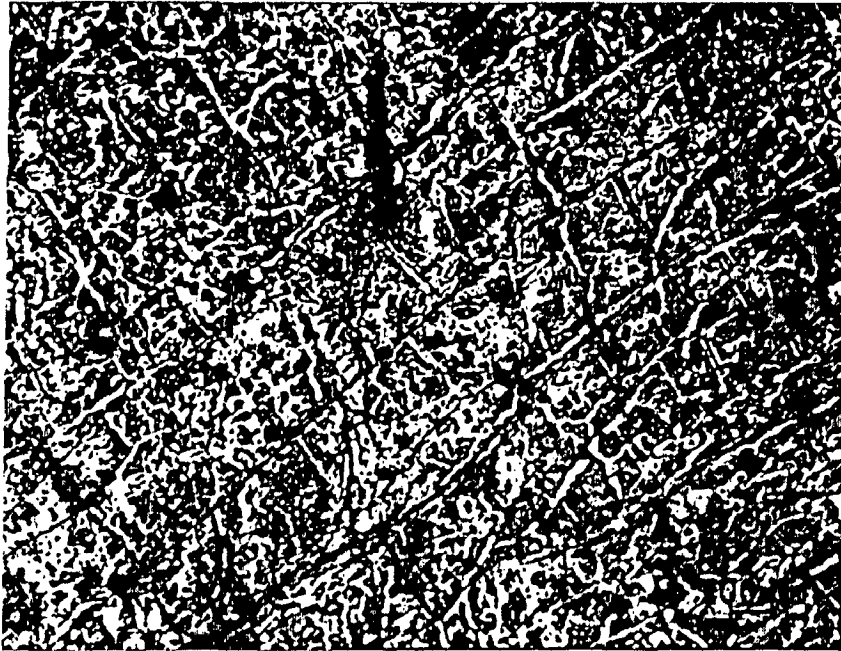
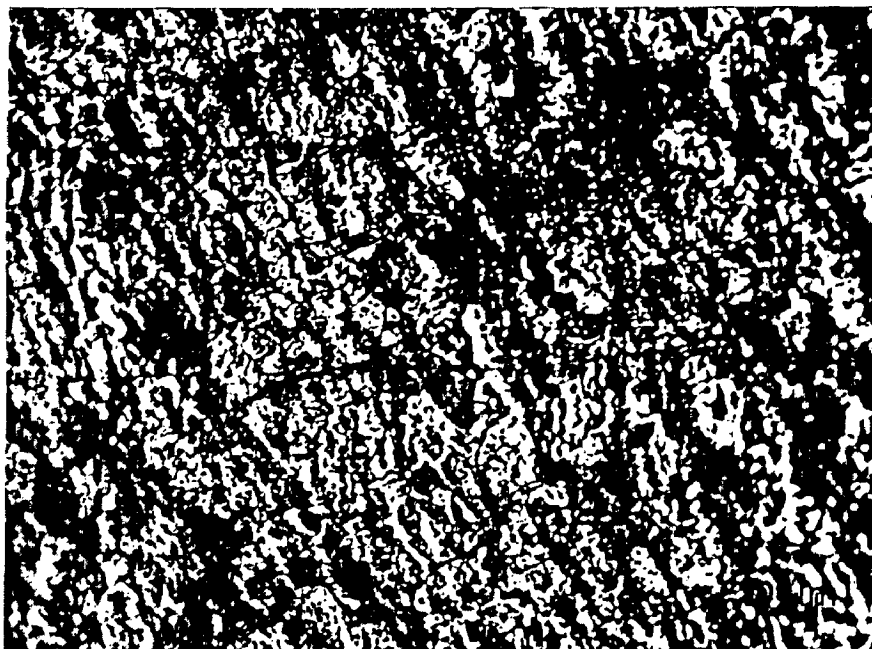


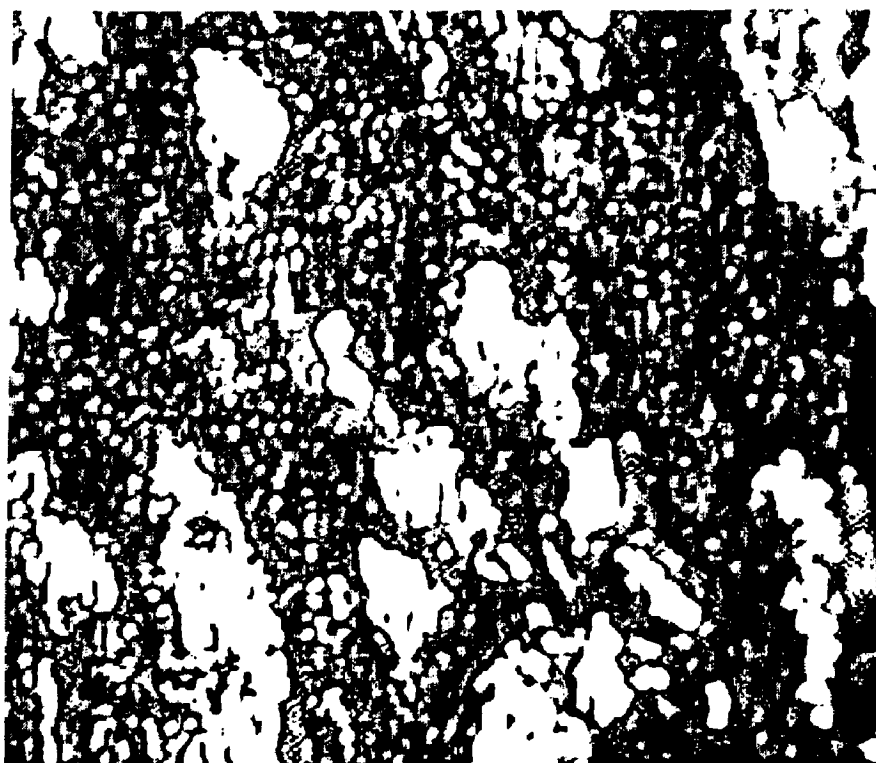
Fig.4.3.2 shows the effect of 20% reduction rolling on Ni-Ti-Cu SMA reduced  
(Magnification: 100X)



Fig.4.3.3 shows the effect of 30% reduction rolling on Ni-Ti-Cu SMA reduced  
(Magnification: 100X)



**Fig.4.3.4** shows the effect of 40% reduction rolling on Ni-Ti-Cu SMA reduced  
(Magnification: 100X)



**Fig.4.3.5** shows the effect of 50% reduction rolling on Ni-Ti-Cu SMA reduced  
(Magnification: 100X)

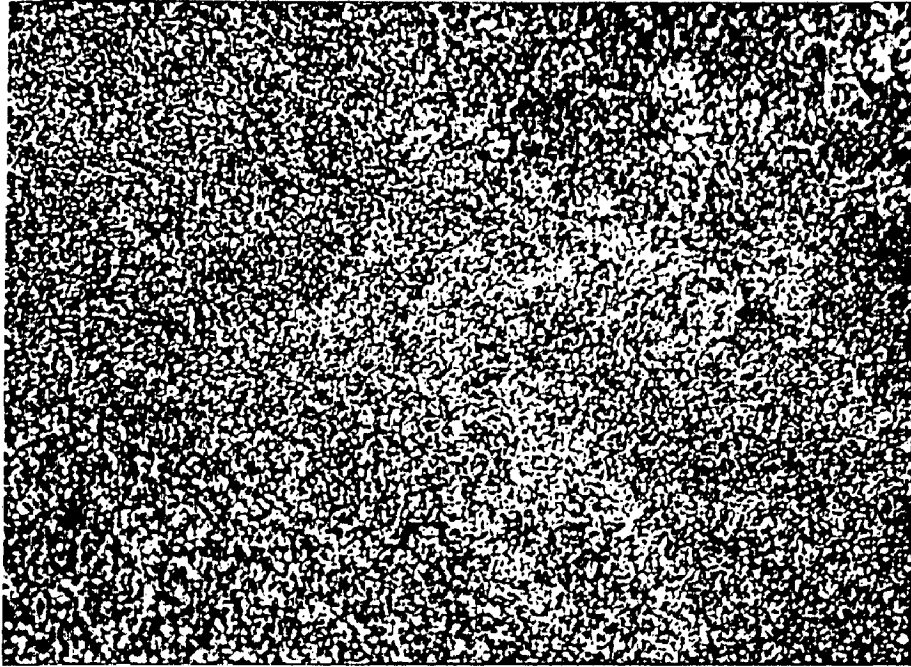


**Fig.4.3.6 shows the effect of 95% reduction (Final) rolling on Ni-Ti-Cu SMA reduced (Magnification: 100X)**

**Effect of rolling on the microstructural changes in Ni-Ti as rolled:**

A series of the optical microstructures were performed in after rolling. This was shown in Fig.4.3.7 to 4.3.8. All these microstructures were taken in after hot rolling.

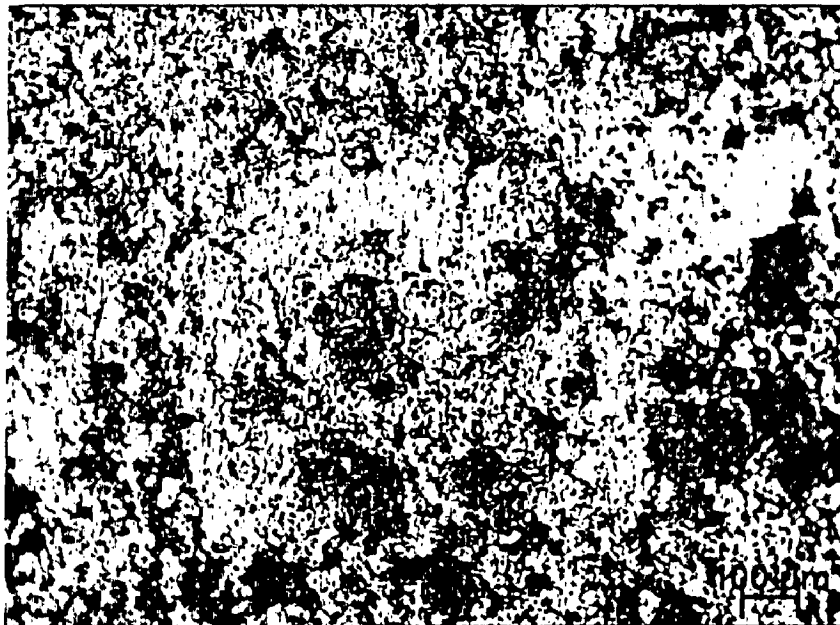


**Fig.4.3.7 shows the effect of 40% reduction rolling on Ni-Ti SMA reduced (Magnification: 100X)**

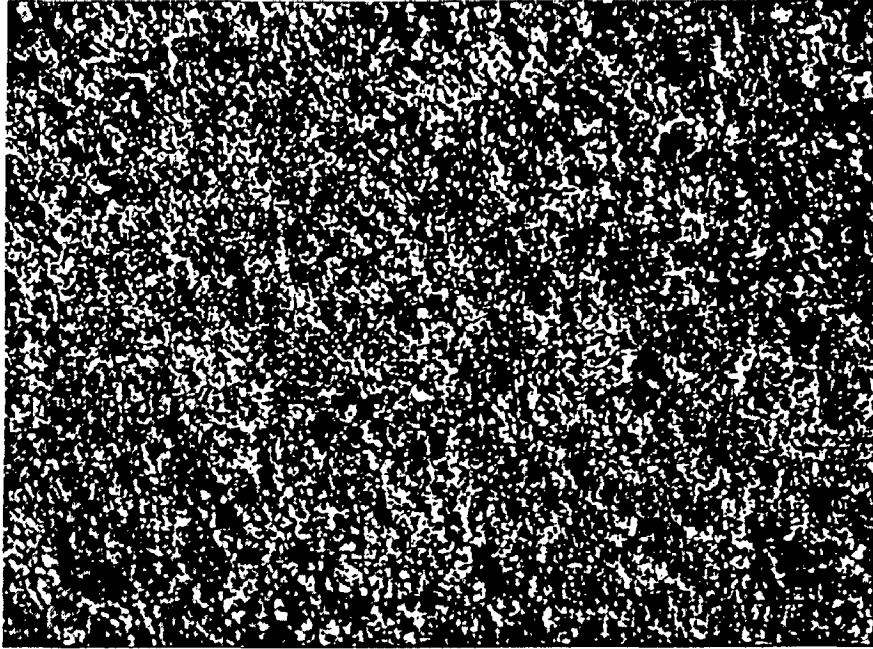


**Fig.4.3.8 shows the effect of 60% reduction rolling on Ni-Ti SMA reduced  
(Magnification: 100X)**

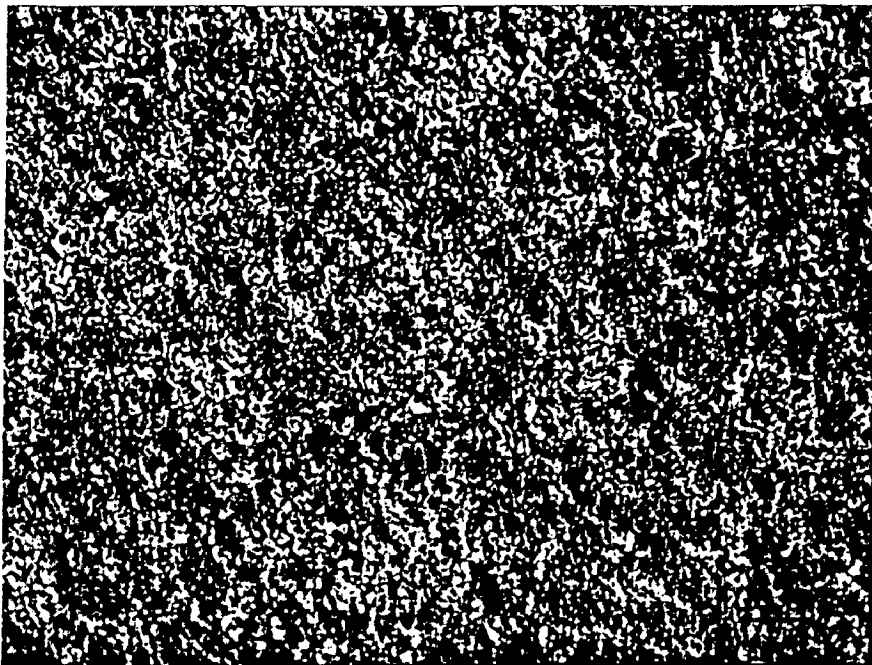


**Fig.4.3.8.1 shows the effect of 70% reduction rolling on Ni-Ti SMA reduced  
(Magnification: 100X)**



### 4.3.2 Effect aging treatment on Ni-Ti and Ni-Ti-Cu.

Optical microscope studies were used to study the changes in martensite needles with respect to ageing temperature and time. But, it is not used to study the identify R-Phase precipitates ( $\text{Ni}_4\text{Ti}_3$ -Rhombohedral or B19 martensitic structures). Martensite needles were appeared clearly on 1000X magnification. So, in all the microstructures were taken at constant magnifications 1000X.



Fig.4.3.9 Ni-Ti as quenched from 800<sup>0</sup>C (1 hour soaking time). Magnification 1000 X

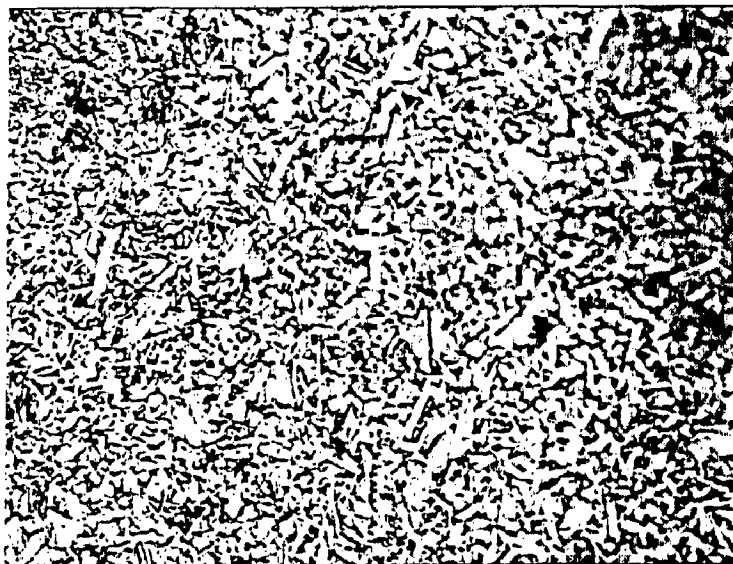


Fig.4.3.10 Ni-Ti aged in 300<sup>0</sup>C at 24 hrs. Magnification 1000 X



Fig.4.3.11 Ni-Ti aged in 300<sup>0</sup>C at 48 hrs (Magnification 1000X).



Fig.4.3.12 Ni-Ti aged in 300<sup>0</sup>C at 72 hrs (Magnification 1000X).

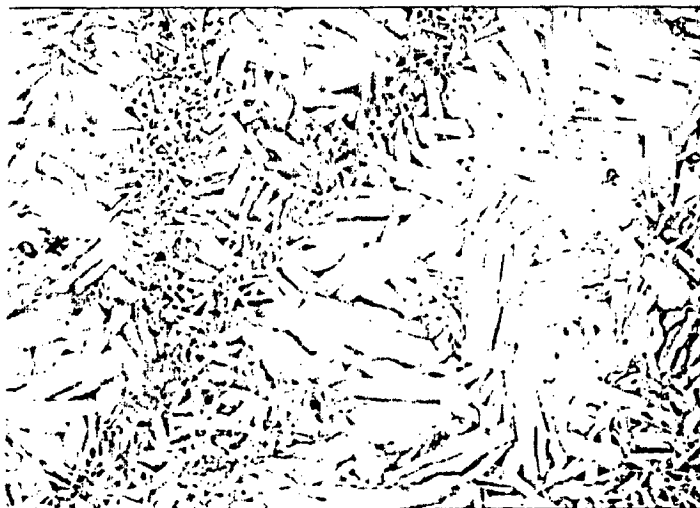


Fig.4.3.13 Ni-Ti aged in 300<sup>0</sup>C at 96 hrs (Magnification 1000X).

Ni-Ti-Cu aged in 300<sup>0</sup>C

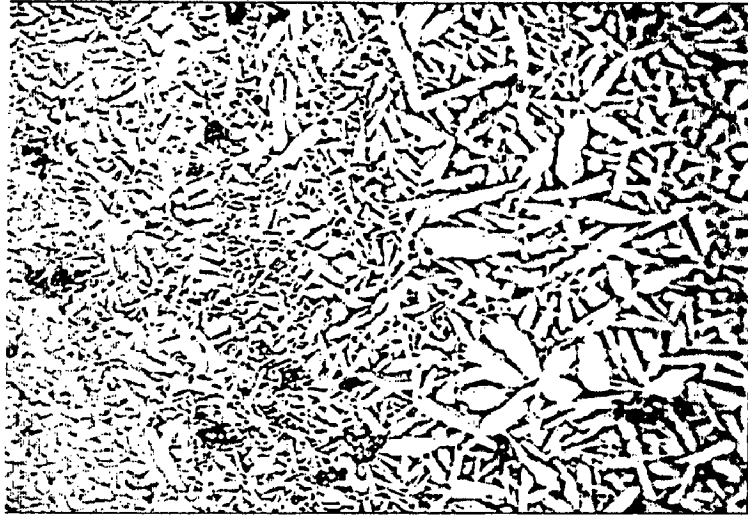


Fig.4.3.14 Ni-Ti-Cu aged in 300<sup>0</sup>C at 24 hrs (Magnification 1000X).

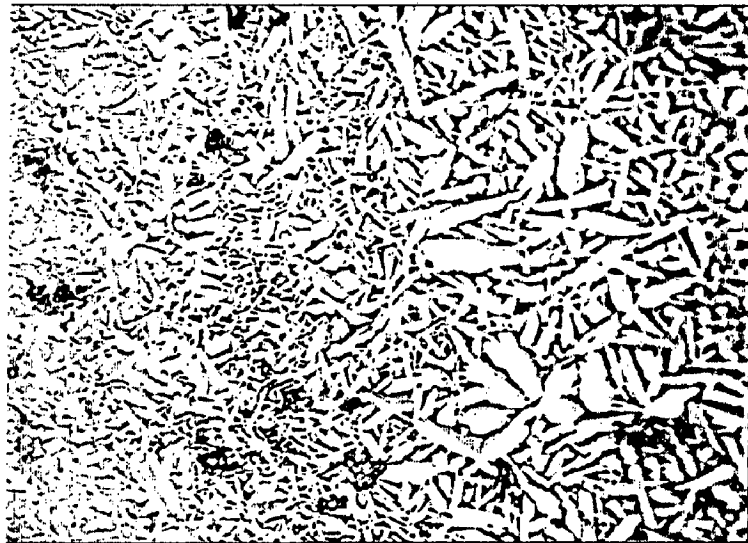


Fig.4.3.14 Ni-Ti-Cu aged in 300<sup>0</sup>C at 48 hrs (Magnification 1000X)

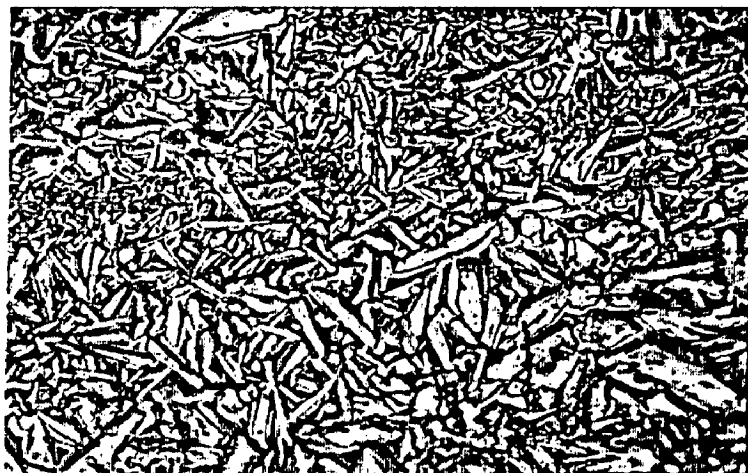
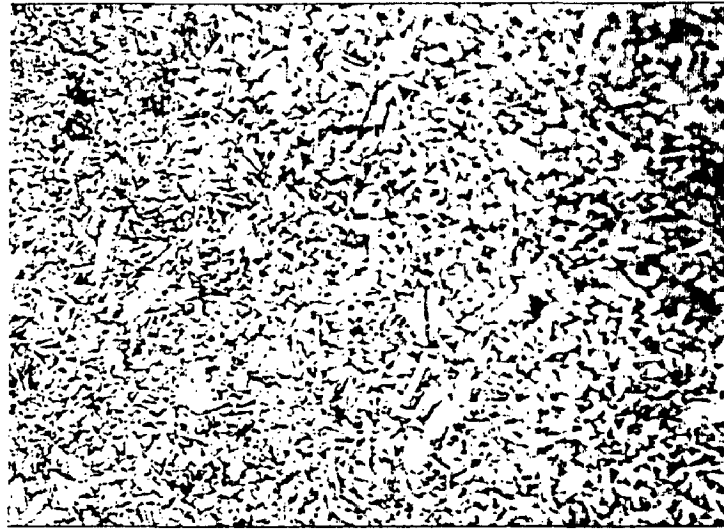
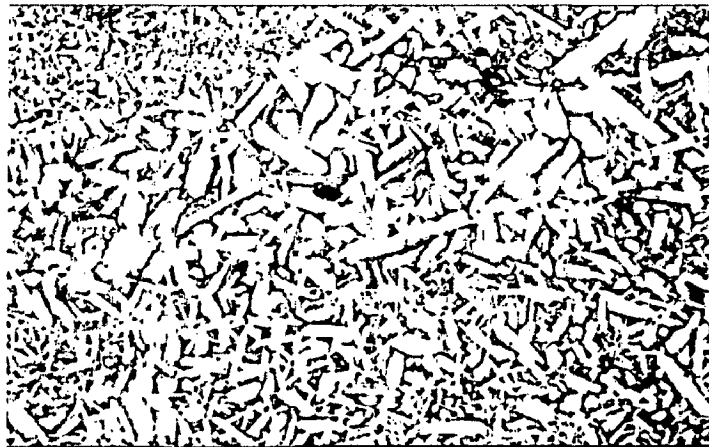


Fig.4.3.14.1 Ni-Ti-Cu,aged in 300<sup>0</sup>C at 72 hrs (Magnification 1000X)



**Fig.4.3.15 Ni-Ti aged in 400<sup>0</sup>C at 24 hrs (Magnification 1000X)**



**Fig.43.16 Ni-Ti aged in 400<sup>0</sup>C at 48 hrs (Magnification 1000X)**

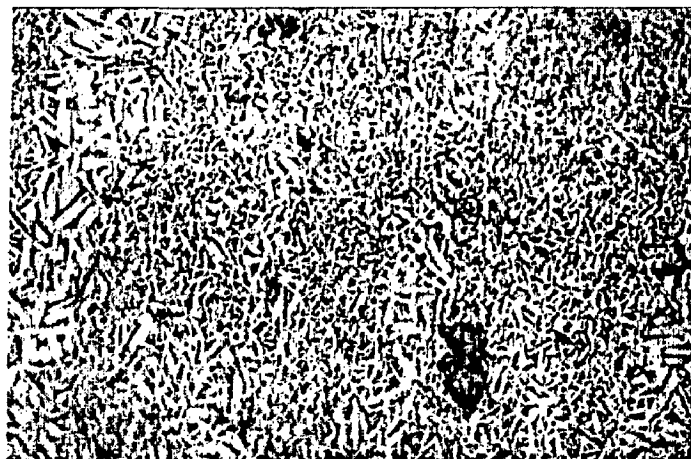


**Fig.4.3.17 Ni-Ti aged in 400<sup>0</sup>C at 72 hrs (Magnification 1000X)**

Ni-Ti aged 150<sup>0</sup>C

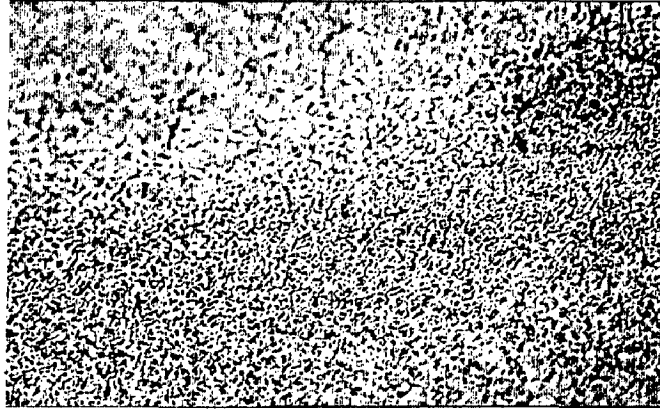


Fig.4.3.18- Ni-Ti as quenched from 850<sup>0</sup>C (Magnification 1000X)

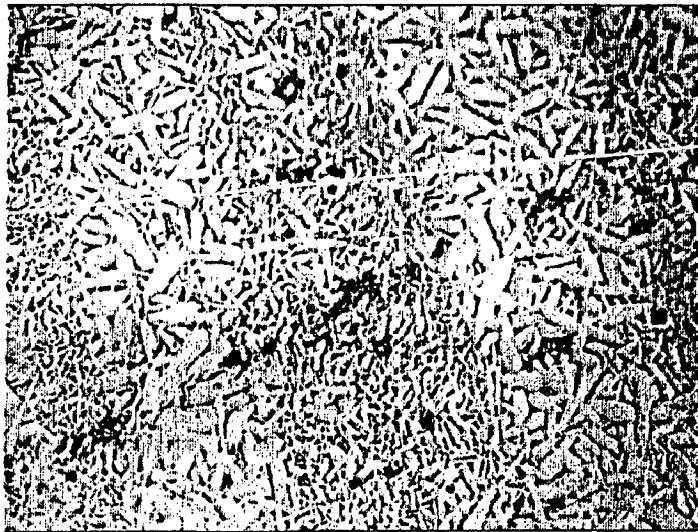


Fig.4.3.19- Ni-Ti aged in 150<sup>0</sup>C at 24 hrs (Magnification 1000X)



Fig.4.3.20 Ni-Ti aged in 150<sup>0</sup>C at 48 hrs (Magnification 1000X)



Fig.4.3.21- Ni-Ti aged in 150<sup>0</sup>C at 72 hrs (Magnification 1000X)

#### 4.4 SEM study:

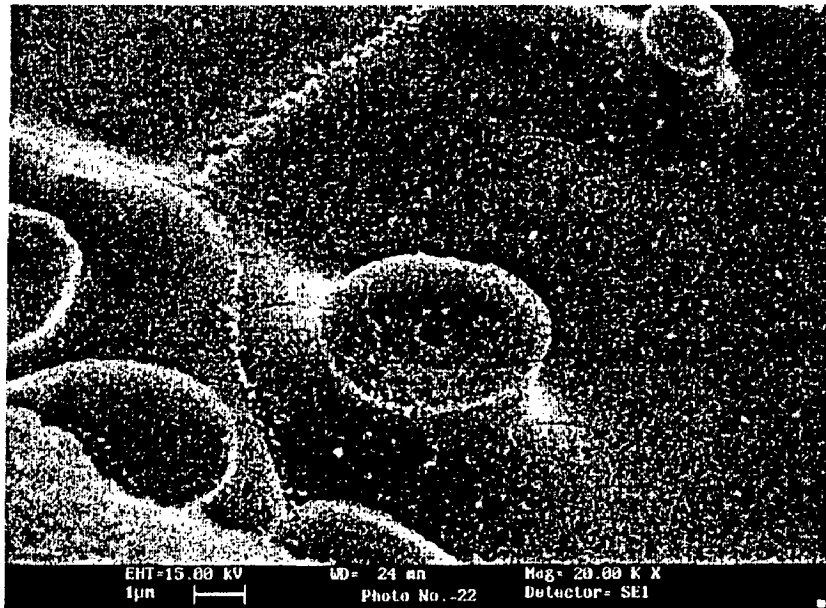


Fig.4.4.1 shows the SEM picture of the aged 150<sup>0</sup>C at 48 hrs and Ni<sub>4</sub>Ti<sub>3</sub> precipitation was formed along the grain boundary and inside the grains.

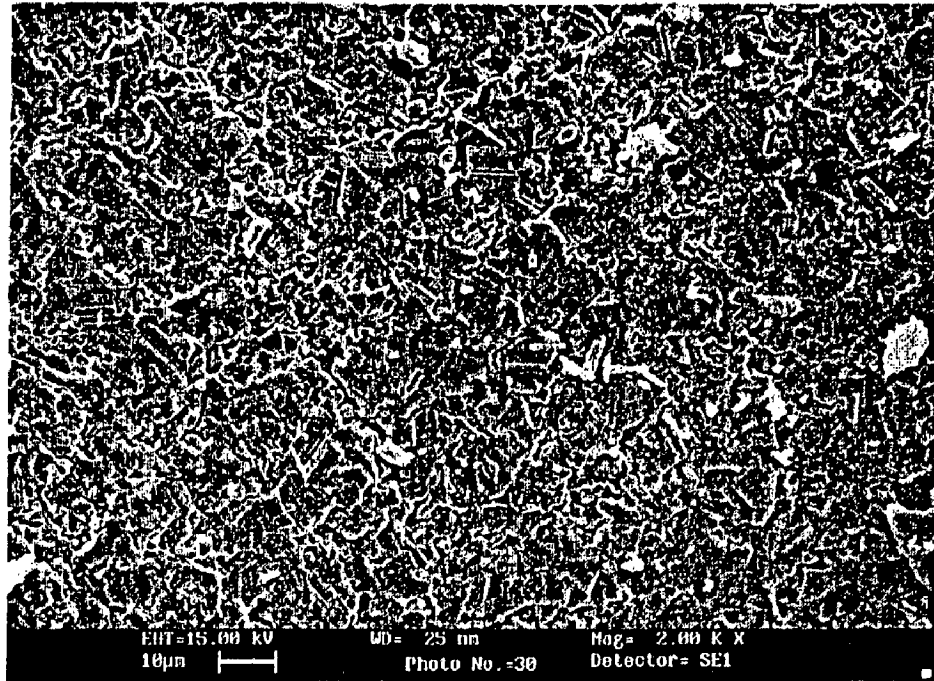


Fig.4.4.2 shows the martensite needles of the Ni-Ti aged in 150<sup>0</sup>C at 24 hrs (at 2000X)

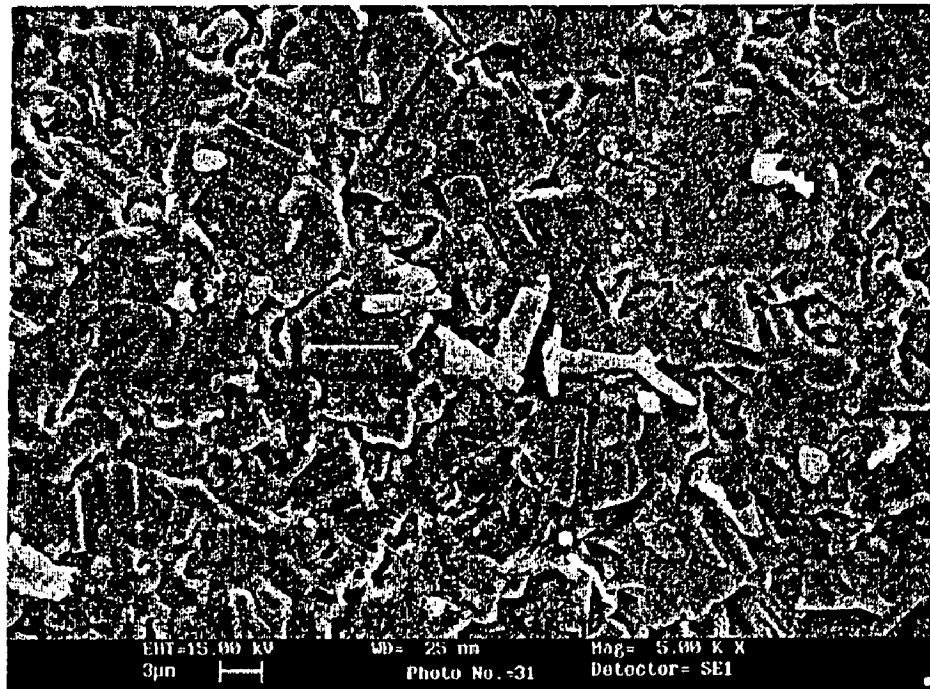
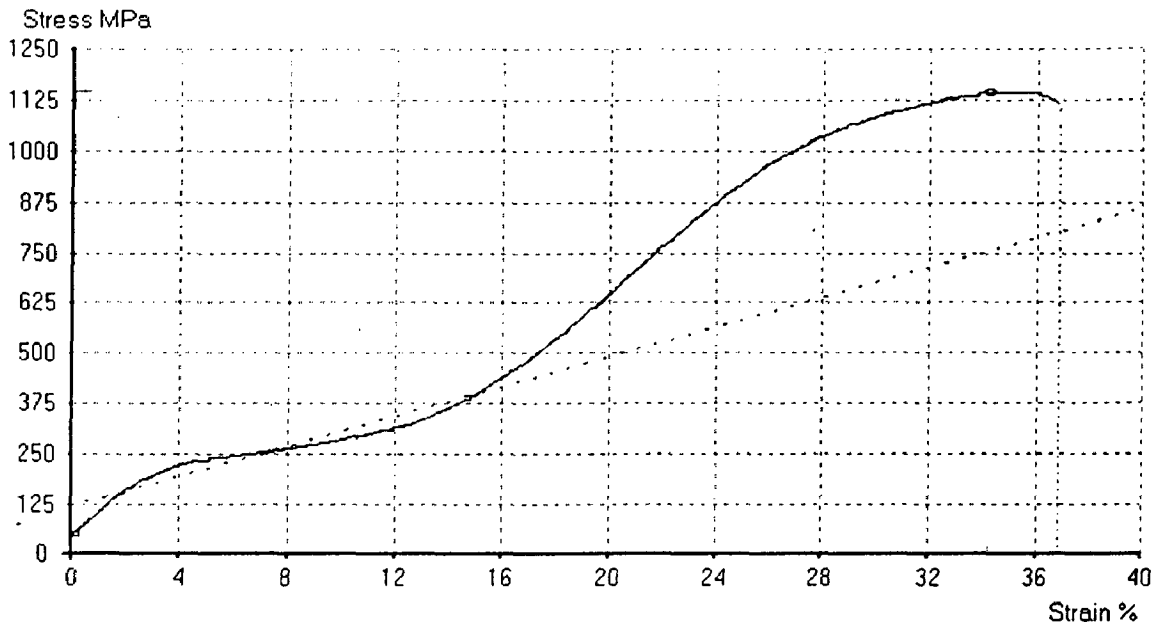


Fig: 4.4.3 shows the martensite needles of the Ni-Ti aged in 150<sup>0</sup>C at 24 hrs (at 5000X)

## 4.5. Tensile Test

Stress-strain curve for the nitinol alloys are characterized by discontinuous yielding and large luder strains when tested at temperature at room temperature and above AF at a temperature above 373 K (100°C). The luder strain does not appear and more than 15% elongation absorbed before fracture [36].



**Fig: 4.5.1** shows tensile stress –strain curve of the annealed 400°C in 1 hr.

Fig.4.5.1 shows the tensile stress/strain curve of wire specimens of a Ti alloy (dia 0.5 mm). The specimen was annealed for 1 hr at 400°C after cold drawing and tested at 40°C which is below  $R_f$  and above  $M_s$  and thus the specimen was entirely in the R phase state when tested on stressing the first yielding occur at  $Y_R$  in which is the starting part of the deformation during to rearrangement of the R phase variants. This first shape due to the variant rearrangement gives due to an elongation of above 0.3%.

The second yielding occurs at  $Y_M$  which is the starting part of the deformation due to stress induced of the B19' Martensite form from R phase. This second step due to the stress induced B19' Martensite rise to an elongation of about 5% including to that of the R-phase. After this, the rate of stress increase becomes larger and slip deformation begins. Finally fracture occurs at about 15% elongation. If the test temperature is below  $M_f$ , the



first step does not occur, since R-phase exists. In this case, only one large step which is due to rearrangement of the variants of the B19' appears before slip deforms starts.

The characteristics of the stress-strain in terms of annealing, ageing and thermally cycled wires.

#### 4.5.1 Effect of annealing on stress-strain curve:

Fig.4.5.2 shows the effect of annealing on the 30% cold work wire. Wire samples taken in the same gauge length 50mm in order to compare the properties of the pseudo elasticity of this Ni-Ti wire 0.5mm diameter wire sample.

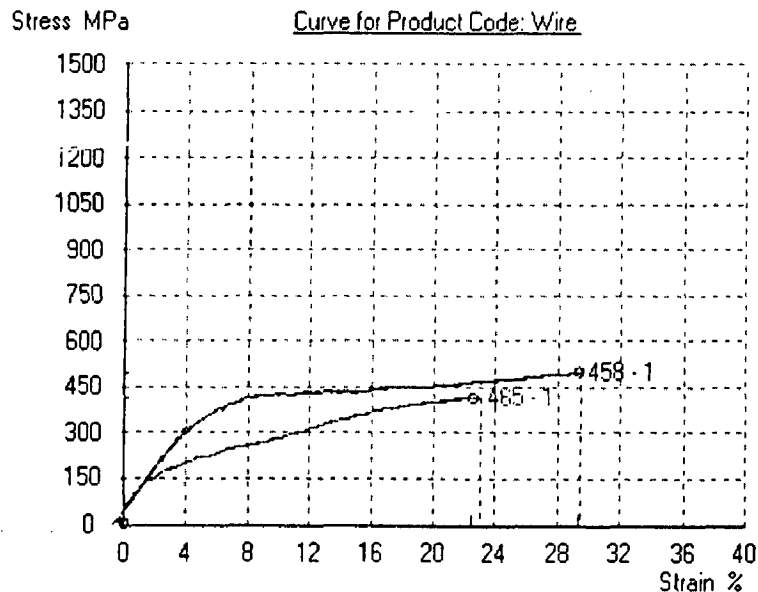


**Fig .4.5.2 shows effect on temperature on tensile stress- strain curve of the Ni-Ti SMA.**

Product code: 458-1- represents Ni-Ti annealed in 1000<sup>0</sup>C

Product code: 465-1 represents Ni-Ti annealed in 900<sup>0</sup>C

Specimens are solution-annealed at 900<sup>0</sup>C which represents the product code 465-1 and solution annealed at 1000<sup>0</sup>C which represents product code 458-1. Solution annealed 1000<sup>0</sup>C wire having proof stress 2.445 MPa as compared to solution annealed 900<sup>0</sup>C wire having 2.979MPa. 1000<sup>0</sup>C annealed Ni-Ti having high values of the stress-assisted transformation. In the relatively soft Ni-Ti is a compressed by as significant amount of

concurrent plastic deformation. Initial stress-assisted Martensite transformation occurs in those martensite domains which are mostly favorably oriented with respect to the applied stress. As transformation proceeds, however, the continuing stress- arrested transformation must set in others, progressively less formerly oriented domains. Therefore, its interaction requires progressively higher stresses. It follows that the relative properties of the plastic deformation to the transfer matrix deformation progressively increases. Finally at  $Y_2$ , essentially at the favourably oriented martensite domains have under transformation. In a random polycrystalline martensite specimen until the

Solution annealed  $1000^{\circ}\text{C}$  specimen may have  $M_s$  temperature below room temperature. Presently, the specimen was in austenite  $B_2$  structure. If while stressing the material in tensile loading stress-assisted martensite was formed and it may spread over the material and finally after reaching 420 MPa, started to plastic deformation (work hardening); It was gaining the strain up to 30%. This 30% strain the material covered on heating above  $A_s$  temperature of the material. This concept was Pseudo- elasticity.

Specimen was quenched from  $900^{\circ}\text{C}$  having proof stress 2.979 MPa. This was higher than stress induced martensite formed at lower stress level than quenched from  $1000^{\circ}\text{C}$ . It may due to  $M_s$  Temperature of the sample was more than  $M_s$  temperature of the  $1000^{\circ}\text{C}$  solution annealed sample. Solutionized at  $900^{\circ}\text{C}$  may not have complete  $B_2$  structure some amount of retained martensite appeared in this wire sample. As quenched from  $900^{\circ}\text{C}$  mixture of  $B_2$  cubic structure and Martensite plate, triggering the formation of additions martensite plate at this low stress level. So strain hardening will take place at very low stress level. After 24% straining the specimen, permanent plastic deformation was started. So we can use shape memory alloy is SAM up to thermal-elastic recovery stress. If second yielding due to permanent plastic deformation started, then the efficiency of the SME was decreased.

Up to the range, where Recoverable plastic deformation occurs, that range was called pseudo elasticity. Certainly, those metals, which cannot possess thermal martensite or

non-thermo elastic martensite characteristics phase transformation, they cannot produce SME or pseudo elasticity.

Second yield was not occurs in this transformation in As – solutionized sample, so use may concluded that, no chances for the appearances of the R-phase in these samples.

#### 4.5.2 Effect of ageing on the tensile stress-strain Curve:

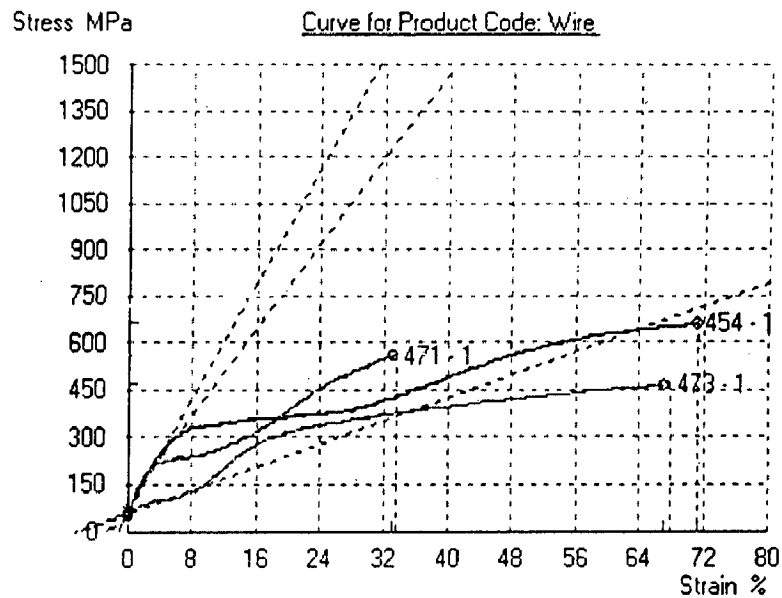


Fig: 4.5.3 shows effect of ageing characteristics of the stress-strain curve of the constant ageing time (24 hrs) in Ni-Ti-Cu SMA.

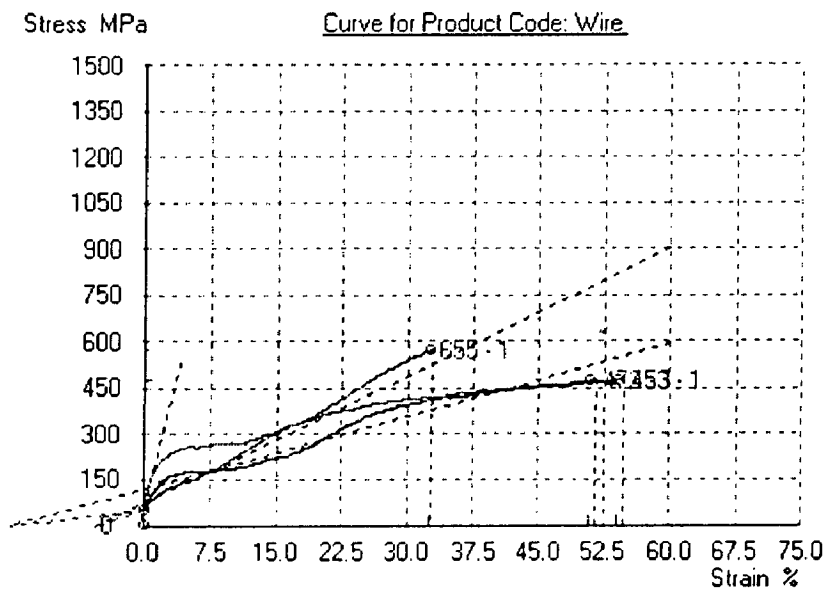
Product code 471-1 designates the Ni-Ti-Cu aged in 150°C at 24 hrs. Product code 471-h designates the Ni-Ti-Cu aged in 150°C at 24hrs after first thermal cycle (T>Rf). To be the test temperature .To was achieved by formation of electric current through the tensile test wire. While passing current (1-1.5A) through the wire temperature of the wire may reach around 100°C above Rs temperature. So the test temperature was adjusted to 100°C to 150°C.

Fig 4.5.3 shows the product code of the 471-1 the Ni-Ti-Cu aged sample exhibits the proof stress value 54.7MPa is much greater than 2.822 MPa in high temperature tensile

test ( $T > R_s$ ). In room temperature tensile test specimen shows two stage strain hardening characteristics the first yielding was started at the strain level of 3% which is usually designated at  $Y_r$ , responsible to the formation of the R phase variant. This first step due to the variant re-arrangement goes rise to an elongation of about 3%.

The second yielding occurs at 10%. Strain which is the starting point of the deformation due to stress induced of the B19' martensite form from the R phase. This second yielding represent at  $Y_m$ . After this 10% strain, the rate of stress increases layer and slip deformation begins. When the test temperature ( $T > R_s$ ), should be above  $R_s$  and below  $A_f$ , specimen completely M austenite B<sub>2</sub> (cubic) structure [38]. Stress strain curve on this temperature regions shows, only one yielding due to formation of stress assisted martensite. So, the proof stress was dropped low values as compared to the room temperature tensile test. First yielding due to formation of the R-phase was concluded in this aged sample [39]. After first yielding, specimen starts to fractured. But very high amount of first stage strain stored in this material.

Comparison on the stress-strain



**Fig.4.5.4 shows the comparison of the ageing characteristics of the Ni-Ti in different temperatures.**

Product code 472-1 shows Ni-Ti aged in 150°C at 24 hrs

Product code 453-1 shows the Ni-Ti aged in 200°C at 24 hrs

Product code 655-1 shows Ni-Ti aged 300°C at 24 hrs.

In Ni-Ti system, R-phase was started high yield strength than only B2 phase Ni-Ti. Due to this R-phase transformation two yields,  $Y_R$  and  $Y_m$  occurred correspondingly. The product code 655-1 shows only one yield point, which represents the formation of B19' martensite variants.

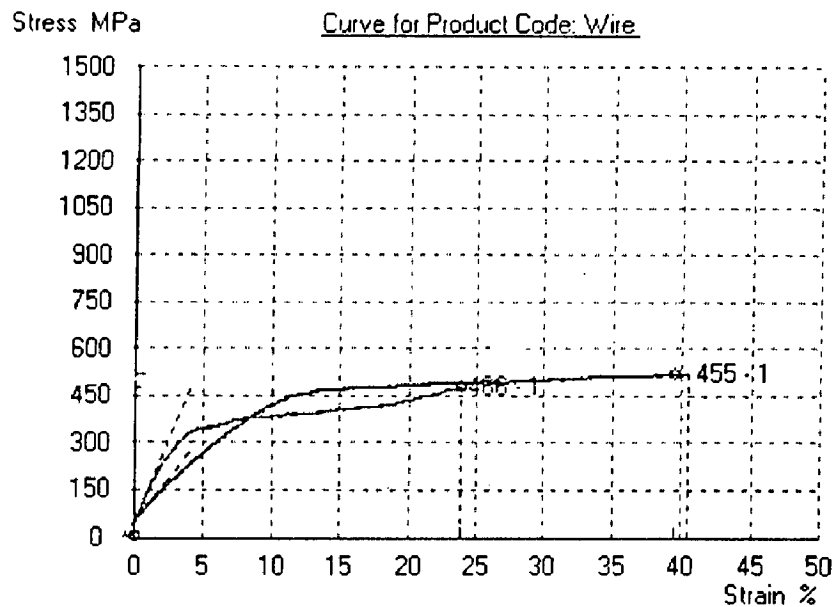


**Fig: 4.5.5 compares the stress-strain behaviour of the aged sample with as-quenched Ni-Ti SMA**

455-1 – Aged in 200°C at 24 hrs, Ni-Ti system

466-1 – Ni-Ti solution annealed 900°C.

Solution annealed sample having proof stress values 7.33 MPa then aged in 150°C at 24 hrs. Ni-Ti solution annealed at 900°C having only B2 -B19' transformation and  $M_s$  temperature of the sample in the as-solutionized condition was lowered below room temperature. So, straining takes place at 325MPa at 5% strain. But aged 200°C at 24hrs was having  $M_s$  temperature was certainly lesser than the as-quenched form 800°C.  $M_s$  temperature was lowered very low level, certainly formation of the SAM was delayed, to

these reasons. Strain hardening in Martensite phase transformation was delayed upto the stress level of 450MPa corresponds to the 12% Strain comparing these two curves, memory concludes that Ms Temperature lowering means Ym (yielding at martensite) was increased.

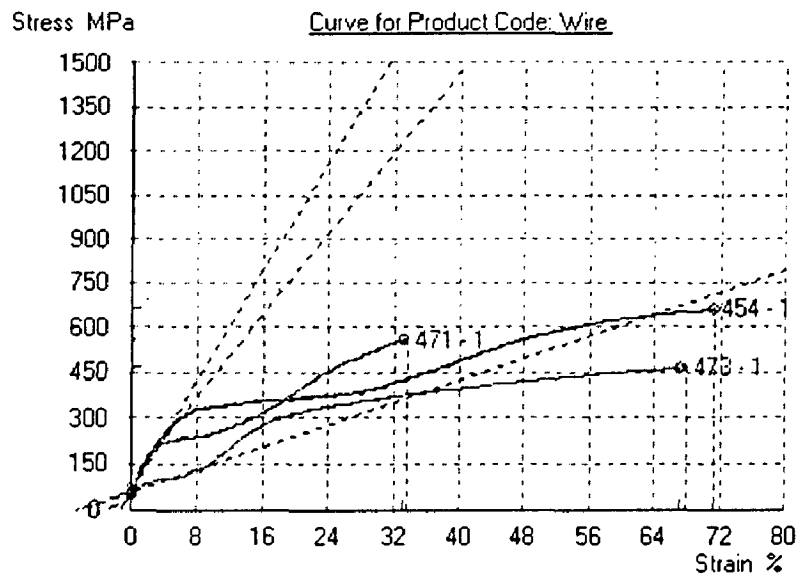


**Fig.4.5.6 shows the comparison of the ageing characteristics of the Ni-Ti-Cu in different ageing temperature.**

Product code –

471-1 – Ni- Ti-Cu aged 150°C in 24 hrs

454-1 – Ni-Ti-Cu Aged 200°C in 24 hrs.

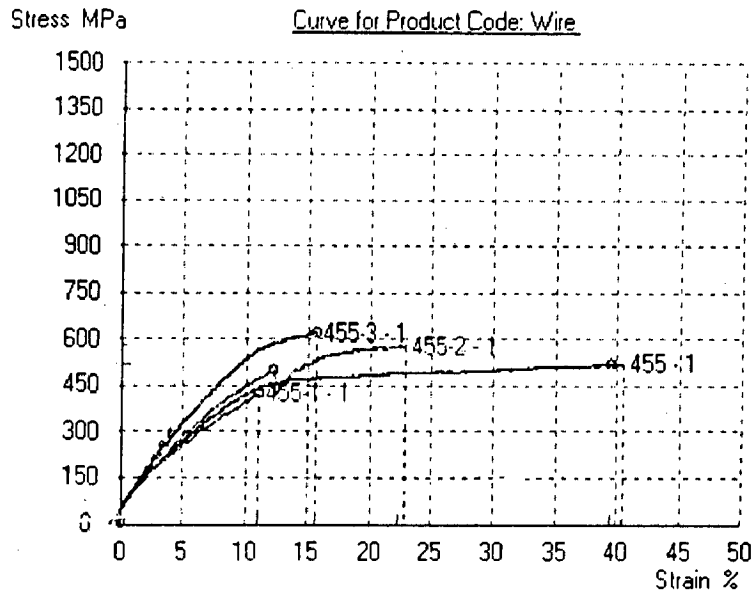
473-1 –Ni-Ti-Cu Aged 300°C in 125 hrs

Fig.4.5.5 shows the comparison of the ageing characteristics of the Ni-Ti-Cu in different ageing temperature. In this figure the product code 454-1 shows the Ni-Ti-Cu aged 200°C in 24 hrs. The only one yielding (Ym) occurred due to high stress level 320 MPa with the 7% strain. No R-Phase transformation was observed in this aged wire Ni-Ti SMA

471-1 shows Ni-Ti-Cu aged 150°C in 24 hrs wire sample. First yielding due to R-phase transformation was started at 3% starts with 200 MPa. Second yielding due to Martensite B19' was started at 12% strain in this wire sample.

454-1 curve shows the aged 200°C at 24hrs. Here the yielding due to Ym martensite starts with 300 MPa with 6% strain.

#### 4.5.3 Effect of temperature on the stress-strain curve of the Ni-Ti SMA.



**Fig: 5.5.7 shows effect of temperature on the stress-strain curve of the Ni-Ti aged in 200°C in 24 hrs Stress-strain Curve.**

455—1 first loading cycle

455-2second loading cycle (Temperature above Ms)

455-3 third loading cycle temperature above Af

Only one yielding occurred on this Ni Ti aged 24hrs at 200°C represents, no R-phase transformation involved in this stress strain curve.

The each loading cycle was performed with intermediate annealing carried out above Af temperature with help of the electric current (1-2A).

Each and every loading cycle, elastic limit (proportional limit was increased linearly).This may represents SIM formed in first cycle was completely removed by heating above Af temperature. While cooling form B2 phase to room temperature phase, already formed martensite plates were disappeared.

455-1 specimen shows ordinary aging characteristics of the stress-strain curve. Yielding was occurred in Y region. Followed by continues martensite variants were formed in this

specimen. 455-2 shows wire was tested above Ms Temperature. So the yield due to Martensite variants was nil. 455-3 shows wire tested above Af, so there was no chances for presence of the martensite variants in the specimen, no yield occur.

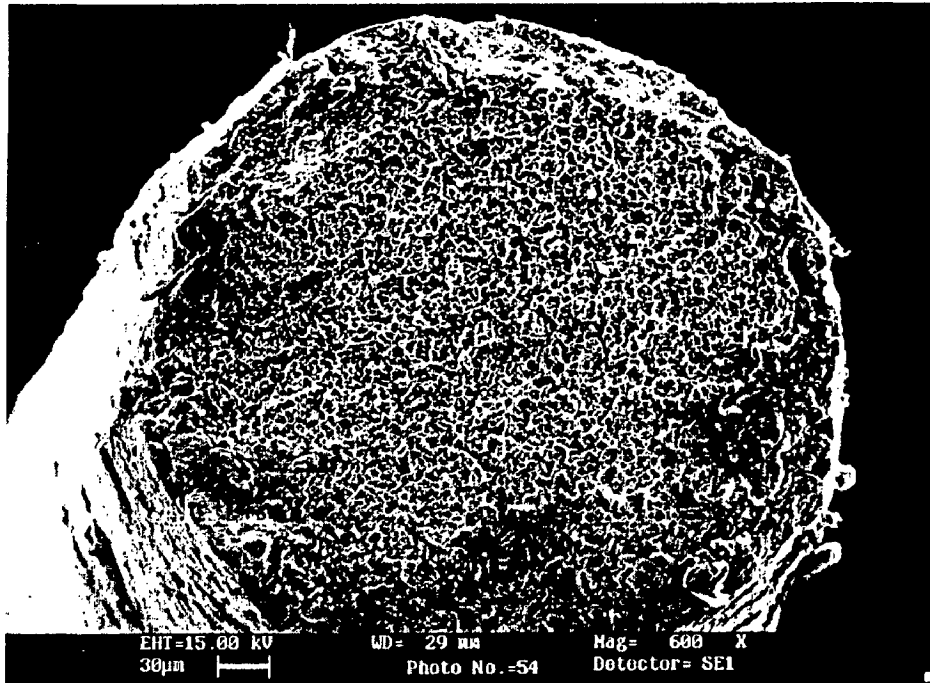


Fig.5.5.7-a shows SEM study of the Ni-Ti annealed 800<sup>0</sup>C

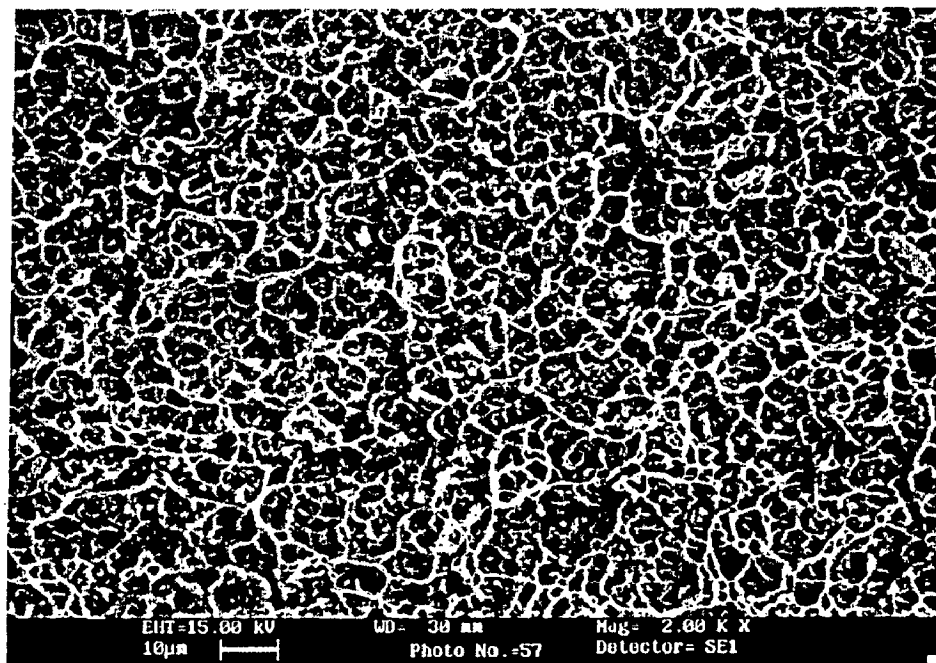


Fig.5.5.7-b shows SEM study of the Ni-Ti annealed 800<sup>0</sup>C



Fig.5.5.7-a shows the position of the fracture surface of the Ni-Ti wire SMA annealed 800°C in 20 minutes. Fig.5.5.7-b shows the same region magnified in 2000X. There was large amount of the equiaxed dimpled surface appeared in this microstructure. This microstructure shows that the large amount of the ductility before fracture behaviour of the Ni-Ti annealed SMA. Thus, it shows that large amount of energy observed before fracture.

#### 4.6. Resistivity Measurements:

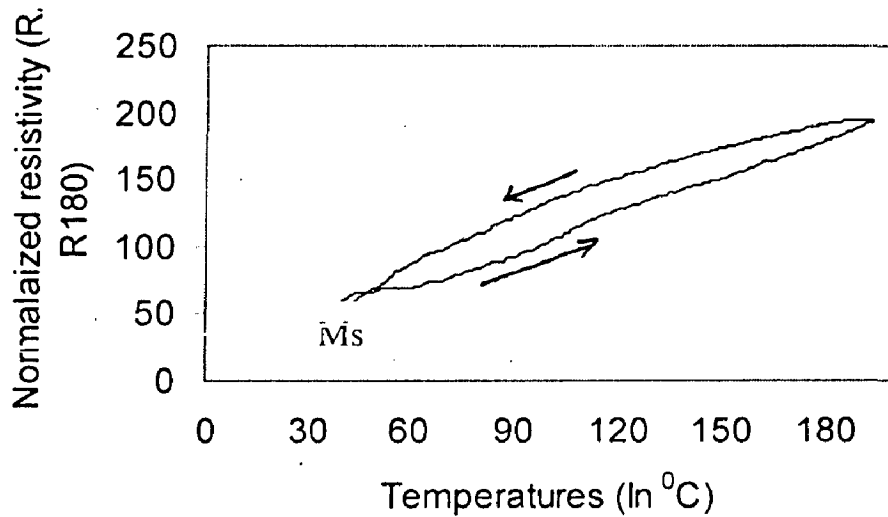


Fig 4.6.1 shows Normalized resistivity curve of the Ni-Ti annealed in 400C at 1hr.

$M_s = 47^\circ\text{C}$ .  $M_f = 30^\circ\text{C}$ . No R-phase transformation in this annealed specimen.

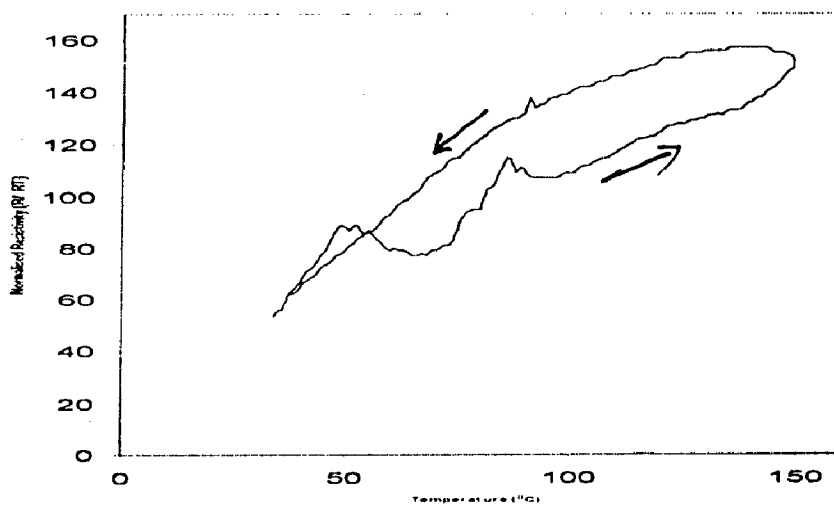
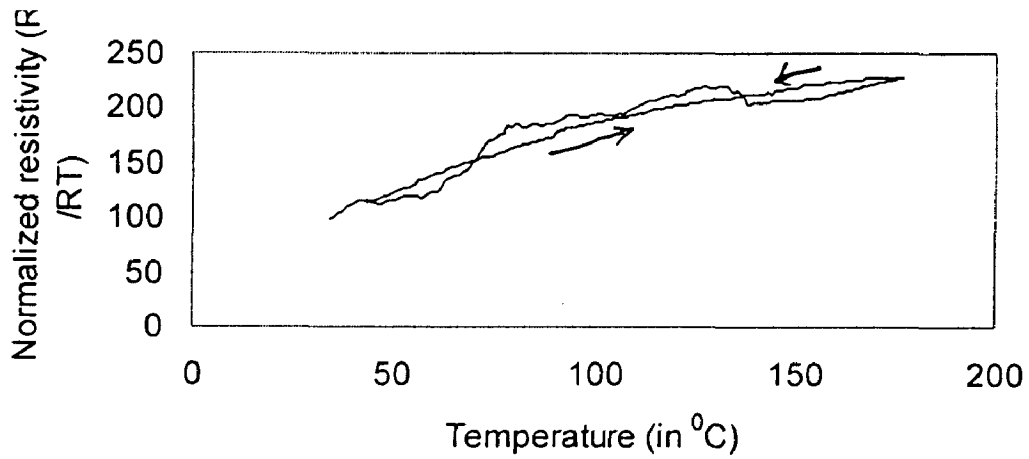


Fig 4.6.2 shows the normalized resistivity curve of the Ni-Ti aged 500°C at 50 hrs.

The resistivity curve of the Ni-Ti aged 500<sup>0</sup>C at 50 hrs was shown in Fig. R1, s= 47<sup>0</sup>C R1,f=54<sup>0</sup>C R2,s= 69<sup>0</sup>C R2,f=98<sup>0</sup>C As=90<sup>0</sup>C Af=98<sup>0</sup>C.



**Fig 4.6.3 shows the normalized resistivity curve of the Ni-Ti 30 % cold reduced sample.**

Fig 4.6.3 shows the normalized resistivity curves of the Ni-Ti 30 % cold reduced sample. From this plot, the following parameters were studied [40-44].

Ms=109<sup>0</sup>C Mf= 69<sup>0</sup>C As=139<sup>0</sup>C Af=176<sup>0</sup>C.

---

## Discussion

### 5.1.1. Aged in 150<sup>0</sup>C in Ni-Ti system:

From the DSC plot provides evidence for the formation of precipitates ( $\text{Ni}_4\text{Ti}_3$ , orthorhombic, R-phase) formation in Ni-Ti system aged in 150<sup>0</sup>C at different intervals 4 hrs, 24 hrs, 48 hrs, 72 hrs.

In solutionized samples, there is no evidence of the formation of R-phase  $\text{Ni}_4\text{Ti}_3$ . The same situation was observed in aged samples up to 24 hrs aged 48 hrs; there were three endothermic peaks along with exothermic peak observed. Currently, I can not say any thing about this new exothermic peak phase transformation; it violates the nature of the law of the phase transformations were occurred in heating especially in this Ni-Ti System.

Thermal hysteresis of this phase transformation was 20<sup>0</sup>C with endothermic energy -4.23 J/g. This phase not certainly R-phase because thermal hysteresis in R-phase transformation should be narrow and formation of R-phase in Ni-Ti system, while heating should be endothermic, certainly not exothermic, based on experimental results.

Based on the literature, a plausible explanation to rationalize three steps endothermic peaks may occur on heating from B19' phase to B<sub>2</sub> phase. In the case of Ni-Ti system, if the formation of R-phase may consist of two R-phases, that is R1 and R2 phases. This phase having high thermal hysteresis 27<sup>0</sup>C with endothermic energy of 7.39 J/g. merging of the two R-phases peak was started between 24 hrs and 48 hrs. B<sub>2</sub> phase was formed with thermal hysteresis of the 10<sup>0</sup>C with 0.7 J/g. While cooling B<sub>2</sub>→R phase temperature was raised from 63<sup>0</sup>C to 73<sup>0</sup>C.

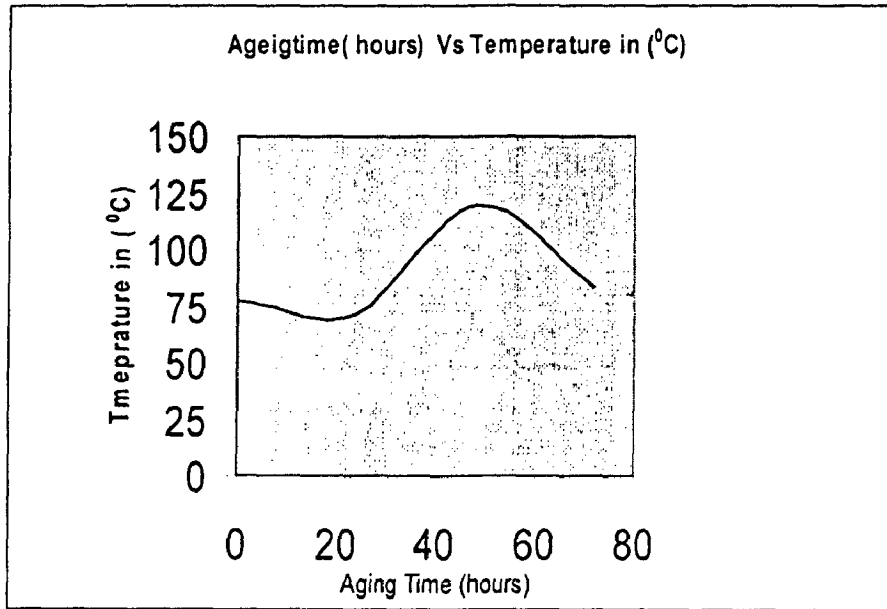


Fig 5.1.1 shows effect of ageing time on As temperature.

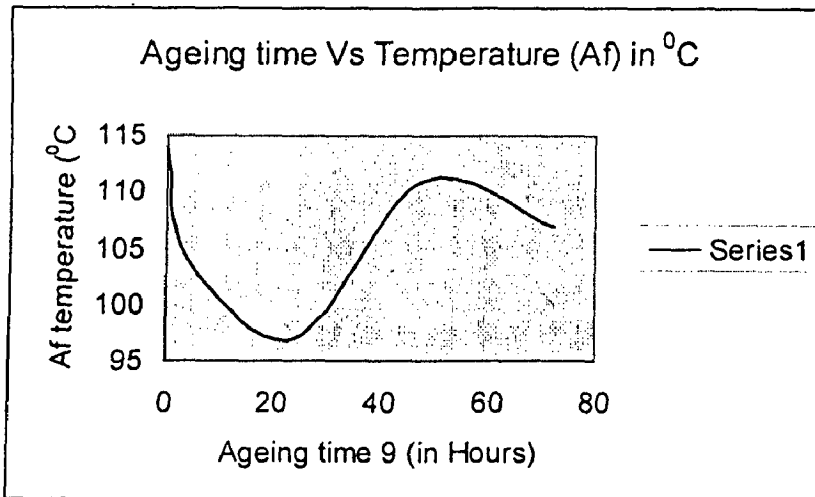
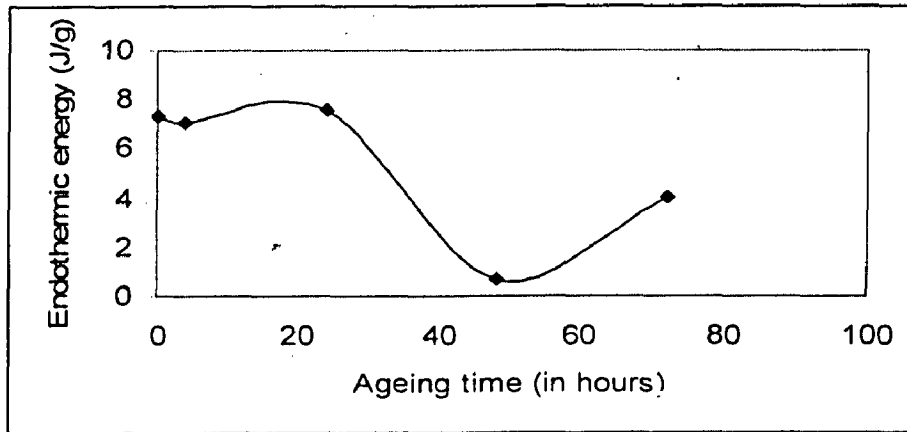


Fig 5.1.2 shows effect of ageing time on Af temperature.

In the above graph (Fig- 5.1.2) shows how the Af temperature of the aged sample varying with respect to ageing time. Those ageing time does not have R-phase transformation ( $B2 \rightarrow B19'$ , phase transformation only) no effects in As temperature of the sample. Aged in between 24 hrs and 48 hrs samples, there is the big variations in As

temperatures, it may be due to formation of intermediate precipitate phases, R-phase- $Ni_4Ti_3$  precipitates [45, 46]. In this low temperature aged samples, R-phase were appeared in heating and cooling also. Af temperature also following the same sequences which was shown in the following Fig.5.1.2.



**Fig 5.1.3 shows effect of ageing time on endothermic energy (J/g)**

Explanation for the  $B_2$  regime isolated to the interaction of the moving Austenite / Martensite boundaries. Here, the first peak on heating represents to the formation of R-phase from  $B19'$  phase. The second peak represents to the R-phase to  $B_2$  cubic phase. The transformation sequences were concluded as follows

In heating  $B19' \rightarrow R \rightarrow B_2$

In cooling  $B_2 \rightarrow R \rightarrow B19'$ .

The  $B19'$  phase growth is interrupted, however, as M/A interfaces are energetically impeded by sub-grain walls (second peak:  $B19' \rightarrow R$ ) until R-phase growth is interrupted by the dislocation walls.

From the Fig.5.1.3, energy consumption in phase transformations were lowered in 48 hrs ageing treatment, this ageing period useful for Actuator or smart structures.

Fig shows tensile stress-strain plot of the aged in 150<sup>0</sup>C at 48 hrs. Proof stress of the sample was very low 2.538 MPa. After cyclic loading with intermediate annealing at 100<sup>0</sup>C at 2 minutes, rises the proof stress 8.59 MPa.

A microstructural scenario suggested which is based on in-situ TEM observations during cooling B2 region / They refers to the presence of the coherency stress fields around meta stable Ni<sub>4</sub>Ti<sub>3</sub> precipitates to rationalize multiple step transformation behaviour. In the first stage of the transformation sequences, B<sub>2</sub> transformation in to R-phase as R-phase nucleates at the particle/ matrix region interface and grows into the matrix (First peak). In the second step, the R-phase transforms in to the B19', but the subsequent growth of B19' is bounded by those regions around particles which are affected by coherency stress fields ( Second peak R-B19') in regions around precipitates affected by coherency stresses [47].

Finally, those regions of the matrix out side the local precipitates coherency stresses are able to transform third peak: R-B19'-in matrix regions which are not affected by coherent stresses.

The present experimental work believed in results obtained from differential scanning calorimetric (DSC) for Ni-rich Ni-Ti-alloys on heating from the B19' regime. In a simplified two-particles/matrix system a multiple step transformation can be explained based on two elements [49]:

- (1) The composition in homogeneity which evolves during aging as Ni<sub>4</sub>Ti<sub>3</sub>, precipitates grow.
- (2) The differences between nucleation barriers for R-phase (small) and B19' (large).

These two elements explain the features of the evolution of DSC charts during aging, which change from two transformation peaks on cooling after long aging times. Another reason for multiple step transformations in Ni-rich Ni-Ti alloys may be that Ni<sub>4</sub>Ti<sub>3</sub>, particles precipitate heterogeneously near grain boundaries. Then the first two (endothermic transformation) peaks can be attributed to the formation of R-phase from B19' in the grain boundary regions while the third peak corresponds to a transformation of

R to B2 phase (high temperature phase). This was confirmed with SEM Fig.4.4.1. Formation of Ni<sub>4</sub>Ti<sub>3</sub> precipitates in grain boundary and grain interiors. This is the reason to exhibit multiple step R-phase transformations in this alloy. We may believe that the same situation was observed while cooling also.

### 5.1.2 Ageing 150<sup>0</sup>C in Ni-Ti-Cu SMA

Although a substitution of the third element Cu in Ni-Ti maintains the Thermo Mechanical Treatment (TMT) in the Ni-Ti-Cu alloys the martensite phase is different depending upon the Cu-content. Up to about > 7 at % of Cu transformation sequences is very similar to the binary one with a cubic body centered (B2) to a monoclinic B19' martensite. Controversial is the presence in these alloys of the R-phase with different experimental findings [50].

We have identified some new experimental evidence with formation of the R-phase transformations in Ni rich Ni-Ti-Cu aged SMA at different temperature intervals.

The chemical composition of the as received sample was Ni<sub>49.14</sub>Ti<sub>45</sub>Cu<sub>6.6</sub>. The amount of at% Cu values less than values predicted by the researches (Cu<7 at. %) favorable for the formation of B19'-phase in stead of B19 martensite phase in Ni-Ti-Cu systems.

We have identified that the formation of R-phase peak was unstable even at these low temperature ageing treatment in 150<sup>0</sup>C. After 96 hrs aged sample shows only B<sub>2</sub> phase with large thermal hysteresis of this transformation. Energy consumption in this transformation + 8.62 J/g, certainly higher than previous 72 hrs aged Ni-Ti-Cu SMA.

This high amount of energy consumption indicates that B<sub>2</sub> phase stabilized in this transformation and R-phase vanishes in this aged Ni-Ti-Cu SMA.

We have identified formation of R-phase occur after short ageing duration in  $150^{\circ}\text{C}$ . It may have high chances to formation of R-phase near 20 hrs. It was completely different from aged in  $150^{\circ}\text{C}$  at 24 hrs Ni-Ti SMA.

After 48 hrs, aged sample shows that the R-phase started to stabilize and energy released in these phase transformation was (total endothermic peak on heating) was 12.9 J/g. This may indicates that the deepening of the R-phase occurred in this 48 hrs aged Ni-Ti SMA.

Fig: shows the Ni-Ti-Cu aged  $150^{\circ}\text{C}$  at different time intervals:

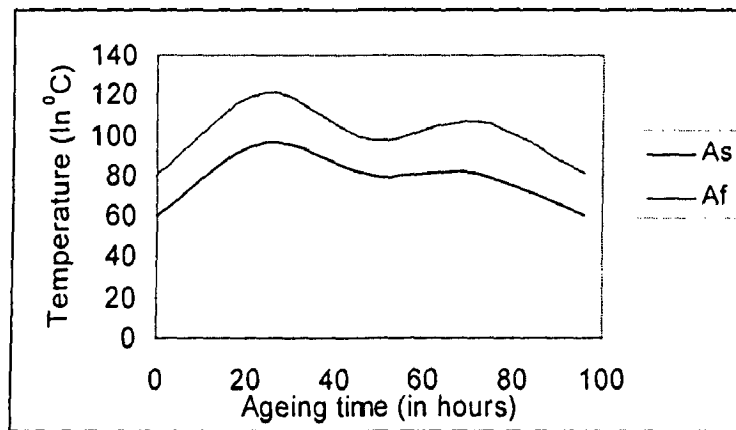


Fig 5.1.4 shows effect of ageing time on As temperature.

From this above fig.6.1.4 shows the effect of As temperature of the as-quenched sample was always lesser than the aged Ni-Ti-Cu SMA. Fig.6.1.4 shows the effect of ageing time in endothermic energy of the transformation. Whenever the R-phase transformations were occurred, energy consumption in that phase transformation was decreased. So, we may conclude that ageing 24 hrs treatments was best suited for Fighter Air-craft Actuator control wire spring. Whenever the energy consumption in phase transformations were increased, that ageing time suitable for pipe coupling. So ageing in 48 hrs best suited for pipe coupling.



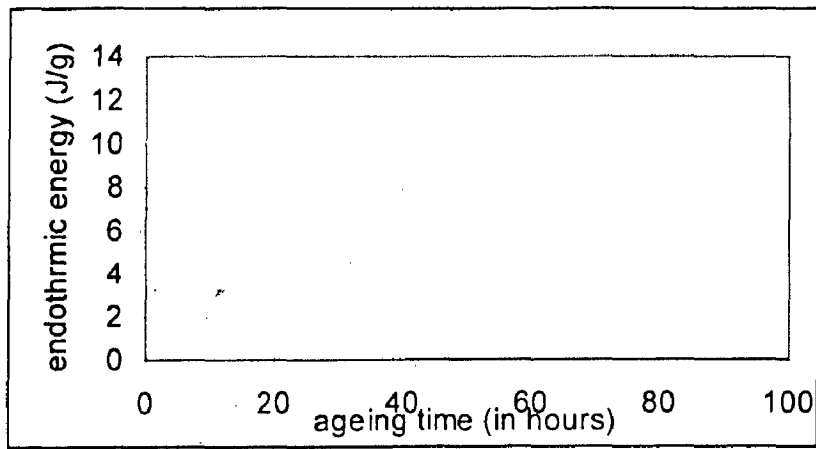


Fig 6.1.5. Shows effect of ageing time on endothermic temperature.

5.1.3 Ageing in 300<sup>0</sup>C Ni-Ti system.

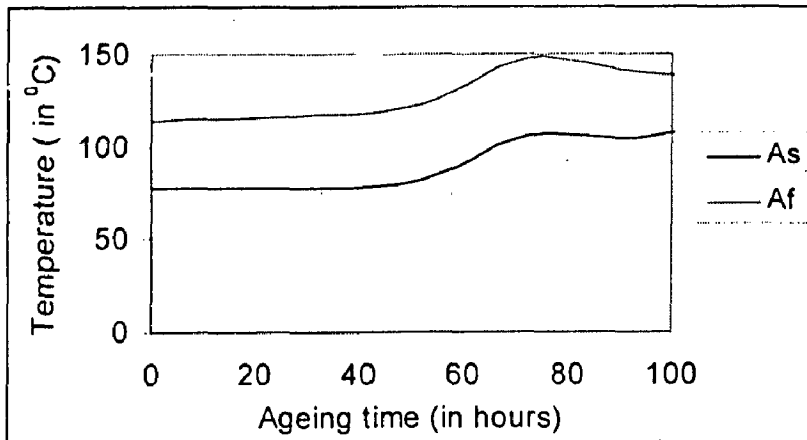


Fig 5.1.6 Shows effect of ageing time on As and Af temperature

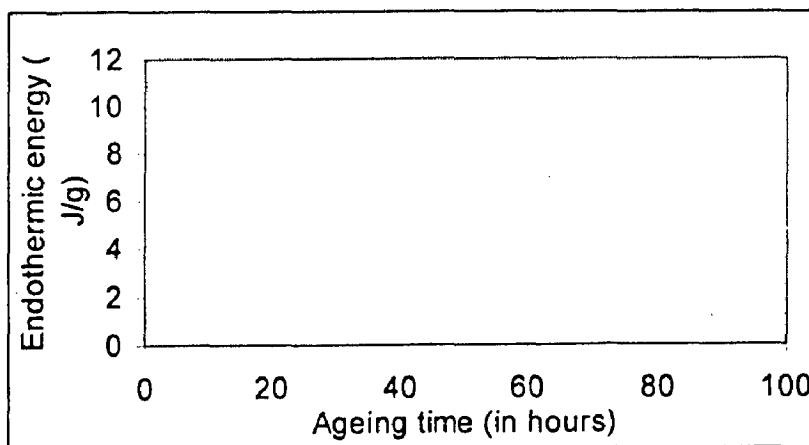
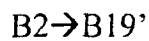


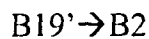
Fig 5.1.7. Shows effect of ageing time on endothermic energy consumption.

Aged up to **48 hrs** observed the following transformation cycles:

On Cooling:

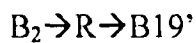


On heating:



Aged up to **72 hrs** observed the following sequences of the transformation cycle:

On Cooling:

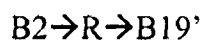


On heating:

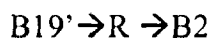


Aged at **96 hrs** observed the following sequences of phase transformations:

On Cooling:

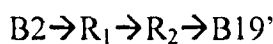


On heating:

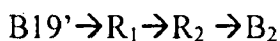


Aged at **125 hrs** observed the following sequences of the phase transformation:

On Cooling:



On heating:



Aged at 125 Hrs Ni-Ti-Cu SMA shows some interesting results between  $R_2$  start and  $R_2$  Finish transformations some intermediate phases were observed because there is no sharp endothermic peak available in this R-phase transformation. Formation of this R-phase transformation was confirmed with help of XRD spectra, which was shown in Fig.4.2.1.  $R_2$  phase transformation thermal ( $R_s$  and  $R_f$ ) hysteresis, multiple step R-phase may form. R-phase transformation of this aged sample was started between 48 hrs and 72 hrs aged sample. It was stabilized at 76 hrs aged sample, because, in 96 hrs aged sample separation of the phases were observed; this was confirmed with XRD spectra Fig.4.2.7. R-phase transformation of this alloy having low thermal hysteresis  $15^\circ\text{C}$  with  $0.54 \text{ J/g}$  energy consumed in this aged at 72 hrs Ni-Ti SMA. From the fig.6.1.6 and Fig.6.1.7 ageing in 125

hrs preferred for actuator control, where energy consumption in phase transformations were lower.

#### 5.1.4 Aged 300°C in Ni-Ti-Cu SMA

Aged up to 48 hrs (No R-phase transformations were observed): the transformation sequences were follows:

**B2-Cubic phase, NiTi (Austenite phase)**

On Cooling:

$B2 \rightarrow B19'$

On heating:

$B19' \rightarrow B2$

Aged up to 72 hrs the transformation sequences were follows:

On Cooling:

$B2 \rightarrow R \rightarrow B19'$

On heating:

$B19' \rightarrow R \rightarrow B2$

Aged at 96 hrs the following transformation sequences were observed:

On Cooling:

$B2 \rightarrow B19'$

On heating:

$B19' \rightarrow B2$

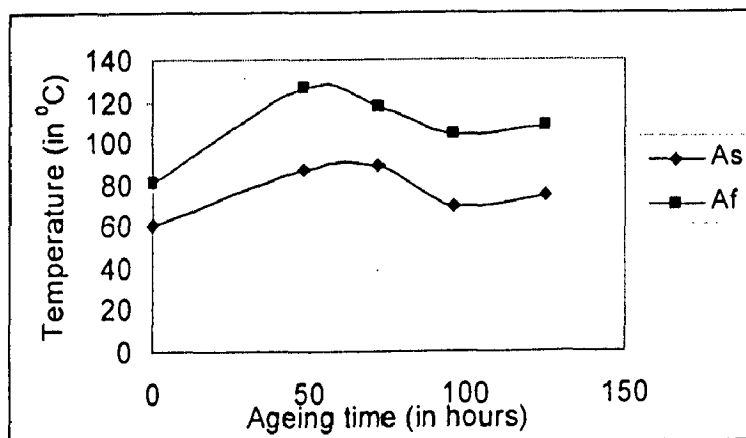
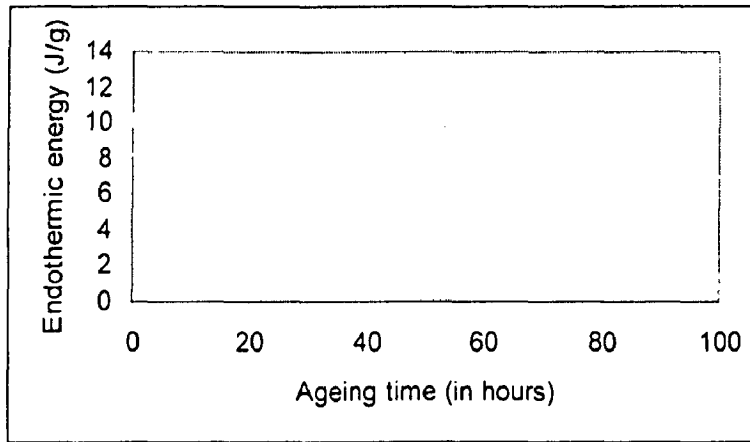


Fig.5.1.8. Shows effect of ageing time on As and Af temperatures.



**Fig 5.1.9. Shows effect of ageing time on endothermic energy consumption.**

R-phase transformations were occurred in between 48 hrs and 72 hrs aged sample. Thermal hysteresis in this R-phase transformation surprisingly was equal to the thermal hysteresis of the B<sub>2</sub> phase transformation. he fig.6.1.8 and Fig.6.1.9 ageing in 78 hrs preferred for actuator control, where energy consumption in phase transformations were lower and hysteresis in phase transformations were also lowered.

#### **Thermally cycled Ni-Ti-Cu wire:**

Fig.4.1.24 shows the Ni-Ti-Cu specimen as quenched from 850°C and given thermal cycles with the help of the constant current source (1 A current in 1.5 minutes), after 1.5 minutes cooling will occur. While thermal cycled wire showing the R-phase transformations, it will be very useful for designing the actuators in Fighter craft.

$$R1,s = 64^{\circ}\text{C} \quad R1,f=72^{\circ}\text{C} \quad R2,s=72^{\circ}\text{C} \quad R2,f=91^{\circ}\text{C}, \quad A_s=131^{\circ}\text{C} \quad \text{and} \quad A_f=135^{\circ}\text{C}.$$

Thermal hysteresis in B<sub>2</sub> phase transformations were lowered very low value only 4°C. This may be due to formation of dislocation sub-structure in each and every thermal cycle. This is the reason why multiple R-phase transformations were observed in thermally cycled Ni-Ti-Cu wire sample.

## **5.2 XRD analysis.**

Fig.4.2.12 shows XRD spectra of the specimen measured at various temperature intervals. The temperatures were reached by cooling down progressively after each measurement. An XRD spectrum was obtained as-rolled sheet.  $d=2.111\text{\AA}$  corresponds to

the B2 cubic (011) structure. B2 cubic was low intensity at room temperature. While temperature of the specimen increases means intensity of the (110) B2 was increased progressively [39].

### 5.2.1 Formation of the B2 cubic structure from R phases from R1 and R2 phase

Fig.4.2.12 shows the super imposed image of the XRD spectra of the Ni-Ti aged in 500°C at 48 hrs specimen measured at various temperature intervals from room temperature to 150°C. The temperature was reached cooling down progressively after each measurement from 150°C. With in 2θ ranges shown in the figure, the B2 phase is easily identified by strong reflection (110) B2 diffraction peak. The shoulder peak on the high angle side of the B2 (100) reflection peak was a double reflection from Cu-Kα<sub>2</sub>. It is seen that above 85°C there is the only one peak observed corresponds to (110) B2. Cooling to 80°C lead to the appearance of R (011) and R (101) reflections in co-existing with B2 (110). The intensity of the R-phase diffraction peaks increased with decreasing temperature whilst that of the B2 (110) peak decreased. At below 80°C, no B2 (110) diffraction peak was detected. It is also seen in the figure that the positions of the R (011) and R (101) peaks shifted during cooling. This may be related to the second order nature of the R-phase transformation i.e., evolution of the Rhombohedral angle upon cooling [40].

$a=11.235 \text{ \AA}$   $c=5.0789 \text{ \AA}$   $C=.4521$  S.G= R3 (148).

### 5.2.2 Effect of the cold work (strain hardening) on Ni-Ti-Cu SMA:

Fig.4.2.11-12, 13, 14 and 15 shows XRD spectra of the effect of the cold work (strain hardening) on the diffraction peak intensity. X-ray diffraction was carried out on the 5%, 10%, 15%, 20% strained Ni-Ti-Cu SMA sample. Initially sample have monoclinic B19' martensitic structure. While straining the specimen intensity of the B19' (monoclinic) phase increases rapidly. And, the major peak was broadening and splitting will occur in the shoulder of the major peaks. This may indicates high amount of dislocation density developed while straining the specimen, due to for that Ms temperature of the SMA was raised. There is no peak was observed the formation of the R-phase (Rhombohedral, Ni<sub>4</sub>Ti<sub>3</sub> precipitates) in this strained Ni-Ti-Cu SMA.

Fig.4.2.11-1 shows XRD spectra of the 5 % strained Ni-Ti SMA sheet. Here, the major peak belongs to the monoclinic B19' phase. There is no sharp peak available in this major peak. It may be due to increase the dislocation density in this 5% strained Ni-Ti-Cu SMA. Fig.4.2.11-2 shows XRD spectra of the 5 % strained Ni-Ti SMA sheet. Here, the major peak belongs to the monoclinic B19' phase. There is no sharp peak available in this major peak. It may be due to increase the dislocation density in this 10% strained Ni-Ti-Cu SMA.

Fig.4.2.11-3 shows one additional monoclinic phase was observed at the start of the shoulder in the (111) position. This additional peak may belong to the formation of the Stress Induced Martensite (SIM) (B19' monoclinic) phase in this 15 % strained Ni-Ti-Cu SMA. So the Ms Temperature of the sample was raised progressively in this 15% strained sheet. Fig.4.2.11-4 shows, numerous number of diffuse diffraction peaks were observed in this 20% strained Ni-Ti-Cu SMA. Intensity of the B19' phases increases and some additional streaks were formed in the bottom of the shoulder of the major peak.

Fig.4.2.13 and 4.2.13-1 to 8 shows the XRD spectra of the Ni-Ti-Cu aged in 500<sup>0</sup>C at 48 hrs. The next series of the diffraction patterns of the (110)<sub>B2</sub> peak was obtained by using a specially designed heating stage that the sample could be heated at 100<sup>0</sup>C / minute with a temperature stability of  $\pm 1^{\circ}\text{C}$ . Series of experiments were carried out at different temperatures intervals 25<sup>0</sup>C, 35<sup>0</sup>C, 40<sup>0</sup>C, 45<sup>0</sup>C, 50<sup>0</sup>C, 100<sup>0</sup>C, 150<sup>0</sup>C, 200<sup>0</sup>C and 700<sup>0</sup>C.

From the temperature 25<sup>0</sup>C to 40<sup>0</sup>C, no change in the peak (110)<sub>B2</sub>. But after reaching 45<sup>0</sup>C, the progressive broadening of the peak, and intensity of the peak increase. This temperature is called TTR (Temperature transformation region).

At 100<sup>0</sup>C, peak was split and intensity of the peak increases and 150<sup>0</sup>C flattening of the peak was started. At 200<sup>0</sup>C, flattening of the peak disturbed, again splitting of the peak was started. At 700<sup>0</sup>C, peak was having higher intensity than any other peak. From the series of the high temperature XRD measurements, the TTR of the Ni-Ti-Cu aged 48Hrs was 45<sup>0</sup>C. At 45<sup>0</sup>C, B2 phase (110) cubic austenite phase was started.

## FUTURE WORKS

1. SEM with EDX analysis should be carried out to identify the precipitates in aged samples.
2. TEM study should be carried out to identify the martensite plate orientation.

## CONCLUSION

1. We were characterized R-phase transformation in Ni-Ti and Ni-Ti-Cu SMA with help of DSC and XRD spectra, very useful for actuator or smart structures.
2. Ageing in 150°C at 72 hrs, R-phase transformation of the Ni-Ti-Cu SMA having low thermal hysteresis 15°C with 0.54 J/g energy consumed Ni-Ti SMA. Ageing in 300°C at 125 hrs yields low endothermic energy with narrow hysteresis region. These narrow thermal hysteresis regions were useful in Actuators and smart structures.
3. In the case of Ni-Ti-Cu system, the energy consumption in R-phase transformations were lowered in 24 hrs aged in 150°C treatment and aged in 300°C at 48 hrs yields low endothermic energy with narrow thermal hysteresis. Formation of R-phase was confirmed with XRD results.
4. Thermal hysteresis in B2 phase transformations were lowered very low value only 4°C. This may be due to formation of dislocation sub-structure in each and every thermal cycle. This is the reason why multiple R-phase transformations were observed in thermally cycled Ni-Ti-Cu wire sample. Thermo cycled methods very useful for stabilizing the R-phase transformation in Ni-Ti-Cu system.



## REFERENCES

---

1. W.J Buelher, J.V. Gilfrich, and R.C. Wiley, J.A.P 34, 1475 (1963).
2. Garica. Scripta materialia, Volume 42, issue 6, 28 Feb 2000, Pages-531-536
3. K.Otsuka and K.Shinizu .M.Athlers Materials sciences and engg A, Volume 273-275,15 Dec1999,Pages 595-599.
4. R.W.Cahn Act. Met. 149(1955).
5. Yan Li, Chengobao Jiang, Ting liang –Scripta Materilia48 (2003) 1255-1258.
6. X.M.Zhang .J.Fernandance and J.M.Gliemany Materials and Design, volume-21,issue-6,Dec-2000,pages 557-559.
7. R.J.Wasilewski, Metallurgical Trans. 1971, Vol-2, pages (1953).
8. L .C. Chang and T.A.Read Transactions, AIME, 1991, 47(1957)
9. D.P. Dunne, materials science Forum, Vol 327-328, (2000), PP 315-322.
10. D.P.Dunne and C.M Wayman, Met. Transaction, 4(1973) P.137.
11. L.Hou, O.S., Grummon, scripta Metal and Materials Vol-33(1995) ,P-989.
12. Y.C.Lo, S.K.WuJournal of material Science-30, 1995, 1577-1583
13. P.Arneodo Larochette, M.Ahelrs, Materials sci and engg A 361 (2003) 249-257)
14. J.D.Eissenwasser and L.Brown Metal transaction, 1971, Vol-3-P 1359.
15. H.Tobushi, T.Hachisuka, T.hachisuka Transaction, ASME, Journal of Engg Materials and their tech, Vol 120(1998), P.64-70
16. Ling HC, Kaplow R. Met Trans A 1981;11:77–83.
17. Hwang CM, Meichle M, Salamon MB, Wayman CM. Phil Mag A 1983;47:9–30.
18. Hwang CM, Wayman CM. Scripta Metall 1983;17:1449–53.
19. Miyazaki S, Otsuka K. Met Trans A 1986;17A:53–63.
20. Miyazaki S, Wayman CM. Acta Metall 1988;36:181–92.
21. Miyazaki S, Kimura S, Otsuka K. Phil Mag A 1988;57:467–78.
22. Lin HC, Wu SK, Chou TS, Kao HP. Acta Metall Mater 1991;39:2069–80.
23. Todoroki T, Tamura H. Trans JIM 1987;28:83–94.
24. Miyazaki S, Ohmi Y. Otsuka K. Suzuki Y. J de Phys 1982; 43(suppl. 12):C4-255.

25. Miyazaki S. In: Duerig TW et al., editors. Engineering aspects of shape memory alloys. Butterworth-Heinemann: 1990. p. 394–413.
26. Miyazaki S, Igo Y, Otsuka K. *Acta Metall* 1986;34:2045–51.
27. McCormick PG, Liu Y. *Acta Metall Mater* 1994; 42:2407–13.
28. Liu Y, Chen X, McCormick PG. *J Mater Sci* 1997; 32:5979–84.
29. Miyazaki S, Otsuka K. *Phil Mag A* 1984; 50:393–408.
30. Zhu JS, Gotthardt R. *Phys Lett A* 1988;132:279–82.
31. Favier D, Liu Y, McCormick PG. *Scripta Metall Mater* 1993;28:669–72.
32. Stroz D, Kwarciak J, Morawiec H. *J Mater Sci* 1988;23:4127.
33. Bataillard L, Bidaux J-E, Gotthardt R. *Phil Mag A* 1998;78: 327–44.
34. Saburi T, Watanabe Y, Nenno S. *ISIJ Internat* 1989;29:405.
35. J.I. Kim, Yinong Liu, S. Miyazaki *Acta Materialia* 52 (2004) 487–499
  
36. J. Spielfeld *Materials Science and Engineering A* 273–275, (1999), 639–643
37. J.I. Kim, Yinong Liu, S. Miyazaki *Acta Materialia* 52 (2004) 487–499
38. P. Shi, D.Z. Yang, H.M. Shen, F.X. Chen, *Materials and Design* 21, 2000, 521-524
39. S.P. Thompson, J. Loughlan. *Composite Structures* 51 (2001) 21-36
40. Y.F. Zheng, L.C. Zhao, H.Q. Ye *Materials Science and Engineering A* 297 (2001) 185–196
41. T. Mineta et al., *Sensors and Actuators A* 88 (2001) 112-120
42. Guojun Suna, U, Shuangshuang Suna, Xiaodong Wub, Jianshen Wub *Materials and Design* 21, 2000, P.525-528
43. S.K. Wu, H.C. Lin, H. Chena *Materials Chemistry and Physics* 68 (2001) 149–156
44. Sergey A. Egorov, Margarita E. Evard, Alexandre E. Volkov *Computational Materials Science* 19 (2000) 77-80
45. C. Messner, G. Reisner a, Q.P. Sun b, E. Werner *Computational Materials Science* 19 (2000) 313-319
46. Fumihito Nishimura<sup>1</sup>, Noriko Watanabe, Kikuaki Tanaka *International Journal of Mechanical Sciences* 42 (2000) 347-365
47. Y. F. ZHENG<sup>1</sup>, W. CAI<sup>1</sup>, J. X. ZHANG, L. C. ZHAO<sup>1</sup> and H. Q. YE *Acta mater.* 48 (2000) 1409-425.